UNIVERSIDADE FEDERAL DE MINAS GERAIS
Escola de Engenharia
Programa de Pós-graduação em Engenharia Elétrica

Diego Andrés Parada Rozo

PARABOLIC EQUATION AND RAY TRACING FORMULATIONS FOR THE DEVELOPMENT OF RADIOWAVE PROPAGATION MODELS IN NON-HOMOGENEOUS MEDIA

Belo Horizonte
2023

Diego Andrés Parada Rozo

PARABOLIC EQUATION AND RAY TRACING FORMULATIONS FOR THE DEVELOPMENT OF RADIOWAVE PROPAGATION MODELS IN NON-HOMOGENEOUS MEDIA

Versão final

Tese de Doutorado apresentada ao Programa de Pós-Graduação em Engenharia Elétrica da Universidade Federal de Minas Gerais, como requisito parcial para obtenção do título de Doutor em Engenharia Elétrica.

Orientador: Cássio Gonçalves do Rego
Coorientador: Dinael Guevara Ibarra

Belo Horizonte
2023

Parada Rozo, Diego Andrés.
P222p Parabolic equation and ray tracing formulations for the development of radiowave propagation models in non-homogeneous media [recurso eletrônico] / Diego Andrés Parada Rozo. - 2023.
1 recurso online (97 f. : il., color.) : pdf.

Orientador: Cássio Gonçalves do Rego.
Coorientador: Dinael Guevara Ibarra.

Tese (doutorado) - Universidade Federal de Minas Gerais, Escola de Engenharia.

Bibliografia: f. 93-97.
Exigências do sistema: Adobe Acrobat Reader.

1. Engenharia elétrica - Teses. 2. Ondas de rádio - Propagação - Teses. 3. Sistemas de comunicação sem fio - Teses. 4. Velocidade - Teses. 5. Algoritmos - Teses. 6. Telecomunicações - Teses. 7. Raios - Teses. 8. Refração - Teses. I. Rego, Cássio Gonçalves do. II. Guevara Ibarra, Dinael. III. Universidade Federal de Minas Gerais. Escola de Engenharia. IV. Título.

CDU: 621.3(043)

Ficha catalográfica elaborada pela bibliotecária Ângela Cristina Silva CRB/6 2361
Biblioteca Prof. Mário Werneck, Escola de Engenharia da UFMG

UNIVERSIDADE FEDERAL DE MINAS GERAIS
ESCOLA DE ENGENHARIA
PROGRAMA DE PÓS-GRADUAÇÃO EM ENGENHARIA ELÉTRICA

FOLHA DE APROVAÇÃO

"PARABOLIC EQUATION AND RAY TRACING FORMULATIONS FOR THE DEVELOPMENT OF RADIOWAVE PROPAGATION MODELS IN NON-HOMOGENEOUS MEDIA"

DIEGO ANDRÉS PARADA ROZO

Tese de Doutorado submetida à Banca Examinadora designada pelo Colegiado do Programa de Pós-Graduação em Engenharia Elétrica da Escola de Engenharia da Universidade Federal de Minas Gerais, como requisito para obtenção do grau de Doutor em Engenharia Elétrica. Aprovada em 19 de maio de 2023. Por:

Prof. Dr. Cássio Gonçalves do Rego
DELT (UFMG) - Orientador

Prof. Dr. DINAEL GUEVARA IBARRA
Depto de Electricidad y Electrónica da Universidad Francisco de Paula Santander (Colômbia) - Coorientador

Prof. Dr. Glaucio Lopes Ramos
DETEM (UFSJ)

Prof. Dr. Luiz Alencar Reis da Silva Mello
DEE (PUC Rio)

Prof. Dr. Alberto Resende De Conti
DEE (UFMG)

Prof. Dr. Fernando José da Silva Moreira
DELT (UFMG)

Documento assinado eletronicamente por **Cassio Goncalves do Rego**, **Professor do Magistério Superior**, em 22/05/2023, às 14:28, conforme horário oficial de Brasília, com fundamento no art. 5º do Decreto nº 10.543, de 13 de novembro de 2020.

Documento assinado eletronicamente por **Alberto Resende de Conti**, **Professor do Magistério Superior**, em 22/05/2023, às 15:06, conforme horário oficial de Brasília, com fundamento no art. 5º do Decreto nº 10.543, de 13 de novembro de 2020.

Documento assinado eletronicamente por **Luiz Alencar Reis da Silva Mello**, **Usuário Externo**, em 22/05/2023, às 16:54, conforme horário oficial de Brasília, com fundamento no art. 5º do Decreto nº 10.543, de 13 de novembro de 2020.

Documento assinado eletronicamente por **Dinael Guevara Ibarra**, **Usuário Externo**, em 23/05/2023, às 07:19, conforme horário oficial de Brasília, com fundamento no art. 5º do Decreto nº 10.543, de 13 de novembro de 2020.

Documento assinado eletronicamente por **Fernando Jose da Silva Moreira**, **Professor do Magistério Superior**, em 23/05/2023, às 12:52, conforme horário oficial de Brasília, com fundamento no art. 5º do Decreto nº 10.543, de 13 de novembro de 2020.

Documento assinado eletronicamente por **Glaucio Lopes Ramos**, **Usuário Externo**, em 24/05/2023, às 22:28, conforme horário oficial de Brasília, com fundamento no art. 5º do Decreto nº 10.543, de 13 de novembro de 2020.

A autenticidade deste documento pode ser conferida no site https://sei.ufmg.br/sei/controlador_externo.php?acao=documento_conferir&id_orgao_acesso_externo=0, informando o código verificador **2305869** e o código CRC **BC5F9962**.

Este trabajo es dedicado,

En primera instancia a Dios, por orientarme en cada paso y decisión, por hacerme comprender su voluntad de seguir y construir este camino, por colmarme de sabiduría, de fortaleza y reconfortarme en momentos de incertidumbre.

A mi hermanito Miguel Ángel, quién partió de este mundo, por marcar dulcemente mi historia y la de mi familia, sé que desde cielo nos acompañas; seguirás siendo nuestro motivo de unión, amor y superación. Te recordaré cada día de mi vida.

A mis padres, Maria Isabel Rozo y José Miguel Parada, por su ejemplo de entrega y amor, por apoyarme en mis proyectos y comprender el motivo de mi ausencia durante estos años; por ser mi principal motivación para lograr nuevos y grandes objetivos. Para ellos mi esfuerzo, amor y gratitud.

A mi abuelita Ana Matilde, quién también partió durante este tiempo, gracias por todo tu cariño.

Diego Andrés Parada Rozo.

Acknowledgements

O autor desta tese expressa seus agradecimentos:

Ao meu orientador Cássio Gonçalves do Rego, pela amizade, confiança, motivação e apoio durante o doutorado, pela tranquilidade transmitida nos momentos mais críticos deste processo.

A mi coorientador Dinael Guevara Ibarra, por la amistad, colaboración e incentivo para continuar con mis estudios de posgrado.

A Diego Tami, por la amistad y el apoyo incondicional que me ha brindado desde el inicio de esta experiencia en Brasil.

A Olger Vargas, Luilly García y Marlon Lizarazo, por ser colegas y amigos de tantas batallas, gracias por los buenos momentos compartidos, ustedes son personas de calidad.

A mis amigos Fabián Martínez (Q.E.P.D), David Morales, Andreina Martínez, Lina Calderón, Juan David León, Fabián Rangel y Mateo Soler, gracias por estar siempre presentes a pesar de la distancia.

Ao Prof. Fernando Moreira, pelos ensinamentos e aulas impecáveis, ao Prof. Jhonattan Córdoba pelas discussões acadêmicas, e aos meus colegas e amigos do GAPTEM.

Aos meus colegas de trabalho e estudantes do Instituto Federal do Sul de Minas Gerais - Campus Inconfidentes, especialmente aos professores Thiago Zucarelli, Helder Caldas e Matheus Guedes pela amizade, convívio e bons momentos.

A Luis Eduardo Royero y al Centro Tecnológico de Cúcuta, por la oportunidad brindada de aplicar parte de mi investigación en los casos de estudio analizados en Cúcuta.

Ao PPGEE pela formação acadêmica e profissional dada neste doutorado.

Ao CNPq, pela bolsa de estudo.

"Imagination will often carry us to worlds that never were, but without it we go nowhere."

Carl Sagan

Resumo

O desenvolvimento de modelos de propagação para a precisa previsão de cobertura de ondas de rádio é um desafio para os pesquisadores. A maior dificuldade na construção desses modelos é a adequada caracterização das condições não homogêneas dos ambientes (variações atmosféricas, caracterização eletromagnética de superfícies, perfis irregulares de terreno, etc.), pois estas afetam a radiopropagação e produzem diversos fenômenos de espalhamento. Esta tese centra-se na exploração da técnica *Ray Tracing* (RT) e do algoritmo numérico *Split-Step Fourier Transform Parabolic Equation* (SSPE). A escolha desses métodos explica-se pelo fato de ambos serem algoritmos de modelagem de propagação eletromagnética rápidos, robustos e promissores para incluir a influência das condições não homogêneas dos ambientes em suas soluções. Esta pesquisa apresenta um algoritmo de radiopropagação baseado na técnica RT que combina um modelo multipercurso modificado para perfis de gradiente de refratividade constante e a Teoria Uniforme de Difração (UTD). Uma nova formulação é proposta para analisar a reflexão no solo das trajetórias dos raios em função da refratividade atmosférica. Paralelamente, o método *Discrete Mixed Fourier Transform* (DMFT) é incluído no algoritmo SSPE, tornando-se uma abordagem DMFT-SSPE para resolver problemas de radiopropagação com impedância de superfície como condição de contorno. Inicialmente, este trabalho avalia os algoritmos obtidos em casos canônicos e em um cenário misto, sob condições de gradiente de refratividade constante, perfis de terreno com perdas e usando bandas de frequências projetadas para aplicações 5G. Com base nos resultados obtidos, é possível afirmar que ambos os métodos têm um comportamento semelhante em todos os casos testados. Posteriormente, os dois modelos de propagação obtidos foram aplicados para prever a cobertura e caracterizar o canal de rádio em cenários suburbanos da região andina e da floresta do Pacífico, ambos na Colômbia. Nestes casos realísticos os resultados mostraram a similaridade das curvas de *pathloss* obtidas com ambas as abordagens. Portanto, os dois modelos de radiopropagação apresentados nesta tese são projetados como ferramentas úteis de previsão de cobertura em áreas remotas da geografia colombiana. Ao longo deste trabalho, o método DMFT-SSPE e uma proposta modificada de RT com efeito de refratividade atmosférica são apresentados como alternativas que garantem resultados razoáveis, demonstrando precisão e notável eficiência computacional para analisar a propagação de ondas de rádio.

Palavras-chave: Radiopropagação. Técnicas RT. Refratividade atmosférica. Modelo multipercurso. SSPE. DMFT. UTD.

Abstract

The development of propagation models for accurate radiowave coverage prediction is a challenge for researchers and radio engineers. The greatest difficulty in the construction of these models is the appropriated characterization of the factors that affect the radiowave propagation, such as the non-homogeneous conditions of realistic environments (atmospheric variations, electromagnetic characterization of surfaces, irregular terrain profiles, etc.), since they produce several scattering phenomena. This thesis focuses on the exploration of the Ray Tracing (RT) technique and the Split-Step Fourier Transform Parabolic Equation (SSPE) numerical algorithm. The choice of these methods can be explained by the fact that both are fast and robust electromagnetic propagation modeling algorithms, widely used, and promising to include within their solutions the influence of the different non-homogeneous environments conditions. This research presents a radiopropagation algorithm based on RT technique that combines a modified multipath model for constant refractivity gradient profiles and the Uniform Theory of Diffraction (UTD). A novel formulation is proposed for calculation and ground-reflection analysis of ray paths depending on atmospheric refractivity. In paralell, the Discrete Mixed Fourier Transform (DMFT) method is included into the SSPE algorithm, becoming a DMFT-SSPE approach to solve radio propagation problems over surfaces with impedance boundary conditions. This work proposes comparative studies with the purpose of validating the proposed formulation for modified RT, and evaluating the DMFT-SSPE implementation. Initially, the algorithms introduced herein were evaluated in canonical cases and a mixed scenario, under conditions of constant refractivity gradient, lossy terrain profiles and using the frequency bands projected for 5G applications. Taking into account the results obtained, it is possible to affirm that both methods have a similar behavior for all the cases tested. A remarkable case study was the application of the two algorithms in Colombian environments, which present challenging conditions for propagation modelling. The propagation models obtained were applied to predict coverage and temporarily characterize the radio channel in suburban scenarios of the Andean region and the Pacific forest, at 5G frequency bands. The results of this case study showed the similarity of the pathloss curves obtained with both approaches. Therefore, the two radiopropagation models presented in this thesis, are project as useful coverage prediction tools in remote areas of the Colombian geography. Throughout this work, the DMFT-SSPE method and a modified RT proposal with atmospheric refractivity effect, are presented as alternatives that guarantee reasonable results, demonstrating precision and remarkable computational efficiency to analyze radiowave propagation.

Keywords: EM propagation. RT tecniques. Atmospheric refractivity. Multipath model. SSPE. DMFT. UTD.

List of Figures

List of Tables

List of Symbols

$\mathbf{E}$	Electric field intensity
f	Frequency
k	Free-space wavenumber
M	Modified refractivity
m	Modified refractive index
N	Refractivity
n	Refraction index
u	Reduced auxiliary function
x	Range coordinate
z	Height coordinate
δ	Gradient of refractive index
Δx	Range increment
Δz	Height increment
ϵ	Permittivity or dielectric constant
ϵ_r	Relative permittivity
i	Unit imaginary number $\sqrt{-1}$
λ	Wave length
ψ	Scalar component of field
σ	Conductivity

List of abbreviations and acronyms

2D	Two-dimensional
3D	Three-dimensional
5G	Fifth-Generation
BC	Boundary Conditions
DMFT	Discrete Mixed Fourier Transform
DST	Discrete Sine Transform
EFIE	Electric Field Integral Equation
EM	Electromagnetic
FD	Finite Difference
FDTD	Finite Difference Time Domain
FEM	Finite Element Method
FFT	Fast Fourier Transform
GO	Geometrical Optics
MFT	Mixed Fourier Transform
mmWave	milimetre waves
MoM	Method of Moments
NAPE	Narrow Angle Parabolic Equation
PEC	Perfectly Electrical Conducting
PE	Parabolic Equation
PL	Pathloss
RL	Ray Launching
RT	Ray Tracing
SPE	Standard Parabolic Equation

SSFT	Split Step Fourier Transform
SSPE	Split Step Parabolic Equation
TEM	Transverse Electromagnetic
UHF	Ultra High Frequencies
UTD	Uniform Theory of Diffraction
VHF	Very High Frequencies
WAPE	Wide Angle Parabolic Equation

Contents

1 Introduction

This chapter presents a brief description of the main challenges in the current characterization of radio channels, and the need for researchers and engineers to obtain efficient and accurate radiowave propagation algorithms. The contextualization, objectives and contributions of this work are also exhibited. Finally, an outline of the text structure introduces the content of the following chapters.

1.1 Contextualization

The advancement and dramatic improvement of wireless communication technologies imply the need to develop accurate and robust coverage prediction models that guarantee lower computational cost and obtain fast results. The appropriated characterization of the factors that affect radiowave propagation, such as atmospheric variations, electromagnetic characterization of the surfaces and scenery elements (such as terrain profiles, obstacles, etc.), is a challenge for researchers and radio engineers (Ozgun et al., 2011). The precise characterization is a costly process, because such factors vary considerably depending on the analyzed environment and, therefore, constitutes great difficulties in the consolidation of a radiopropagation model (Apaydin; Sevgi, 2017).

Latest technologies of Fifth-Generation (5G) wireless networks are aimed to the meeting of the objectives of high-speed transmission and large increase in channel capacity (Rappaport et al., 2017; Navarro; Guevara; Gomez, 2015). It is awaited that 5G systems configure heterogeneous networks of overlapping cell, also composed of macrocells for wide coverage. Several sub-6 GHz frequencies are being tested for pioneering 5G services, specifically, 750 MHz, 2.5 GHz, 3.5 GHz and 5.4 GHz bands are proposed in Latin American countries to be used in 5G applications (Leonor et al., 2022). Within this framework, one of the main challenges of these technologies is to guarantee connectivity and to provide broadband services in rural and sub-urban areas. Thus, improved, quick and refined propagation models must be proposed to predict coverage and characterize the radio channel in this kind of scenarios, and at the mentioned frequency bands.

Lossy irregular terrains and atmospheric conditions produce several scattering phenomena in radiowave propagation. Radio waves from the Very High Frequency (VHF) range to the millimeter waves (mmWave), specifically in applications of 5G wireless networks, are affected by phenomena such as reflection, refraction and diffraction. The analysis of irregular terrains should consider that the portion of reflected and diffracted energy influences significantly the pathloss of the radiation, thus, the analysis of the problem becomes more complex (Ozgun et al., 2010). In addition, it is known that radiopropagation

can be strongly influenced by the non-uniform spatial distribution of the refractivity in the atmosphere (Valtr; Pechac, 2005b). This interaction can result in multipath fading events and interference effects, significantly affecting the performance of long-distance communications (Karimian et al., 2011; Wagner; Gerstoft; Rogers, 2016).

Refractivity variation is a relevant characteristic affecting the radio wavepropagation. Several refractive conditions, such as sub, super, normal, and duct, can be defined depending on the gradient value of the refractivity index (Wang et al., 2020; AbouAlmal et al., 2015; Dinc; Akan, 2015; Sirkova, 2011; Dinc; Akan, 2014; Bean; Thayer, 1959). The ducting conditions is the most significant influencing factor for long-distance radio interference. Although the ducts, in general, have a significant impact on the radar and communication systems operating in the microwave range, if the antennas are not in specific positions in the duct, then it would not be a major radio interference factor (Wang et al., 2020; Sirkova, 2011). For example, it has been reported that the pathloss is about 20-30 dB lower when the receiving antenna is located inside the duct in comparison to when it is located just outside of it (Yang et al., 2015).

With the increasing improvement of the computational systems, it was possible to use deterministic approaches to model the electromagnetic propagation. Many two-dimensional (2-D) space implementations can be found in the literature to solve radio-propagation problems, where Ray Tracing (RT) methods and numerical techniques, such as Parabolic Equation (PE) model, Finite Difference (FD), Method of Moments (MoM), Finite Element Method (FEM) and Finite-Difference Time-Domain (FDTD) method have been implemented in closed and open environments (Sevgi; Uluisik; Akleman, 2005; Janaswamy, 1994; Johnson et al., 1997; Akleman; Sevgi, 2007; Parker; Chuprin; Langley, 1999; Yun; Iskander; Zhang, 2004; Hviid et al., 1995). Among these, the solutions based on RT and PE algorithms are proposed to be the most attractive and effective (Apaydin; Sevgi, 2017).

This work focuses on the application of the optical RT technique and the Split-Step Fourier Transform PE numerical algorithm, which are analytical approximations to the wave equation, and generally, less demanding computationally methods (El Ahdab; Akleman, 2017). RT requires appropriate algorithms to estimate the multiple directions in the propagation environment (Sevgi, 2014), and it is based on the asymptotic solutions of Geometrical Optics (GO) and the Uniform Theory of Diffraction (UTD). GO determines incident and reflected fields and UTD solves the edge diffraction (Kouyoumjian; Pathak, 1974). PE method consists of splitting the wave equation into two paraxial terms and provides highly accurate results for radiowave propagation over irregular terrain and lossy surfaces in the observed region, which is determined through detailed characterization (Ozgun et al., 2011; Zhang et al., 2016). The choice of these methods can be explained by the fact that both are fast and robust electromagnetic propagation modeling algorithms,

widely used, and promising to include (or adapt) within their solutions the influence of the different non-homogeneous environments conditions. (Apaydin; Sevgi, 2017; Valtr; Pechac, 2005b).

In this context, it is necessary to comment that numerical techniques, like PE model, are convenient to estimate coverage, however, bandwidth wireless communications require an suitable channel characterization. In this sense, numerical techniques are not so intuitive when it comes to temporarily characterizing the radio channel, instead, RT algorithms are speculated to be the most attractive in such situation (Navarro; Guevara; Gómez, 2019).

Recently, many studies have shown the importance of GO method in the analysis of tropospheric propagation. In GO, the electromagnetic wave is represented by rays that form trajectories perpendicular to the wave front. Knowing the trajectory, is possible to define the amplitude and the phase, point to point. In this method, a large number of rays are emitted by the transmitter at different angles, to the positions of the points at which the rays reach the receivers (Valtr; Pechac, 2006).

On a terrestrial radio link, a single path between the transmitter and receiver is seldom the only physical means for propagation. Possibly, a direct ray and a ground-reflected ray arrive at a certain point. In this conditions, RT formulation to predict the direct ray paths under a refractivity gradient is, in the most cases, inaccurate when used alone. To consider refractive properties of the atmosphere, Valtr and Pechach introduced a RT formulation for the analytical description of ray paths under a constant refractivity gradient along the height (i.e., the variation of the refractive index value only depends on the height) (Valtr; Pechac, 2005b; Valtr; Pechac, 2006). A previous work by these same authors described an analytical RT approach for a horizontally variable refractivity height profile (Valtr; Pechac, 2005a). Nevertheless, the applicability of these models is limited to cases of line-of-sight between transmitter and receiver, and to cases where the terrain influence is not significant. These works focused on solutions and results for direct ray paths considering atmospheric refractive, and to the best knowledge of the author of this research, ray paths solutions associated with other propagation mechanisms have not been published.

The current numerical strategy reduces the 3D problem into 2D distance-height scenarios (Apaydin; Sevgi, 2017). For this purpose, PE algorithms are the most attractive, since the others techniques require high processing resources. PE model is an approximation of the wave equation which models energy propagating in a cone centered on a preferred direction, the paraxial direction (Levy, 2000) . It was introduced by Leontovich and Fock to study the problem of diffraction of radio waves around the earth (Lentovich; Fock, 1946). Two numerical techniques may be used to solve the PE: Split-Step Fourier Transform (SSFT) method (Tappert, 1977) and Crank–Nikolson FD scheme (Levy, 2000;

Valtr; Pechac, 2005b). The numerical solution based on SSFT algorithm is used in this work.

The application of SSFT method for solving numerically PE model is known as Split-Step Parabolic Equation (SSPE) method, it consists in determining a vertical field profile, which is calculated step by step. The main advantage of the SSPE approach is the possibility to use of larger range increments. Therefore, it is a faster solution for long-distance propagation scenarios (Barrios, 1994), with high-performance. The disadvantage of the method, however, is the laborious accounting of boundary conditions (Lytaev, 2018).

A remarkable advance in SSPE technique was the introduction of the Discrete mixed Fourier transform (DMFT) (Kuttler; Dockery, 1991; Dockery; Kuttler, 1996; Kuttler; Janaswamy, 2002). This allowed the extension of the split-step method from propagation over only smooth perfectly conducting surfaces to surfaces satisfying impedance boundary conditions, and in this way, the application of the split-step approach has also been extended to general terrain problems (Donohue; Kuttler, 2000). The algorithms used to implement the DMFT have been improved in the years since its introduction to make it faster and more robust (Dockery; Kuttler, 1996). However, certain combinations of parameters can occasionally cause numerical instabilities in the method (Kuttler; Janaswamy, 2002). This research uses the DMFT approach of the SSPE numerical solution (referred to as DMFT-SSPE throughout this work) and implements algorithms proposed in the literature to avoid the occurrence of these numerical instabilities.

1.2 Objectives and contributions

This work aims to obtain radiopropagation algorithms, based on RT techniques and PE numerical solutions, that guarantee fast and accurate solutions when applied in long-distance scenarios considering non-homogeneous media. In addition, the obtained propagation models must demonstrate their ability to be used at 5G frequency bands.

Hence, founded on the general objective, the specific objectives of this research are defined:

- Provide analytical descriptions of ray paths for different conditions of atmospheric refraction.
- Propose a modified multipath model with atmospheric refractivity effect and UTD.
- Obtain a numerically stable radio propagation algorithm based on the DMFT-SSPE method.
- Simulate and evaluate the obtained algorithms in radiopropagation problems involving realistic scenarios and 5G frequencies.

In Section 1.1, it was reported that analytical solutions of ray paths under refractivity effect have not been published for propagation mechanisms other than the direct ray paths. Therefore, with the objective of developing a RT technique to estimate coverage and characterize the radio channel in more realistic scenarios (considering atmospheric refractivity and terrain influence), this research proposes to complement the analytical RT approach presented in (Valtr; Pechac, 2005b; Valtr; Pechac, 2006; Valtr; Pechac, 2005a). In this work, it is deduced a formulation to incorporate ground-reflection analysis, on both flat and sloping terrain. Furthermore, UTD principles are employed for the inclusion of terrain diffraction. This means that the RT algorithm, proposed in this doctoral thesis, predicts multipath components for the launched rays from a transmitter to a receiver point through the processing of specular reflections, diffractions, free space attenuation, and multiple combinations of those effects. In such a way that the main contribution is to obtain an algorithm based on a RT technique that combines a modified multipath model with atmospheric refractivity effect and UTD.

This research assumes an academic challenge when it decides to novelly obtain a complete multipath model that considers the atmospheric refractivity effect in RT techniques from the calculation of ray paths. This implies deduction of new formulation and combination with UTD principles. The purpose is to offer a more complete solution with respect to other approaches, such as the spherical Earth model, which deform space or approximate terrain profiles. Therefore, a properly deterministic approach is proposed.

The computational implementation of a numerically stable radiopropagation algorithm based on the DMFT-SSPE method is another of the results obtained in this work. This radiopropagation tool contributes as a benchmark and consolidated coverage prediction algorithm to compare and validate the results obtained with other propagation models that are currently implemented in the works of the research group of antennas, propagation and electromagnetic theory (GAPTEM by its acronym in Portuguese).

1.3 Thesis Organization

This thesis is organized as follows. Chapter 2 presents the PE model. Mathematical formulation and implementation details of the SSPE numerical algorithm, are described. The DMFT approach is explained in order to include lossy ground surfaces within the solution. The canonical tests are proposed to validate the SSPE and DMFT implementations, and demonstrate their computational efficiency when compared to the FD numerical solution.

Chapter 3 provides the theoretical foundations of Optical RT method and presents a radiopropagation algorithm based on a RT technique that combines a modified multipath model with atmospheric refractivity effect and UTD. A novel formulation is proposed

for calculation and ground-reflection analysis of ray paths depending on atmospheric refractivity. The algorithm introduced is evaluated in a canonical tests under conditions of constant refractivity gradient. Pathloss results are obtained and compared with Parabolic Equation (PE) numerical solution results.

In Chapter 4, Modified RT and DMFT-SSPE radiopropagation techniques are applied in Colombian environments in order to predict radio coverage in environments that demand radiopropagation modeling challenges. The two tested algorithms offer the possibility to include most of the non-homogeneous conditions of the environments. In order to demonstrate its applicability, two realistic case studies are carried out: the first, in a mountainous terrain in the Andean region, and the second, in a tropical rain forest in the Pacific region. The tests use frequencies of 2.0 GHz, 3.6 GHz and 580 MHz, respectively, and the simulation results show the similarity of the pathloss curves obtained with both approaches.

In Chapter 5, it is developed a novel radiopropagation multipath technique for Horizontally Variable Refractivity for long-range communications. Thus, a formulation is deduced for ground-reflection analysis, which considers the horizontally stratified variation of the refractivity gradient over flat terrain.

Finally, Chapter 6 summarizes the conclusions of this research, and presents the proposal for continuity on activities that can be developed as future works.

2 Fourier Split-Step Methods for solving the Parabolic Equation Model

The PE model and the SSPE numerical solution are presented in the first part of this chapter. Next, the DMFT method is described as a complement of the SSPE approach to include lossy ground surfaces in radiopropagation problems. Finally, some canonical tests are proposed.

2.1 Parabolic equation model (PE model)

The literature has proposed two types of problems to study radiopropagation problems numerically (Boan, 2009). Scattering algorithms seek, generally, a solution of Maxwell's equations or a derivate, for instance, the Electric Field Integral Equation (EFIE) approach. The implementation of these algorithms address the solution EM fields of small or medium size structures, with respect to wavelength. Propagation algorithms are a second type of problem, which are more interested in longer propagation analysis. In order to achieve an efficient solution over long distances, these algorithms use an approximation to Maxwell's equations. Recently, propagation algorithms based on PE methods are the more attractive (Apaydin; Sevgi, 2017).

PE model was first applied to the underwater acoustic propagation modeling by Leontovich and Fock in the 1940s (Tappert, 1977). Later, it was aimed by the same authors to solve the problem of vertical stratification in tropospheric atmospheric propagation and thus proposed the PE, a forward full-wave analysis method. (Lentovich; Fock, 1946). Two numerical methods may be used to solve the PE: FD techniques and SSFT algorithm (Levy, 2000). The application of SSFT to solve the PE model is known as SSPE method, this numerical solution provides the use of larger range increments and a faster solution for long-range propagation scenarios (Barrios, 1994). PE approach becomes famous after the introduction of the Fourier SSPE algorithm, and since then, has been improved and applied to a variety of complex radiopropagation problems (Tappert, 1977).

Throughout the work, the suppressed time-dependence is assumed to be e^{-iwt}, where w and t are the angular frequency and time, respectively, and i represents the unit imaginary number ($i = \sqrt{-1}$). In order to obtain the Standard Parabolic Equation (SPE), the two-dimensional Helmholtz's equation is used (Ozgun et al., 2011):

$$\frac{\partial^2 \psi}{\partial x^2} + \frac{\partial^2 \psi}{\partial z^2} + k^2 n^2 \psi \;=\; 0 \;, \tag{2.1}$$

where $k = 2\pi/\lambda$ represents the free-space wavenumber, n is the refractive index and ψ

denotes the electric or magnetic field in horizontal or vertical polarization, respectively. In equation (2.1) x and z represent, respectively, range and altitude coordinates. In the direction x (*paraxial direction*) is employed a reduced auxiliary function $u(x,z) = e^{-ikx}\psi(x,z)$ (Levy, 2000). Then, (2.1) is rewritten in terms of $u(x,z)$:

$$\left[\frac{\partial^2}{\partial x^2} + 2ik\frac{\partial}{\partial x} + \frac{\partial^2}{\partial z^2} + k^2(n^2-1)\right] u(x,z) \;=\; 0. \tag{2.2}$$

Equation (2.2) may be divided into two equations for computing the forward and backward propagation waves, as follows:

$$\frac{\partial u}{\partial x} = \begin{cases} -ik(1-Q)u & \text{for forward,} \\ \\ -ik(1+Q)u & \text{for backward,} \end{cases} \tag{2.3}$$

where,

$$Q = \sqrt{1+q} \quad \text{and} \quad q = \frac{1}{k^2}\frac{\partial^2}{\partial x^2} + (n^2-1). \tag{2.4}$$

The formal solution of the forward propagation in equation (2.3) is given by:

$$u(x+\Delta x, z) = e^{-ik\Delta x(1-Q)}u(x,z). \tag{2.5}$$

Backward propagating is omitted in the SPE. The operator Q is approximated by using the first-order Taylor expansion (i.e. $\sqrt{1+q} \approx 1 + q/2$). Therefore, we obtain the SPE for forward propagation:

$$\left[\frac{\partial^2}{\partial z^2} + 2ik\frac{\partial}{\partial x} + k^2(n^2-1)\right] u(x,z) \;=\; 0. \tag{2.6}$$

The accuracy of the SPE is limited to propagation angles less than 10°-15°. Hence, the SPE is known as the *Narrow Angle Parabolic Equation* (NAPE) approximation to the wave propagation (Apaydin; Sevgi, 2017). As the propagation angles encountered in long-range propagation problems are usually less than a few degrees, the accuracy of the SPE is adequate for numerical modeling (Ozgun et al., 2011). Nevertheless short-range propagation or situations that present strong multipath effects involve large propagation angles and, therefore, a more accurate expansion of the operator Q must be made. Thus, the *Wide Angle Parabolic Equation* (WAPE) approach is written as follows:

$$\frac{\partial u(x,z)}{\partial x} - \left[ik^{-1}\left(\sqrt{1+\frac{1}{k^2}\frac{\partial^2}{\partial z^2}}+1\right)^{-1} + ik(n-1)\right] u(x,z) = 0. \tag{2.7}$$

2.2 Split-step parabolic equation (SSPE)

The numerical solution of the PE is reached by the SSFT method, which is a widely-used and robust algorithm. Generally, SSPE method is an initial-value problem starting

from a reference range, and marching out in range by obtaining the field along the vertical direction at each range step, through the use of step-by-step Fourier transformations (Kuttler; Dockery, 1991; Levy, 2000).The split-step solution of the NAPE equation in (2.6) is given by:

$$u(x+\Delta x, z) \;=\; e^{[ik(n^2-1)\frac{\Delta x}{2}]} F^{-1}\left\{ e^{(-ip^2\frac{\Delta x}{2k})} F\{u(x,z)\}\right\}, \tag{2.8}$$

and, the solution of the WAPE equation in (2.7) is determined by:

$$u(x+\Delta x, z) \;=\; e^{[ik(n-1)\frac{\Delta x}{2}]} F^{-1}\left\{ e^{[-\frac{ip^2\Delta x}{k}(\sqrt{1-(\frac{p}{k})^2}+1)^{-1}]} F\{u(x,z)\}\right\}. \tag{2.9}$$

In the equations (2.8) and (2.9), F and F^{-1} denote the fast Fourier transform and the inverse fast Fourier transform, respectively. Also in (2.8), $p = k\sin\theta$, where θ is the propagation angle from the horizontal.

In order to apply SSPE algorithm, an initial vertical field profile is calculated at a reference range or initial distance (x_0). The solution marches in range using equations (2.8) and (2.9), in a way such that it obtains the vertical profile at a given range by using the field at the previous range, and with appropriate boundary conditions at the top and bottom boundaries of the domain (Sekmen, 2014). The initial vertical field profile at the reference range position (i.e. $x = x_0$) must be properly determined in accordance with the parameters of the antenna pattern being modeled (Sevgi; Uluisik; Akleman, 2005). Figure 1 depicts an idea or outline about the method's approach.

In SSPE, two computational domains are defined, as shown in Figure 2. A first region (Region 1), from $x = 0$ to $x = x_0$, is known as *analytical-domain* and, a second region (Region 2), from $x = x_0$ to $x = x_{max}$, is defined as the *numerical-domain*, which is, specifically, resolved through SSPE algorithm.

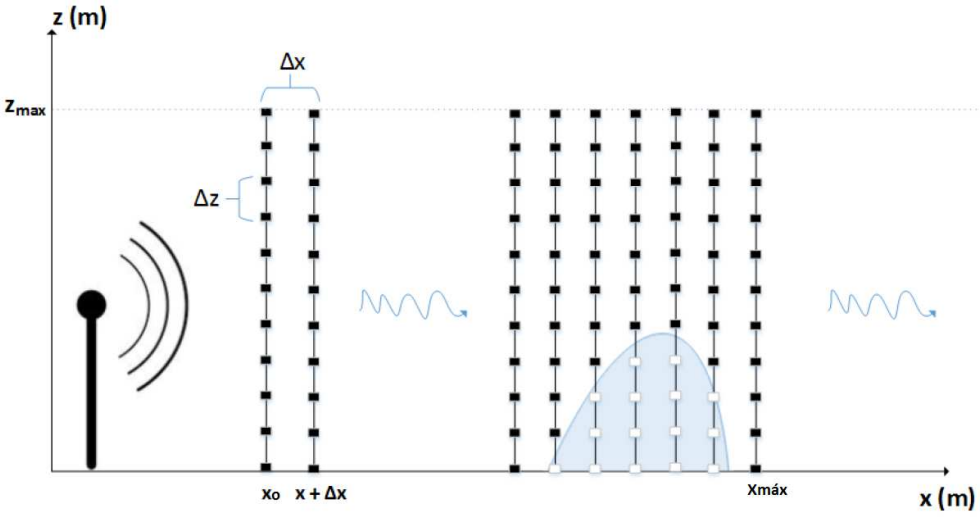

Figure 1 – SSPE approach (Sekmen, 2014).

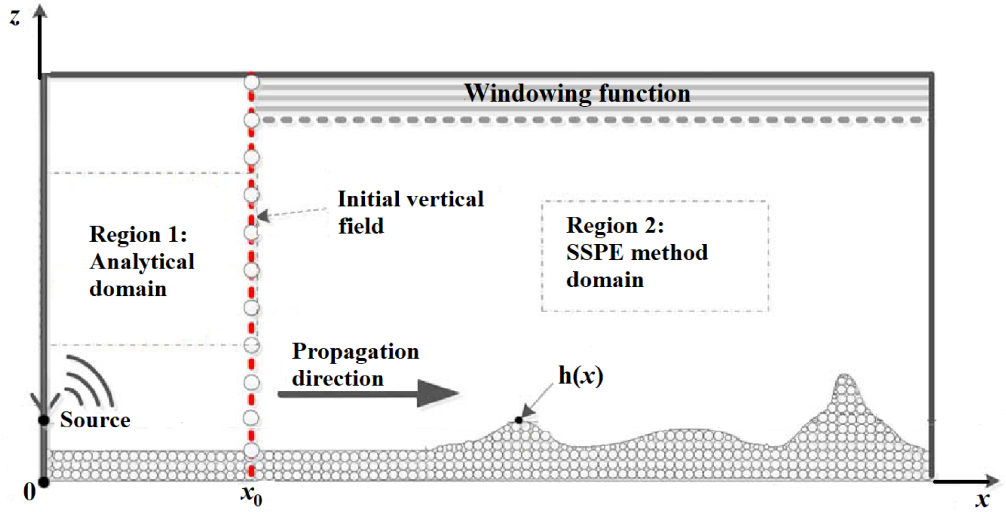

Figure 2 – Computational domains in SSPE algorithm (Wang et al., 2015).

2.2.1 Boundary conditions

In order to apply appropriately the SSPE method, boundary conditions must be imposed on the upper and lower terminations of the computational numerical domain. The propagation problem involves a vertically open region, and therefore, radio wave propagation within limited height must satisfy the Sommerfeld radiation condition, i.e. $u(x,z)|_{z\to\infty} = 0$, which means radio waves are completely absorbed in when arriving the top boundary and non-physical reflections, from the upper boundary, don't arrive towards the computational domain (Zhang et al., 2014). Since the field is truncated abruptly along z, in order to avoid strong reflections above the computational region, which affect the numerical results, it is required to handle the field within the top boundary to be slowly reduced to zero (Valtr, 2017). This can be reached by using absorbing regions or by applying windowing functions (such as Tukey window, Hanning window, Hamming window) or by setting an imaginary part to the refractive index to cause attenuation of radio wave. In this work, a Hanning window is implemented and computed by (Zhang et al., 2014):

$$J(z) = \frac{1 + \cos\left(\frac{\pi z}{H}\right)}{2}, \tag{2.10}$$

where H is the total width of the absorbing layer. Mathematically, this windowing function guarantees that $J(0) = 1$ and $J(H) = 0$.

The comparison between use and non-use of a windowing function in SSPE algorithm is shown in Figure 3. Artificial reflections generated by not using the Hanning Window can be seen in Figure 3a. This figure shows the unwanted effects that cause non-physical reflections within the numerical solution. Figure 3b shows the attenuation of the field in the second half of the vertical domain, due to the appropriate use of the absorbing layer.

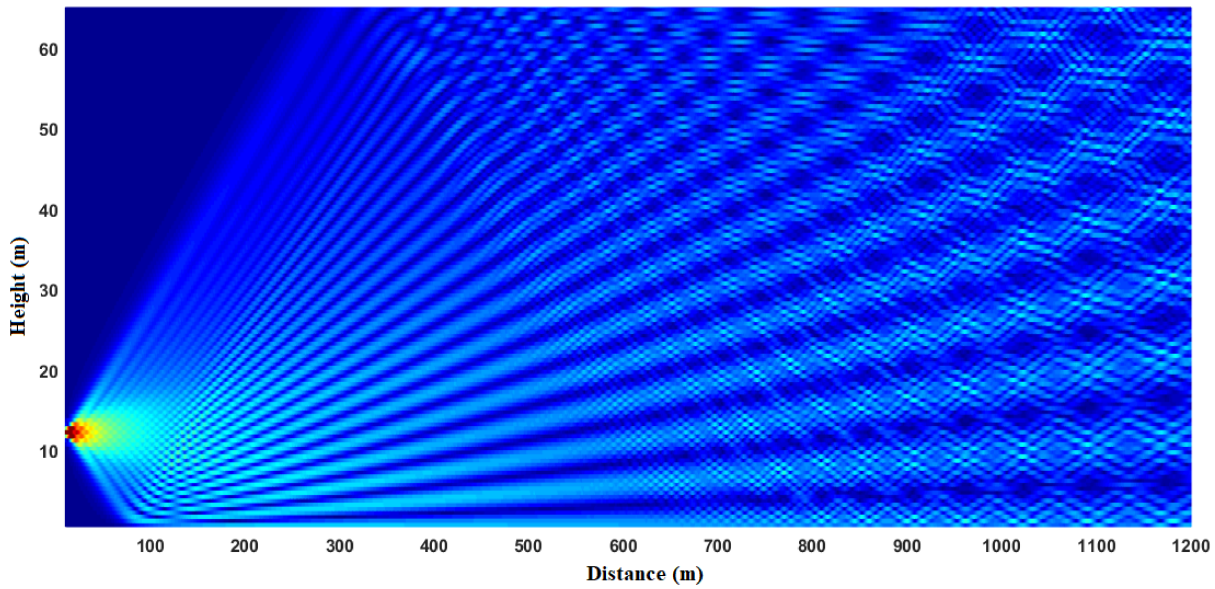

(a)

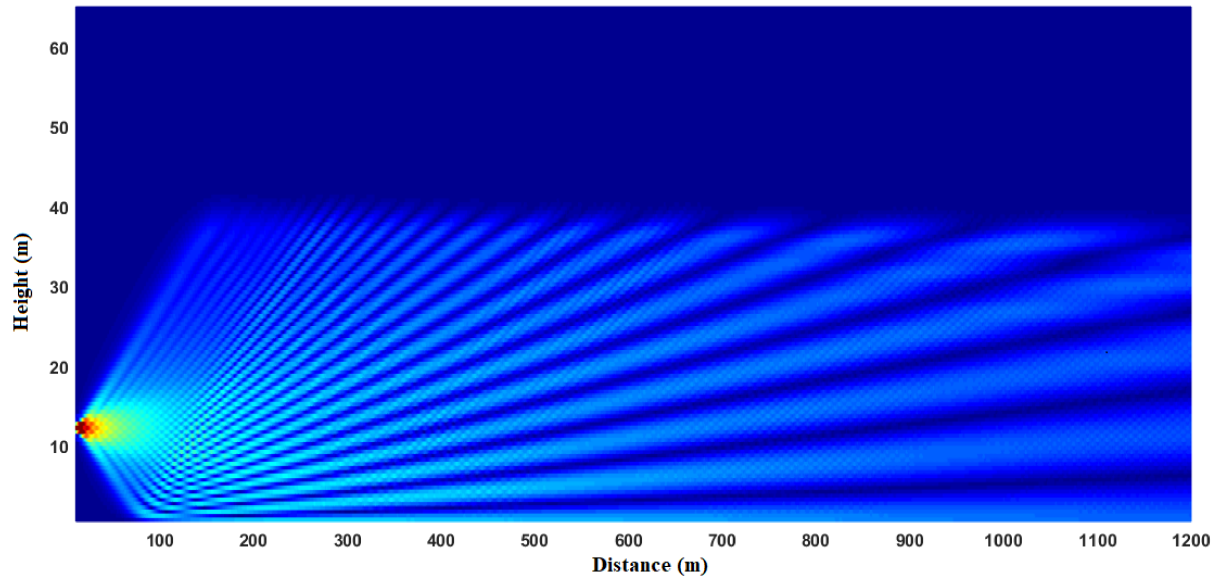

(b)

Figure 3 – Comparison between use and non-use of a windowing function: (a) SSPE without applying Hanning window and (b) SSPE applying Hanning window.

The boundary condition (BC) is also imposed to estimate the loss of interaction between the propagating EM waves and the terrains. Hence, the transverse BC that must be satisfied over the ground surface is expressed as (Ozgun et al., 2011):

$$\left[\alpha_1 \frac{\partial}{\partial z} + \alpha_2\right] u(x, z) = 0, \tag{2.11}$$

where, α_1 and α_2 are constants. For the PEC surface ($\sigma \to \infty$), where $\alpha_1 = 0$ and $\alpha_2 = 0$ make reference to Dirichlet (horizontal polarization) and Neumann (vertical polarization) BCs, respectively. For lossy ground, an impedance BC or the Cauchy-type BC is introduced via $\alpha_1 = 1$, $\alpha_2 = ik\sqrt{\epsilon - 1}$ and $\alpha_1 = 1$, $\alpha_2 = ik\sqrt{\epsilon - 1}/\epsilon$ for horizontal and vertical polarization, respectively. Here, $\epsilon = \epsilon_r + i60\sigma\lambda$ is the complex relative dielectric constant in terms of relative permittivity (ϵ_r) and conductivity (σ) of the lossy ground surface (Wait, 1990). The standard SSPE method cannot handle the BCs automatically, therefore, the lossy ground can be incorporated through the use of mixed Fourier transform (MFT) (Kuttler; Dockery, 1991). Figure 4 shows a general idea of how the SSPE algorithm interacts with the imposed boundary conditions on the top and bottom of the computational domain.

2.2.2 Discretization criterion

SSPE sequentially operates between z and p domains in a consecutive manner, which are the Fourier transform pairs (Apaydin; Sevgi, 2017). The domains are truncated

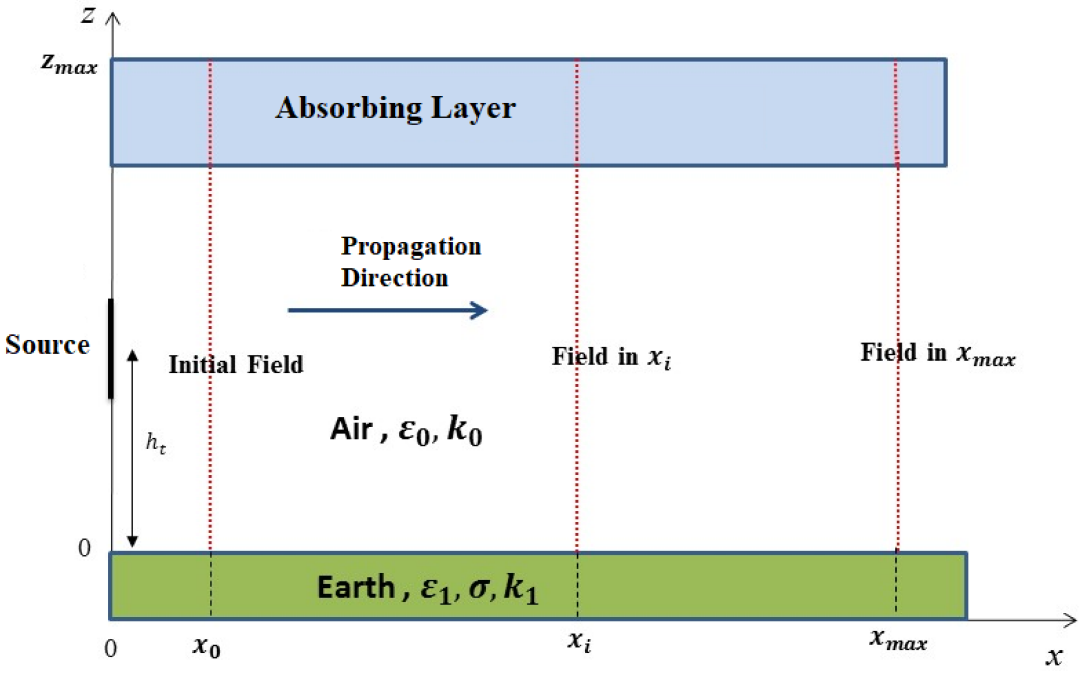

Figure 4 – SSPE algorithm and boundary conditions.

at $z_{\max}$ and $p_{\max}$. Once $z_{\max}$ is decided, $p_{\max}$ is obtained from the Nyquist criterion $z_{\max} \times p_{\max} = \pi N$ where N is the Fourier transform size. Note that $p_{\max} = k \sin\theta_{\max}$, where $\theta_{\max}$ is the maximum allowable propagation angle. Since $\Delta z = z_{\max}/N$, the altitude increment should satisfy $\Delta z \leq \lambda/(2\sin\theta_{\max})$ (Ozgun et al., 2010). The selection of the range increment (Δx) can be much larger than the wavelength. In SSPE implementation, the value of Δx can be up to 900 m and 270 m for lower and higher frequencies, respectively (Barrios, 1992; Valtr; Pechac, 2005b).

2.2.3 Atmospheric effects

As expressed in equations (2.8) and (2.9), the term n (refractive index) in the split-step solution of SPE allows the inclusion of atmospheric effects into numerical algorithm, by setting a refractivity profile. In most cases, n is a function of height z only, i.e. $n(z)$, which means that in each step the vertical field profile propagated by the SSPE method encounters a corresponding refractivity profile. In Chapter 3, the basic concepts of atmospheric refractivity are explained. Furthermore, Figures 13, 21 and 22 illustrated the ability of SSPE to include the effects of atmospheric refractivity in the analysis of radiopropagation problems.

2.2.4 Terrain modeling

Although the backward-propagating waves influence is ignored, terrain factors are an important source of diffraction and multipath effects. Implementation details of SSPE presented in the book by Levy (Levy, 2000) explain two ways to model irregular terrain profiles: staircase terrain modeling and terrain aproximation as a sequence of piecewise linear function. This work implements the first alternative. In this approach, on each segment of the constant altitude, the vertical field profile is calculated in the usual way, applying the desired boundary conditions on the ground surface, and then, is simply set to zero on the vertical terrain facets (Ozgun et al., 2011). Figure 5 shows the approximation of a realistic irregular terrain by using the staircase modeling. The realistic terrain profile is presented in Figure 5a and the terrain approximation is depicted in Figure 5b.

2.2.5 Calculation of path loss (PL)

The calculation assumes propagation in 2D (x and z axis only), therefore, the solution corresponds to cylindrical propagation wave (Valtr, 2017). After calculating the field inside the entire computational domain, the path loss, which is the ratio between the power radiated by the transmitter antenna and the power available at a point in space. In the canonical cases presented in this work, it is assumed zero gain transmitting and

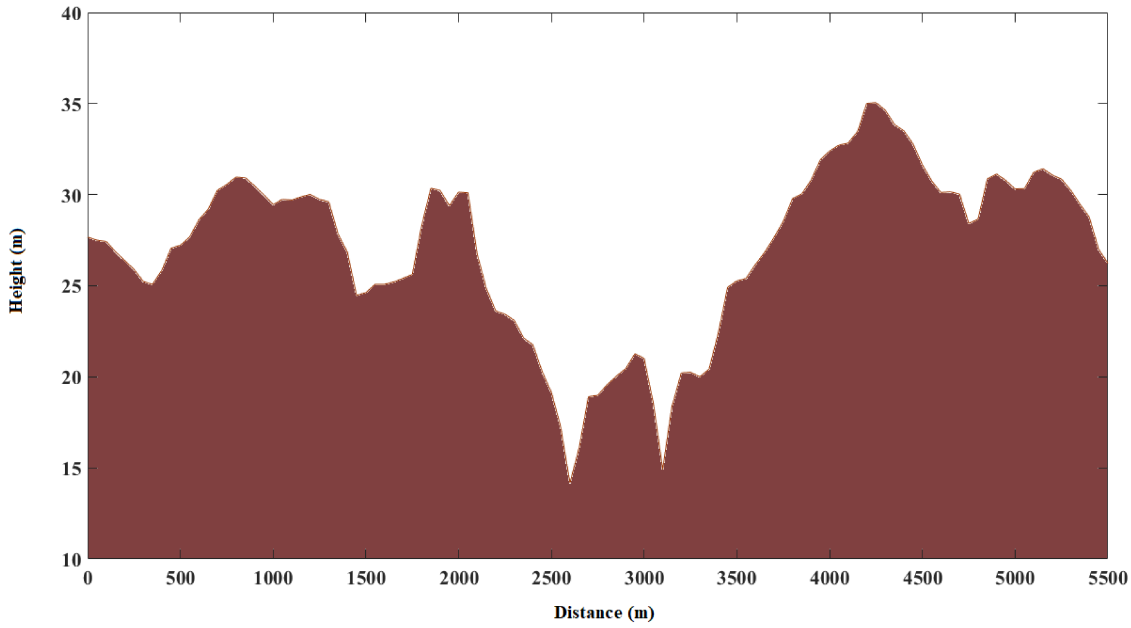

(a)

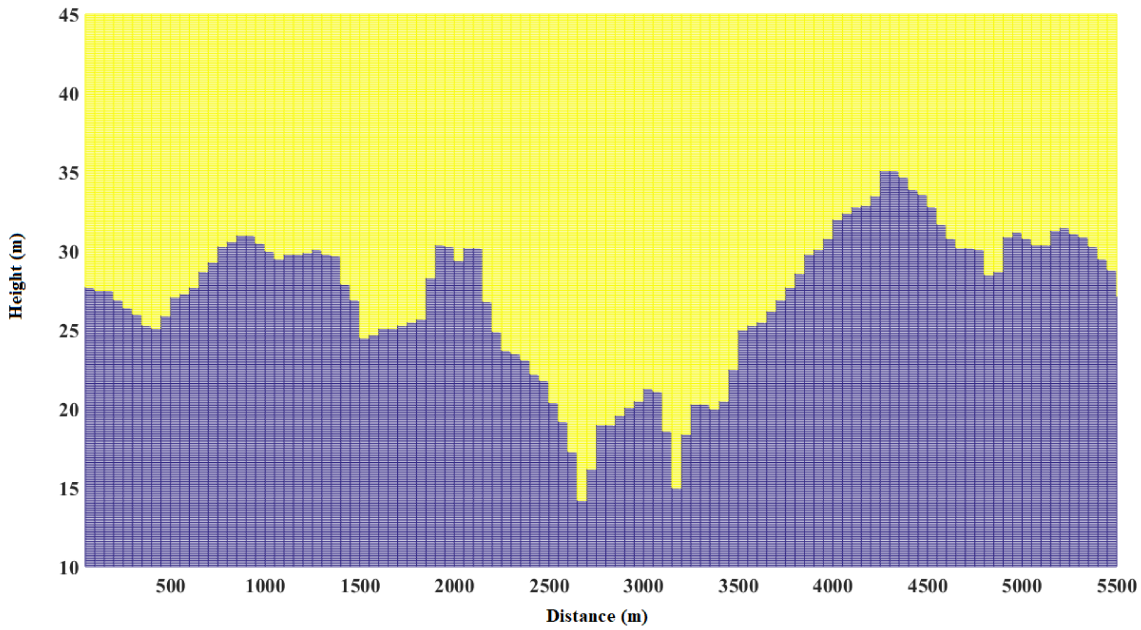

(b)

Figure 5 – Irregular terrain profile (a) Realistic terrain profile and (b) Staircase terrain modeling.

receiving antenna and unitary transmitted power. Thus, PL can be computed by:

$$PL(x,z) = 20\log_{10}\left(\left|\frac{\lambda}{4\pi}\frac{1}{\sqrt{x}}u(x,z)\right|\right). \tag{2.12}$$

2.3 DMFT method

The MFT was introduced into SSPE solution as a rigorous method to include a surface impedance in radio propagation problems (Kuttler; Dockery, 1991). Later, Dockery and Kuttler in (Dockery; Kuttler, 1996) proposed the DMFT algorithm in the SSPE approach.

2.3.1 Mixed Fourier Transform (MFT)

The MFT is given by:

$$F(p) = \int_0^\infty f(z)\left[\alpha\sin(pz) - p\cos(pz)\right]dz \tag{2.13}$$

for the forward (or direct) transform and,

$$f(z) = Ke^{-\alpha z} + \frac{2}{\pi}\int_0^\infty F(p)\frac{\alpha\sin(pz) - p\cos(pz)}{\alpha^2+p^2}dz \tag{2.14}$$

where,

$$K = \begin{cases} 2\alpha\int_0^\infty f(z)e^{-\alpha z}dz, & \mathrm{Re}(\alpha) > 0 \\ \\ 0, & \mathrm{Re}(\alpha) \leq 0 \end{cases} \tag{2.15}$$

for the inverse transform. In radio frequency propagation, generally, $\mathrm{Re}(\alpha) > 0$ for vertical polarization and $\mathrm{Re}(\alpha) < 0$ for horizontal polarization (Kuttler; Janaswamy, 2002).

The MFT split-step solution is determined by:

$$\begin{aligned} u(x+\Delta x,z) = e^{ik(n^2-1)\frac{\Delta x}{2}}\left\{\frac{2}{\pi}\mathcal{F}_s\left[\frac{\alpha}{\alpha^2+p^2}e^{i\Delta x(\sqrt{k^2-p^2}-k)}U(x,p)\right]\right. \\ \left.-\frac{2}{\pi}\mathcal{F}_c\left[\frac{\alpha}{\alpha^2+p^2}e^{i\Delta x(\sqrt{k^2-p^2}-k)}U(x,p)\right] + e^{i\Delta x(\sqrt{k^2-\alpha^2}-k)}e^{-\alpha z}K(x)\right. \end{aligned} \tag{2.16}$$

with

$$U(x,p) = \alpha\mathcal{F}_s\left[e^{ik(n^2-1)\frac{\Delta x}{2}}u(x,z)\right] - p\mathcal{F}_c\left[e^{ik(n^2-1)\frac{\Delta x}{2}}u(x,z)\right] \tag{2.17}$$

and, the sine and cosine transforms are defined as follows:

$$\mathcal{F}_s\left|f(x,z)\right| \equiv \int_0^\infty f(x,z)\sin(pz)dz \tag{2.18}$$

$$\mathcal{F}_c\left|f(x,z)\right| \equiv \int_0^\infty f(x,z)\cos(pz)dz \tag{2.19}$$

For certain values of α some numerical problems can arise. In particular, if the real part of α is very small and the imaginary part is less than p_{max}, then α^2+p^2 approaches zero in the denominator of (2.16) for some value of p. Analytically, there is no singularity at this point, but it is often necessary to decrease the numerical mesh spacing, i.e., increase the transform size beyond what would otherwise be required to accurately represent these expressions. In addition to this behavior, implementation of the MFT requires approximately twice the computations that are required to solve a PEC propagation problem. These characteristics provided the motivation to develop the discrete approach. For convenience, equations (2.16) and (2.17) will be referred to as the "continuous MFT split-step" algorithm, while what follows will be called the "discrete MFT split-step" (DMFT) solution (Dockery; Kuttler, 1996).

2.3.2 The Discrete MFT (DMFT)

The DMFT is the discrete approach of the MFT, and is applied to the field auxiliary function $u(x, m\Delta z)$, which is vertically discretized to $m = 0, 1, 2, ..., N$. The appropriated discretization of equation (2.13) is (Dockery; Kuttler, 1996):

$$U(x, l\Delta p) \equiv \sum_{m=0}^{N}{}' u(x, m\Delta z) \left[\alpha \sin\left(\frac{\pi lm}{N}\right) - \frac{\sin\left(\frac{\pi l}{N}\right)}{\Delta z} \cos\left(\frac{\pi lm}{N}\right)\right], \tag{2.20}$$

Δp is the step size to satisfy $\Delta p \Delta z = \pi/N$. The prime on the summation indicates that in (2.20) a weighted factor of 0.5 is used, for the first and last terms (i.e. $m = 0$, $m = N$).

The following quantities are needed to complete the definition of the transform:

$$C_1 = D \sum_{m=0}^{N}{}' u(x, m\Delta z) r^m \quad \text{and} \quad C_2 = D \sum_{m=0}^{N}{}' u[x, (N-m)\Delta z](-r)^m \tag{2.21}$$

where,

$$D = \frac{2(1-r^2)}{(1+r^2)(1-r^{2N})} \tag{2.22}$$

and r, $-r^{-1}$ are the roots of the quadratic equation:

$$r^2 + 2r\alpha\Delta z - 1 = 0. \tag{2.23}$$

for vertical polarization, the desired root is:

$$r = \sqrt{1 + (\alpha\Delta z)^2} - \alpha\Delta z \tag{2.24}$$

and, for horizontal polarization:

$$r = -\sqrt{1 + (\alpha\Delta z)^2} - \alpha\Delta z. \tag{2.25}$$

Thus, DMFT associates the $N+1$ numbers $u(x, m\Delta z)$, $m = 0, 1, 2, ..., N$ with the $N+1$ numbers $F(x, l\Delta p)$, $l = 1, 2, ..., N-1$ plus C_1 and C_2. Note that C_1 and C_2 correspond to $U(x, 0)$ and $U(x, N\Delta p)$, respectively.

The inverse DMFT which recovers u is given by:

$$u(x, m\Delta z) = \frac{2}{N}{\sum_{l=0}^{N}}' U(x, l\Delta p)\frac{\alpha \sin\left(\frac{\pi lm}{N}\right) - \frac{\sin\left(\frac{\pi l}{N}\right)}{\Delta z}\cos\left(\frac{\pi lm}{N}\right)}{\alpha^2 + \left[\frac{\sin\left(\frac{\pi l}{N}\right)}{\Delta z}\right]^2} + C_1 r^m + C_2(-r)^{N-m} \tag{2.26}$$

A method for implementing the DMFT using only sine transforms is presented in (Kuttler; Janaswamy, 2002). Begin by defining a new function:

$$w(x, m\Delta z) \equiv \frac{u\left[x, (m+1)\Delta z\right] - u\left[x, (m-1)\Delta z\right]}{2\Delta z} + \alpha u(x, m\Delta z) \tag{2.27}$$

for $m = 1, ..., N-1$. Then, the DMFT of u is exactly the discrete sine transform (DST) of w:

$$W(x, l\Delta p) = \sum_{m=1}^{N-1} w(x, m\Delta z)\sin\left(\frac{\pi lm}{N}\right) \tag{2.28}$$

w is recovered from W via the inverse DST:

$$w(x, m\Delta z) = \frac{2}{N}\sum_{l=1}^{N-1} W(x, l\Delta p)\sin\left(\frac{\pi lm}{N}\right) \tag{2.29}$$

and u is calculated by solving the difference equation (2.27) together with (2.22).

As with ordinary differential equations, the solution is a combination of a particular solution u_p of the in-homogeneous equation and an appropriate linear combination of the general solutions to the homogeneous equation:

$$u(x, m\Delta z) = u_p(x, m) + Ar^m + B(-r)^{(N-m)}. \tag{2.30}$$

Finally, the particular solution u_p is found by factoring the difference equation (2.27) into upper and lower triangular terms and using the recursions:

$$y(x, m) - ry(x, m-1) = 2\Delta z w(x, m\Delta z) \tag{2.31}$$

for $m = 1, ..., N-1$, where y(0) is arbitrary, and (back-solving),

$$u_p(x, m+1) + \frac{1}{r}u_p(x, m) = y(x, m) \tag{2.32}$$

for $m = 0, ..., N-1$ where $u_p(x, N)$ is arbitrary. Direct substitution verifies that these are equivalent to equation (2.27). The coefficients A and B are:

$$A = C_1 - D{\sum_{m=0}^{N}}' u_p(x, m)r^m \tag{2.33}$$

$$B = C_2 - D{\sum_{m=0}^{N}}' u_p(x, N-m)(-r)^m. \tag{2.34}$$

2.3.3 An improved DMFT for SSPE numerical solution

In 1996, Dockery and Kuttler proposed a step-by-step procedure to use the DMFT in the SSPE solution. Beginning with the solution from the previous range step $u(x, m\Delta z)$, perform the following (Dockery; Kuttler, 1996; Levy, 2000):

1. multiply by the first half of split z-space operator

$$v(x, m\Delta z) = u(x, m\Delta z) \cdot \exp\left[ik(n^2 - 1)\frac{\Delta x}{2}\right], \tag{2.35}$$

for NAPE solution, and

$$v(x, m\Delta z) = u(x, m\Delta z) \cdot \exp[ik(n - 1)\Delta x] \tag{2.36}$$

for WAPE solution;

2. compute the coefficients $C_1(x)$ and $C_2(x)$ using (2.22) and (2.23) with u replaced by $v(x, m\Delta z)$;

3. construct $w(x, m\Delta z)$ from $v(x, m\Delta z)$ using (2.27) ;

4. perform the discrete sine transform of w

$$W(x, l\Delta p) = \sum_{m=1}^{N-1} w(x, m\Delta z) \sin\left(\frac{\pi lm}{N}\right) \tag{2.37}$$

5. multiply by the p-space operator

$$W(x + \Delta x, l\Delta p) = W(x, l\Delta p) \cdot \exp\left[-ip^2\frac{\Delta x}{2k}\right], \tag{2.38}$$

for NAPE solution and,

$$W(x + \Delta x, l\Delta p) = W(x, l\Delta p) \cdot \exp\left[-\frac{ip^2\Delta x}{k}\left(\sqrt{1 - \frac{p^2}{k^2}} + 1\right)^{-1}\right] \tag{2.39}$$

for WAPE solution ;

6. the coefficients C_1 and C_2 must also be propagated to the new range step using

$$\begin{aligned} C_1(x + \Delta x) &= C_1(x) \cdot \exp\left[\frac{i\Delta x}{2k}\left(\frac{\log\ r}{\Delta z}\right)^2\right] \\ C_2(x + \Delta x) &= C_2(x) \cdot \exp\left[\frac{i\Delta x}{2k}\left(\frac{\log(-r)}{\Delta z}\right)^2\right]; \end{aligned} \tag{2.40}$$

7. perform the inverse DST to obtain $w(x + \Delta x, m\Delta z)$

8. solve for $v(x+\Delta x, m\Delta z)$ using the recursion described in (2.30)-(2.34) ;

9. multiply $v(x+\Delta x, m\Delta z)$ by the other half of the split z-operator in order to obtain $u(x+\Delta x, m\Delta z)$.

The above DMFT version has the advantage of only requiring a sine transform, nevertheless, this version exhibits occasional numerical instability when $\mathrm{Re}(\alpha) \to 0$, which is generally characterized by $|r| \to 1$.

Some algorithms are presented for implementing the DMFT, which will overcome these numerical problems (Kuttler; Janaswamy, 2002). These algorithms will be referred the forward difference and the backward difference methods for the DMFT, and they are most effective when employed in complement to each other.

To obtain a different formulation of the DMFT, replace the central difference equation (2.27) with a forward difference equation:

$$w(x, m\Delta z) \equiv \frac{u\left[x, (m+1)\Delta z\right] - u(x, m\Delta z)}{\Delta z} + \alpha u(x, m\Delta z) \quad \text{for} \quad m = 1 : N-1 \tag{2.41}$$

with $w(x,0) = w(x, N\Delta z) = 0$. This has the advantage of being only a first-order difference equation, thus requiring only one homogeneous solution in the general solution. To analyze the forward difference algorithm, define $r = 1 - \alpha\Delta z$. Then, multiply the above equation by Δz and redefine w by:

$$w(x, m\Delta z) \equiv u\left[x, (m+1)\Delta z\right] - r u(x, m\Delta z) \quad \text{for} \quad m = 1 : N-1 \tag{2.42}$$

After knowing the forward difference algorithm, an idea is to try a backward difference formulation. Instead of (2.27), consider:

$$w(x, m\Delta z) \equiv \frac{u(x, m\Delta z) - u\left[x, (m-1)\Delta z\right]}{\Delta z} + \alpha u(x, m\Delta z) \quad \text{for} \quad m = 1 : N-1 \tag{2.43}$$

with $w(x,0) = w(x, N\Delta z) = 0$. Again, this is only a first-order difference equation. Now, it is defined $r = (1+\alpha\Delta z)^{-1}$, rearrange (2.43), and redefine w by:

$$w(x, m\Delta z) \equiv u(x, m\Delta z) - r u\left[x, (m-1)\Delta z\right] \quad \text{for} \quad m = 1 : N-1. \tag{2.44}$$

2.4 Case studies

The case studies are proposed in order to validate the SSPE and DMFT implementations. The tests are comparisons between FD, SSPE and DMFT-SSPE numerical solutions. In the case studies, Perfectly Electrical Conducting (PEC) flat terrain, lossy ground surfaces and atmospheric refractivity effect are considered.

Table 1 – Simulation times

Technique	**Time Simulation (s)**
FD	1.702607
SSPE	0.369129
Two-Ray Model	0.002846

2.4.1 A comparison between FD technique and DMFT-SSPE method

The numerical algorithms are computationally implemented in MATLAB, and executed on an Intel Core i5-4200U processor and 8.00 GB RAM.

Validation of Numerical Algorithms Implementation

The purpose of this first test is to validate our computational implementation of the FD and SSPE numerical algorithms, comparing the results obtained from a horizontal pathloss profile with the results generated with an analytical solution for the Two-Ray model given in (Apaydin; Sevgi, 2017).

The scenario consists of a PEC flat terrain with a maximum extension of 20 km. A frequency of 1.0 GHz is used, homogeneous atmosphere conditions, a transmitter height of 30 meters and horizontal polarization. The receiver points have a fixed height of 30 meters along the flat terrain.

To carry out the simulations of the numerical techniques, a vertical field profile is calculated analytically at an initial distance of 50 m from the transmitter, and a computational vertical domain of 200 m height is defined.

Figure 6 shows the comparison of the pathloss curves obtained with the FD algorithm, SSPE method and two-ray model, respectively. It is possible to observe the good agreement in the convergence of the results. Additionally, the simulation times of each of the techniques are presented in Table 1.

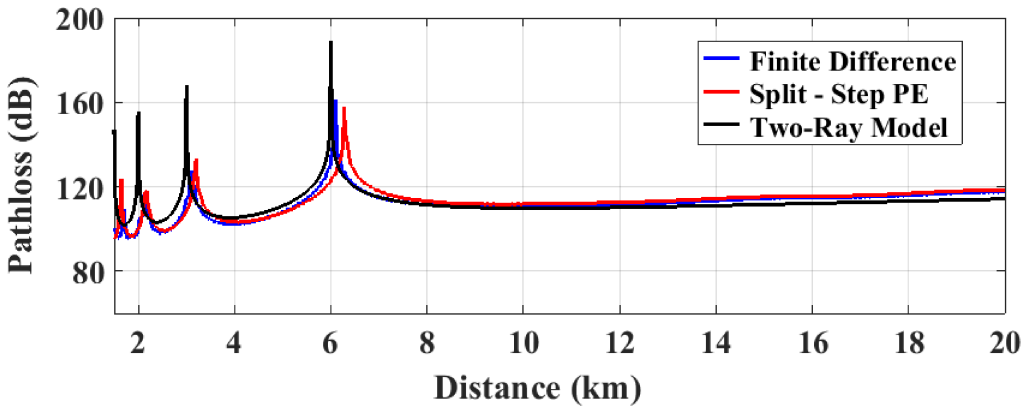

Figure 6 – Comparison between techniques at 1.0 GHz.

Canonical Cases: Inclusion of Ducting Conditions and Lossy Surface

The following canonical cases consider non-homogeneous conditions of the environments. The objective of our study is to compare the convergence of the results of the two implemented numerical solutions of PE model, and to analyze their computational efficiency by comparing the execution times of the algorithms.

The first canonical test consists of a PEC flat terrain and atmospheric conditions of a surface duct, modeled as $N(z) = 304 - 100z$, where $N(z)$ represents the refractivity variation (Akleman; Sevgi, 2000).

The 2D distribution of the auxiliary field function $u(x, z)$ obtained with the FD algorithm and the SSPE technique, at 3.6 GHz, can be seen in the Figures 7a and 7b, respectively.

To obtain pathloss curves, the simulations use the 3.6 GHz frequency band, a

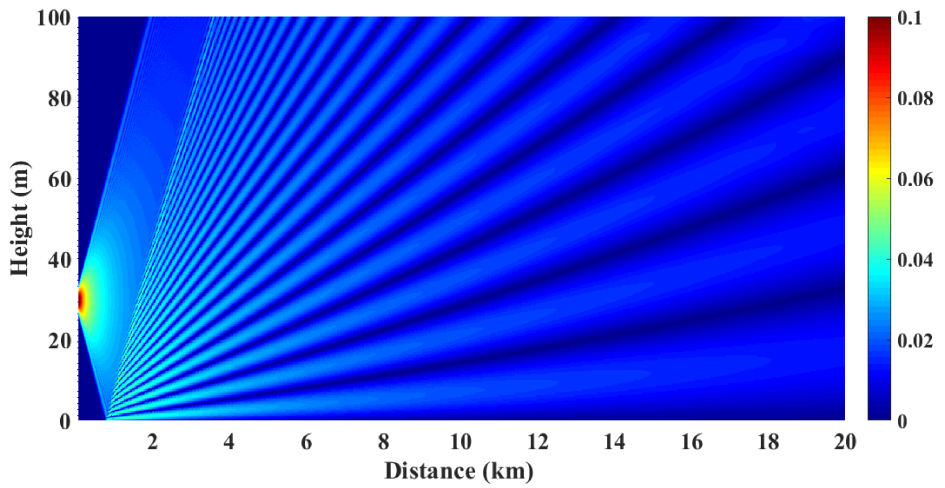

(a)

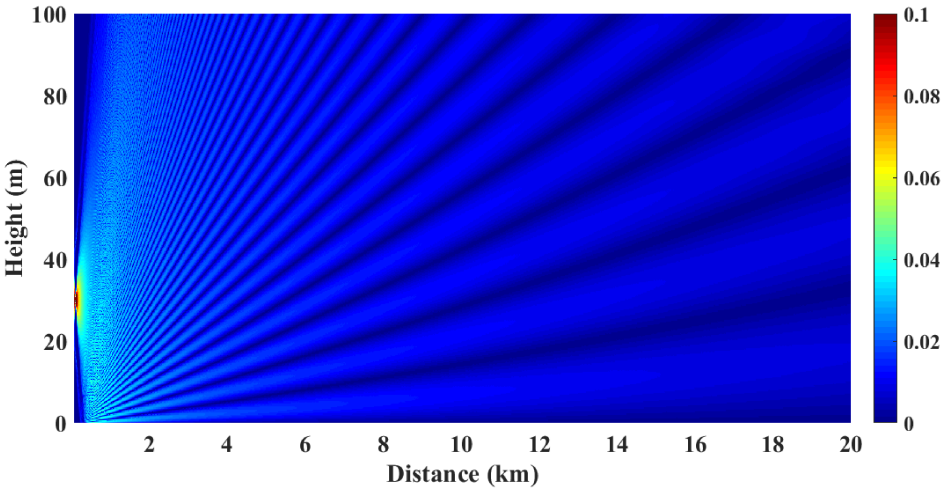

(b)

Figure 7 – 2D Field Distribution at 3.6 GHz obtained with: (a) FD algorithm and (b) SSPE algorithm.

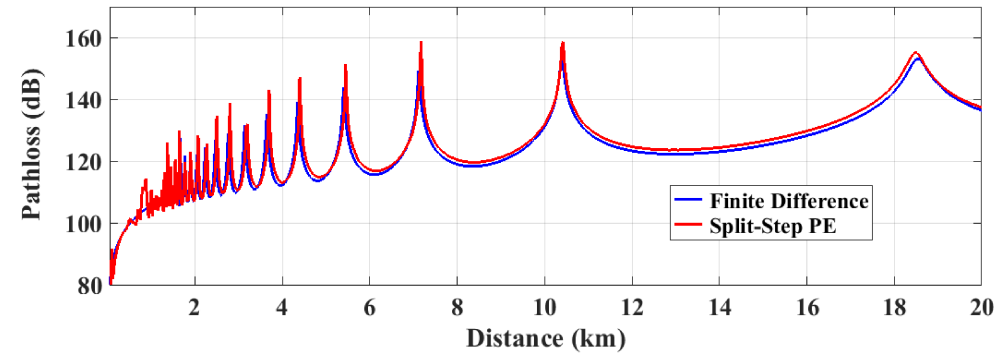

(a)

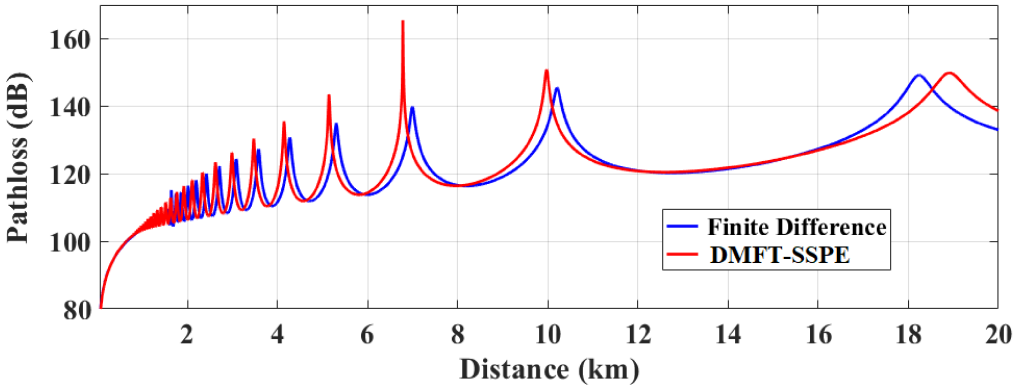

(b)

Figure 8 – Pathloss results - Horizontal Profile at 3.6 GHz including duct conditions: (a) Flat Terrain PEC and (b) Lossy Terrain.

transmitter height of 30 meters and horizontal polarization. The horizontal pathloss profile is calculated at 30 meter high receptor points along the terrain, see Figure 8a. The vertical profile of pathloss is calculated at $x = 20$ km, see Figure 9a.

The second canonical case changes the PEC surface for a Lossy flat terrain, characterized as standard ground ($\epsilon_r = 15$ and $\sigma = 0.012$ S/m). Therefore, the SSPE algorithm is replaced by the DMFT-SSPE approach to obtain the solutions. The frequency, atmospheric conditions, transmitter and receiver heights are maintained with respect to the first canonical situation. In this case, we use vertical polarization.

Figure 8b illustrates the horizontal pathloss profile curves obtained for the case of lossy flat terrain and surface duct conditions. Similarly, Figure 9b shows the vertical pathloss profile curves obtained for this situation.

The results shown in Figures 8 and 9 show the good agreement between the results obtained with both numerical solutions of the PE model. After analyzing the convergence of the results of both numerical approaches, an analysis of the computational efficiency of the algorithms is carried out by comparing their execution time.

The SSPE method (and consequently DMFT-SSPE) has a step size criterion on

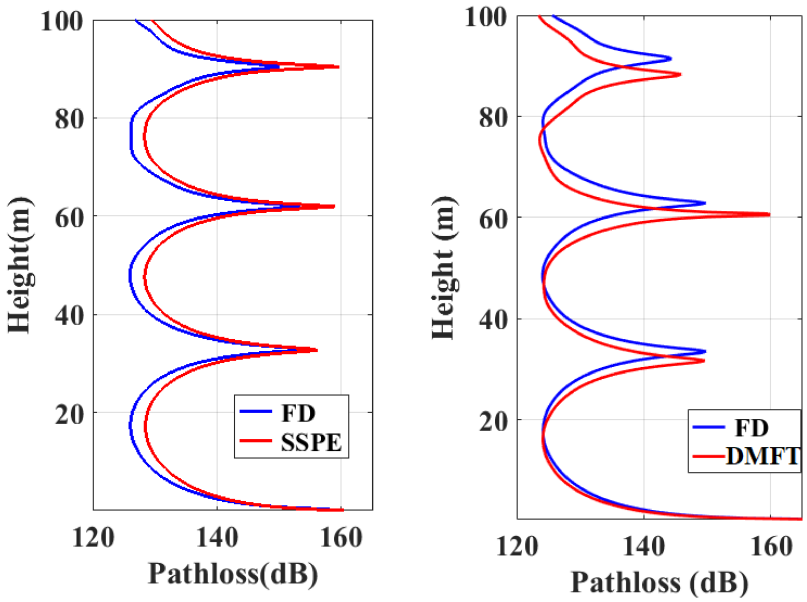

(a) (b)

Figure 9 – Pathloss results - Vertical Profile at 3.6 GHz including duct conditions: (a) Flat Terrain PEC and (b) Lossy Terrain.

the z axis that depends inversely on frequency. This means that the number of steps in the z axis increases when applying the SSPE method in propagation problems that use higher frequencies. In this test, the simulations are carried out in different frequency bands projected for the implementation of 5G networks. The lossy terrain and duct conditions, are maintained. The analyzed scenario considers a maximum extension of 20 km (for longe-distance communications), and a maximum height of computational domain of 200 m.

Table 2 shows the relationship between the simulation frequency, the step size (Δz), and the number of steps on the z axis (N_z).

Figure 10 shows the execution time results of the FD and DMFT-SSPE numerical algorithms. The great difference in the execution time of the algorithm is evident when the number of N_z increases (see Figure 10a), due to this, Figure 10b shows an enlarged

Table 2 – Frequencies and vertical discretization parameters

Frequency	Δz **(m)**	N_z
300 MHz	3.5926	56
750 MHz	1.4371	139
1.4 GHz	0.7699	260
2.5 GHz	0.4311	464
3.6 GHz	0.2994	668
5.4 GHz	0.1996	1002
10 GHz	0.1078	1856

curve of the execution times obtained by the DMFT-SSPE solution.

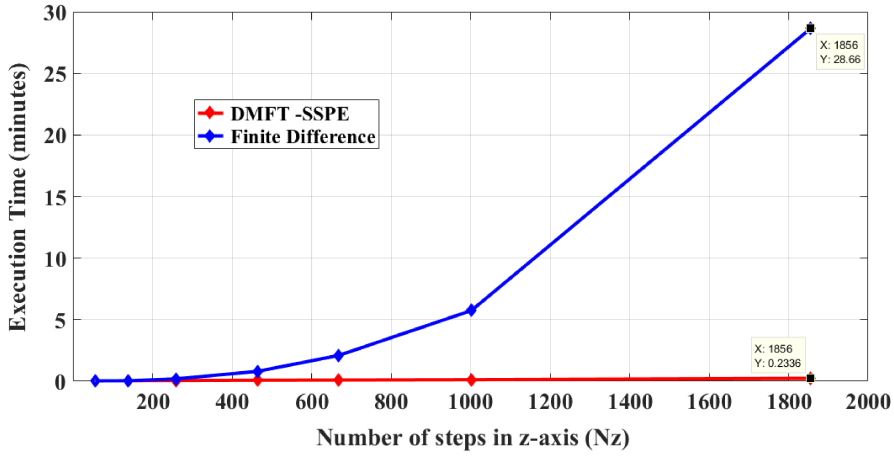

(a)

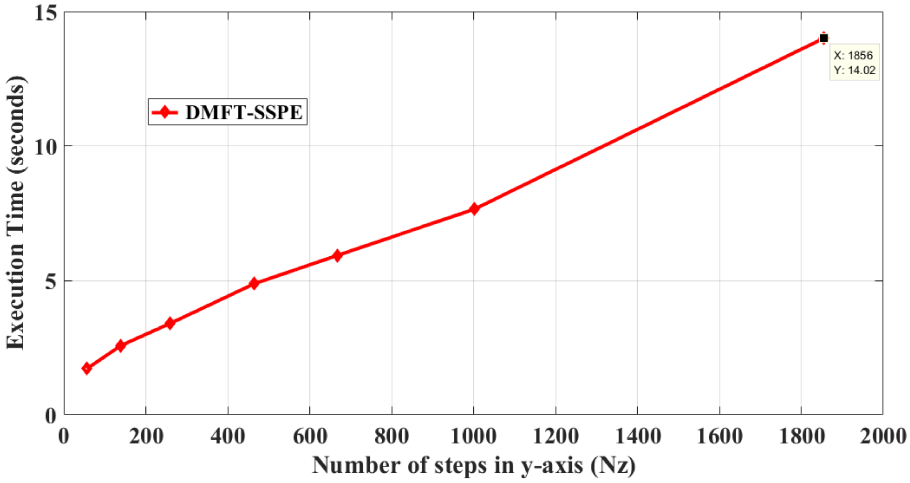

(b)

Figure 10 – Execution time comparisons: (a) DMFT-SSPE versus FD and (b) DMFT-SSPE (zoom).

According to the behavior of the simulation time curves as a function of the number of discretization steps, the literature defines an order of complexity of the algorithms. For numerical techniques based on matrix solutions, such as Finite Differences, the order of complexity is stated to be $O(N_z^2)$. In DMFT-SSPE case, it is given that the order of complexity as a function of N_z is $O(N_z \log N_z)$ (Zhou; Douvenot; Chabory, 2020).

Based on the simulation results, it is possible to conclude the advantages of using the DMFT-SSPE algorithm in radiopropagation problems involving long-distance scenarios and high frequencies. In addition, DMFT-SSPE allows to include non-homogeneous conditions of the environments (lossy terrains, atmospheric conditions, etc), guaranteeing computational efficiency.

2.5 Chapter conclusions

This Chapter presented the SSPE numerical solution to solve the PE model. In radiopropagation problems, SSPE includes irregular terrains by using the staircase approximation, and atmospheric effects are also considered by modeling the refractivity profiles. DMFT was an important advance, since it allowed to incorporate lossy surfaces into the SSPE solution, reaching a DMFT-SSPE algorithm. Comparisons were made through case studies to validate the DMFT-SSPE implementation. The obtained results showed a good agreement with reference to results of FD numerical solution. It is possible to conclude that DMFT-SSPE allows including non-homogeneous conditions of the environments, guaranteeing computational efficiency.

This research uses the DMFT approach of the SSPE numerical solution (referred to as DMFT-SSPE) and implements algorithms proposed in the literature to avoid the occurrence of these numerical instabilities. The computational implementation of a numerically stable radiopropagation algorithm based on the DMFT-SSPE method is one of the results obtained in this work. This radiopropagation tool contributes as a benchmark and consolidated coverage prediction algorithm to compare and validate the results obtained with other propagation models that are currently implemented in the works of the research group of antennas, propagation and electromagnetic theory (GAPTEM by its acronym in Portuguese).

3 A Proposal of a Modified RT with Atmospheric Refractivity Effect

This chapter contains the theoretical foundation on GO, UTD and atmospheric refractivity. The chapter focuses primarily on the mathematical description of the ray paths under different refractivity conditions. A modified multipath model is introduced for the case of a constant refractivity gradient. In addition, canonical cases are defined to validate our proposal of a Modified RT with atmospheric refractivity effect.

3.1 Ray optical technique

Asymptotic methods provide approximate solutions that are widely used when analyzing high-frequency systems in large environments. In these situations the precision increases, since the dimensions of the objects are considered much greater than the wavelength. Ray optical is a deterministic technique used to characterize radio communication channels, based on the asymptotic methods of GO and UTD (Wald et al., 2009; Ufimtsev, 2014). GO determines incident and reflected fields and UTD resolves edge diffraction. The two techniques approach the representation of incident, reflected and diffracted rays, through individual and rectilinear paths, created by the ray optical tracing algorithms.

The ray optical technique mainly proposes two methods, called *ray tracing* (RT) and *ray launching* (RL) (Gómez Rojas, 2018). RT is used, generally, in scenarios with low complexity geometries and few reflections. RL is employed in environments with complex geometries and considers multiple reflections, diffractions or combinations of them. In this research, we use a RT technique. The advantage of using RT approach is its characteristic to distinguish between different propagation paths.

3.1.1 Basic principles of GO

The GO analyzes the incident and reflected rays in order to obtain the field at a given point. It is based on the ray approximation, which assumes that the wavelength is small enough compared to the dimensions of the obstacles ($\lambda \to 0$), allowing to consider the electromagnetic fields as TEM (Transverse Electromagnetic) waves and locally plane at any point of the propagation of the ray. GO is a special case of wave optics, where the meaning of the terms *ray* and *wave-front* can be deduced from Maxwell's equations (Valtr; Pechac, 2005b; Valtr, 2017). Such an assumption is generally valid in urban radio propagation and allows the calculation of the scattered field in terms of electromagnetic

variables (Tami Lopez, 2015). Each ray has an associated electric field, which depends on the emitted field by the transmitter, loss in free space, reflections and diffractions.

3.1.2 Direct electric field at a point

In order to use RT technique, it is necessary to estimate the electric field at a specific receiver point. Then, the antenna is approximated to a point source and the irradiated electric field in the far field region can be predicted according to (Razavi-Ghods, 2007):

$$E(\theta,\phi) = \left(\frac{e^{ikR}}{R}\right)\sqrt{\frac{P_t G_t(\theta,\phi) G_r(\theta,\phi)\eta}{4\pi}}, \tag{3.1}$$

where, e^{ikR} is the plane wave equation, R is the distance from the source to the observation point, k is the wavenumber, P_t is the transmitter power in watts (W), $G_t(\theta,\phi)$ and $G_r(\theta,\phi)$ are the gain of transmitter and receiver respectively, and η is the intrinsic impedance of the propagation medium.

Equation (3.1) is used to characterize the field associated with the direct ray that reaches the receiver and the field of the ray that hits a reflection plane or a diffraction edge, coming directly from the transmitter. Every ray that propagates in the free space suffers losses during its path (*path loss*). The Friis formula allows to calculate *path loss* (Iskander; Yun, 2002), which establishes the ratio between the transmitter power (P_t) and that received at the receiver point (P_r):

$$\frac{P_r}{P_t} = G_t G_r \left(\frac{\lambda}{4\pi R}\right)^2, \tag{3.2}$$

where λ is the wavelength, and antenna gain considers linearly polarized and aligned antennas for maximum radiation.

3.1.3 Reflected electric field

Figure 11 shows an electromagnetic wave incident at an angle α_i with the plane of the boundary between two media. As shown in the figure, part of the energy is reflected back to the first media at an angle α_r, and part of the energy is transmitted (refracted) into the second media at an angle α_t. The nature of reflection varies with the direction of polarization of the E-field. The plane of incidence is defined as the plane containing the incident, reflected and transmitted rays. In Figure 11, the E-field is parallel with the plane of incidence (that is, the E-field has a vertical polarization, or normal component, with respect to reflecting surface). The subscripts i, r, t refer to the incident, reflected, and transmitted fields, respectively. Parameters ϵ_1, μ_1, σ_1, and ϵ_2, μ_2, σ_2 represent the permittivity, permeability, and conductivity of the two media, respectively. Often,

the dielectric constant of a perfect (lossless) dielectric is related to a relative value of permittivity, ϵ_r, such that $\epsilon = \epsilon_0\epsilon_r$, where ϵ_0 is a constant given by 8.85×10^{-12} F/m. If a dielectric material is lossy, it will absorb power and may be described by a complex dielectric constant given by (Rappaport, 1996):

$$\epsilon = \epsilon_0\epsilon_r + i\epsilon' \tag{3.3}$$

where,

$$\epsilon' = \frac{\sigma}{\omega} \tag{3.4}$$

and σ is the conductivity of the material measured in S/m.

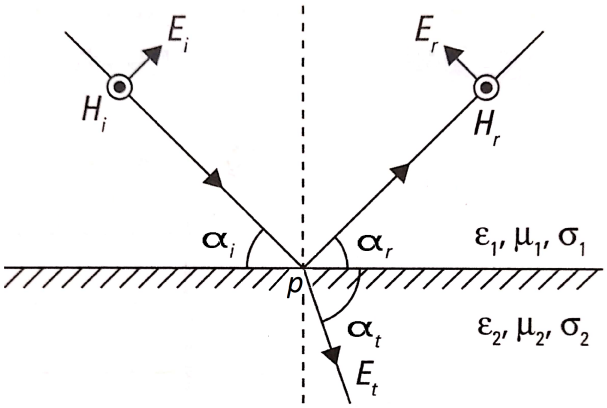

Figure 11 – Field electric in the plane of incidence (Rappaport, 1996).

When a ray hits a surface whose roughness is less than its wavelength, it can be treated with the Fresnel reflection principle (Fuschini; Degli-Esposti; Vitucci, 2010). At the point p (see Figure 11), the reflected electric field at the interface that separates the two media $E_r(p)$ can be found by:

$$\begin{bmatrix} E_r^{\perp} \\ E_r^{\parallel} \end{bmatrix} = \begin{bmatrix} R_s^{\perp} & 0 \\ 0 & R_s^{\parallel} \end{bmatrix} \begin{bmatrix} E_i^{\perp} \\ E_i^{\parallel} \end{bmatrix}, \tag{3.5}$$

where R_s is the Fresnel coefficient for the reflection of a plane wave, and is either $R_s^{\perp}$ or $R_s^{\parallel}$, depending on polarization. When the first medium is free space and $\mu_1 = \mu_2$, the reflection coefficients for the two cases of vertical and horizontal polarization can be obtained through:

$$R_s^{\parallel} = \frac{\hat{\epsilon}_r \sin\alpha_i - \sqrt{\hat{\epsilon}_r - \cos^2\alpha_i}}{\hat{\epsilon}_r \sin\alpha_i + \sqrt{\hat{\epsilon}_r - \cos^2\alpha_i}} \tag{3.6}$$

and,

$$R_s^{\perp} = \frac{\sin\alpha_i - \sqrt{\hat{\epsilon}_r - \cos^2\alpha_i}}{\sin\alpha_i + \sqrt{\hat{\epsilon}_r - \cos^2\alpha_i}}. \tag{3.7}$$

In (3.6) and (3.7) α_i corresponds to the angle of incidence with respect to the normal, and $\hat{\epsilon}_r$ represents the complex relative permittivity given by $\hat{\epsilon}_r = \epsilon_r + i\sigma/\omega\epsilon_0$.

3.1.4 UTD principles

The UTD is an asymptotic solution widely used to predict scattering propagation. The diffraction occurs when a ray encounters a wedge, which generates multiple new rays determined by a diffraction cone according to the Huygens principle. The UTD formulation is rigorous because the diffraction coefficients and angular definitions are quite complex and have many exceptions, depending on the wedge geometry and the positions of the transmitter and receiver (Tami et al., 2018).

We consider the two-dimensional problem of diffraction by a semi-infinite wedge with straight edges, exterior angle $n\pi$, and lossy conducting boundary surfaces in a homogeneous, linear, and isotropic medium (Navarro et al., 2020). In the chosen coordinate system, the straight edge of the wedge is along the z-axis, the plane faces of the wedge are at $\varphi = 0$ (0 face) and $\varphi = n\pi$ (n face), the radio source is at $\varphi = \phi_i$ and distance $\rho = s_i$ from the edge of the wedge, and the observation point is at (s_d, ϕ_d). The distances s_i and s_d are calculated with the optical length equation (Valtr; Pechac, 2006). Besides, ϕ_i is the angle of the trajectory of the ray at the end of the linear segment and ϕ_d is the angle of the trajectory of the ray diffracted at the beginning of the linear segment. Figure 12 shows the geometry of the problem.

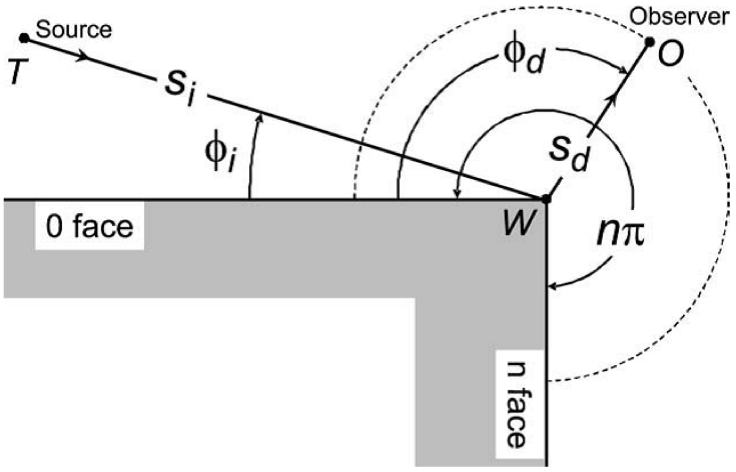

Figure 12 – Geometry and wedge diffraction variables (Tami et al., 2018).

The general UTD solution for the electric field at the observer's point is:

$$E_d(O) = E_i(W) \cdot \overline{D} A(s_d) e^{iks_d} \tag{3.8}$$

where, $E_i(W)$ is the incident electric field at the edge, $A(s_d)$ is the amplitude factor, s_d is the distance between wedge and observer, and $\overline{D}$ is the dyadic diffraction coefficient. Adopting the classical notation of (Kouyoumjian; Pathak, 1974), the dyadic soft and hard is given by:

$$\overline{D}^{s,h} = G_0^{s,h}\left[D_2 + R_0^{s,h}(\alpha_0)D_4\right] + G_n^{s,h}\left[D_1 + R_n^{s,h}(\alpha_n)D_3\right] \tag{3.9}$$

where D_i, for $i = 1, \ldots, 4$, are the UTD diffraction coefficients, G_0 and G_n, are grazing incidence factor, R_0 and R_n are Fresnel reflection coefficients, for the 0 and n faces, respectively.

The UTD formulation is based on the Fresnel reflection coefficients, specifically, the Lubbers Coefficients (Luebbers, 1989) defining the incidence and reflection angles of the incident and diffracted rays. Luebbers' definition for the angles α_0 and α_n, used in the Fresnel reflection coefficients, are $\alpha_0 = \phi_i$ and $\alpha_n = n\pi - \phi_d$ (Tami et al., 2018).

3.2 Ray tracing with atmospheric effects

The main challenge in this chapter is to obtain a propagation model based on RT and that includes atmospheric effects. For this purpose, a brief description of the refractive index is necessary, and then a proposal for a modified two-ray model is explained. The mathematical description of the ray path under different refractivity conditions must be defined, it is essential to apply the principles of RT technique.

3.2.1 Basic concepts of atmospheric refractivity

The non-uniform nature of the lower troposphere causes EM waves to be bent or refracted. Refraction of EM waves is due to the variation of the velocity of propagation with altitude. It is known that refraction index (n) is the ratio of the velocity in free space to the velocity in the medium of interest (atmosphere in our case), and is caused by pressure, temperature, and water vapor variations in both space and time (Apaydin; Sevgi, 2017).

Radio wave propagation behaviour and the refractive properties of the atmosphere are related through the refractive index of air (Bean; Dutton, 1966). For the sake of convenience, refractivity is generally used instead (Valtr; Pechac, 2006). Refractivity (N) is defined as:

$$N = (n - 1) \times 10^6. \tag{3.10}$$

Then, it is conventional to define a new quantity, so called Modified Refractivity (M), which takes the Earth's curvature into account (Ozgun et al., 2011; Valtr; Pechac, 2005b):

$$M = N + \frac{z}{a_e} \times 10^6 = N + 157z, \tag{3.11}$$

where z is the height above surface in km and a_e is the Earth's radius. Consequently, the modified refractive index (m) is defined, as follows:

$$m = 1 + M \times 10^{-6}. \tag{3.12}$$

The vertical variation of N with respect to height (dN/dz) is called refractivity gradient. The rays propagating under positive refractivity gradients are bent upwards.

The standard refractivity gradient ($dN/dz = -40$ N/km) causes rays to bend downwards. Ray propagating under a refractivity gradient equal to $dN/dz = -157$ N/km is exactly parallel to the surface of the earth (Valtr; Pechac, 2005b). Gradients of less than -157 N/km produce ducting.

In order to work with a flat Earth, the refractive index gradient is to be replaced by a gradient of modified refractive index, $dm/dz = dn/dz + 1.57 \times 10^{-7} = dN/dz \times 10^{-9} + 1.57 \times 10^{-7}$ (Valtr; Pechac, 2005a).

Figure 13 shows the radio propagation behavior under atmospheric refractivity effects. The results were reached through SSPE algorithm.

3.2.2 A modified two-ray model

The Introduction chapter mentioned that the two-ray model is a useful approach to analyze radio links. However, it has not been modified (or adjusted) to include curved paths, in other words, a two-ray model that includes refractivity gradients. Therefore, to the best knowledge of the author, it is a novelty to present a modified two-ray model to incorporate the effects of atmospheric refractivity.

The proposed approach guarantees the arrival of a direct ray and a reflected ray at a specific receiver point. Knowing the transmitter height, the location of the receiver point and the refractivity gradient, it is possible to define, firstly, the path of the direct ray. Next, satisfying Snell's law, it is possible to find the distance (from the transmitter) where an incident ray hits, guaranteeing the existence of a ground-reflected ray that reaches at the reception point. Once known the distance where the ground-reflection occurs, it is possible to calculate the launch angle of the incident ray. For each reflected ray is calculated its corresponding launch angle.

In this Chapter, three refractivity situations are addressed: constant refractivity gradient, ducting conditions and horizontally variable refractive conditions. The rest of the chapter provides the formulation of the direct ray path for the three refractivity situations. For the case of constant refractivity gradient, the formulation of the point reflection calculation, in both flat terrain and sloping terrain, is deduced.

3.2.3 Ray paths under constant refractivity gradient

Under the assumptions GO, the following equation can be used to express the path of the rays dependent on the refractivity gradient (Levy, 2000).

$$\frac{d}{dl}\left(n(\mathbf{r})\frac{dr}{dl}\right) = \nabla n(\mathbf{r}), \tag{3.13}$$

where $\mathbf{r}$ represents the position vector and l is the coordinate associated with the path. The following simplifications are made (Valtr, 2017):

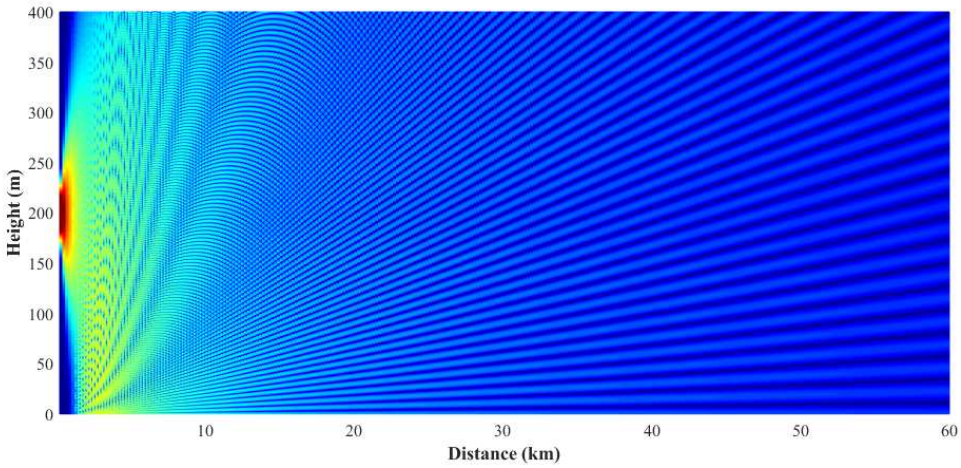

(a)

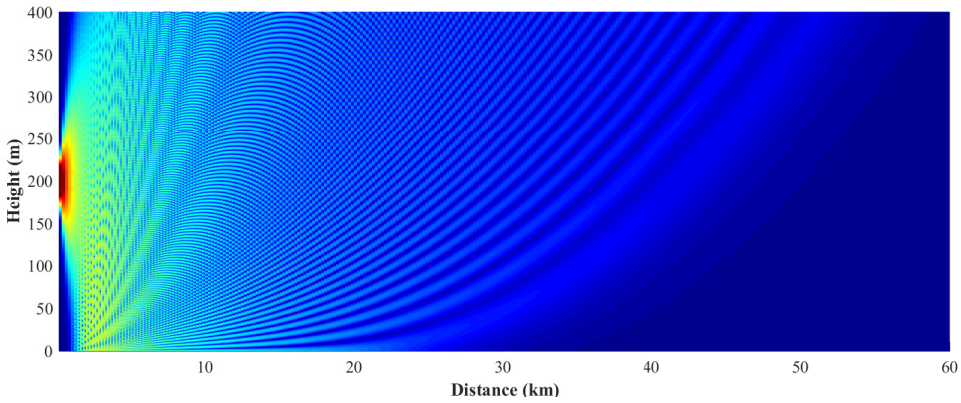

(b)

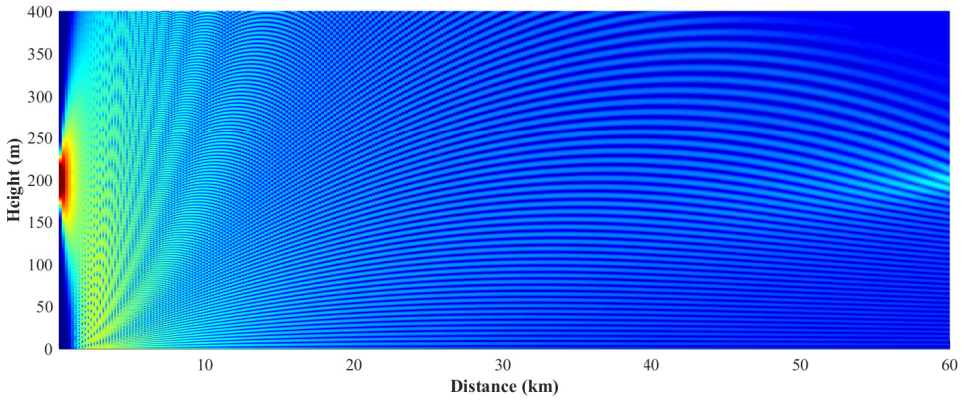

(c)

Figure 13 – Radiowave propagation behavior at 2 GHz: (a) Homogeneous conditions, (b) Under a refractivity gradient $dN/dz > 0$ and (c) Under a refractivity gradient $dN/dz < 0$.

- 2-D propagation in cartesian $x - z$ coordinate system (x is distance and z is height).
- $dl \sim dx$ (predominantly horizontal propagation).
- n is a function of height z only, $n(\mathbf{r}) = n(z)$.

Thus, equation (3.13) is represented as:

$$\frac{d}{dx}\left(n(\mathbf{z})\frac{dz}{dx}\right) = \nabla n(\mathbf{z}). \tag{3.14}$$

Solving the equation (3.14):

$$\frac{\mathrm{d}n(z)}{\mathrm{d}x}\cdot\frac{\mathrm{d}z}{\mathrm{d}x} + n(z)\cdot\frac{\mathrm{d}^2z}{\mathrm{d}x^2} = \frac{\mathrm{d}n(z)}{\mathrm{d}x} + \frac{\mathrm{d}n(z)}{\mathrm{d}z} \tag{3.15}$$

where,

$$n(z) = n_0 + \delta z. \tag{3.16}$$

Equation (3.16) indicates the height dependency of the refractive index of the atmosphere. In this equation, n_0 is the value of the refractive index on the ground surface, and δ is the gradient of refractive index (dn/dz) (Valtr; Pechac, 2006). Moreover, it is possible to affirm that $dn(z)/dx = 0$. Therefore, equation (3.15) is rewritten as:

$$n(z)\cdot\frac{\mathrm{d}^2z}{\mathrm{d}x^2} = \frac{\mathrm{d}n(z)}{\mathrm{d}z} \tag{3.17}$$

or otherwise:

$$\frac{\mathrm{d}^2z}{\mathrm{d}x^2} = \frac{1}{n(z)}\cdot\frac{\mathrm{d}n(z)}{\mathrm{d}z}, \tag{3.18}$$

where $n(z)$ is very close to 1 for all heights. Then, equation (3.18) is rewritten:

$$\frac{\mathrm{d}^2z}{\mathrm{d}x^2} = \frac{\mathrm{d}n(z)}{\mathrm{d}z}. \tag{3.19}$$

Equation (3.19) is a Non-Linear Differential Equation of Second Order.

Substituting equation (3.16) into equation (3.19) :

$$\frac{\mathrm{d}^2z}{\mathrm{d}x^2} = \frac{\mathrm{d}}{\mathrm{d}z}(n_0 + \delta z), \tag{3.20}$$

$$\frac{\mathrm{d}^2z}{\mathrm{d}x^2} = \frac{\mathrm{d}}{\mathrm{d}z}(n_0 + \delta z) = \frac{\mathrm{d}(n_0)}{\mathrm{d}z} + \frac{\mathrm{d}(\delta z)}{\mathrm{d}z} = \delta. \tag{3.21}$$

$$\therefore \quad \frac{\mathrm{d}^2z}{\mathrm{d}x^2} = \delta. \tag{3.22}$$

Equation (3.22) is a Second-Order Linear Ordinary Differential Equation. It was possible

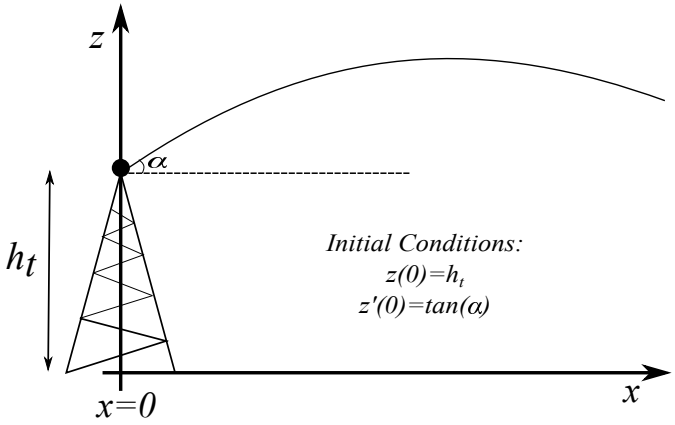

Figure 14 – Ray Path.

to arrive at this differential equation type by working with a constant refractivity gradient along the z-axis.

According to Figure 14 the following initial conditions can be established:

$$z(0) \;=\; h_t \tag{3.23}$$

and,

$$\frac{\mathrm{d}z(0)}{\mathrm{d}x} = z'(0) = \tan\alpha, \tag{3.24}$$

α is the initial launching angle.

Solving equation (3.22):

$$\frac{\mathrm{d}z}{\mathrm{d}x} = \int \delta dx \qquad \rightarrow \qquad \frac{\mathrm{d}z}{\mathrm{d}x} = \delta x + C_1 \tag{3.25}$$

$$\int dz = \int (\delta x + C_1) dx \tag{3.26}$$

$$\therefore \qquad z = \frac{\delta x^2}{2} + C_1 x + C_2. \tag{3.27}$$

The initial conditions are used to find the C_1 and C_2 values. Using equation (3.23) into equation (3.27):

$$\frac{\delta(0)^2}{2} + C_1(0) + C_2 = h_t \qquad \rightarrow \qquad C_2 = h_t \tag{3.28}$$

and equation (3.24) into equation (3.25):

$$\delta(0) + C_1 = \tan\alpha \qquad \rightarrow \qquad C_1 = \tan\alpha = K \tag{3.29}$$

Finally, the following equation is obtained:

$$z = \frac{\delta x^2}{2} + Kx + h_t. \tag{3.30}$$

Analysis of direct ray

In this work, the most relevant contribution is the deduction of a modified two-ray model that considers refractive effects of the atmosphere to estimate radio wave coverage. The proposed formulation guarantees the arrival of a direct line ray and a reflected ray at a specific receiver point. The launch angle of the ray depends on the location of the receiver point, that is to say, for each reflected ray is calculated its corresponding launch angle.

According to Figure 15 can be defined:

$$\alpha \;=\; \arctan\left(\frac{\Delta h_R + h_R - h_t}{X_R}\right). \tag{3.31}$$

In order to deduce the value of Δh_R, the coordinate (X_R, h_R) is used, and substituting those values in equation (3.30):

$$h_R = \frac{\delta X_R^2}{2} + \tan\alpha \cdot X_R + h_t. \tag{3.32}$$

Geometrically: $h_R = \tan\alpha \cdot X_R + h_t$. Therefore, the term Δh_R is:

$$\Delta h_R \;=\; \frac{\delta {X_R}^2}{2} \tag{3.33}$$

Analysis of reflected ray

Figure 16 shows the path of a incident and reflected ray, the ray path to the incident wave front, at $x = X$, makes an angle α_1 with the parallel to plane earth and the reflected wave also makes an angle α_2 with the parallel to plane earth. From Snell's law, the angle of reflection is equal to the angle of incidence, it follows that the two angles must be equal:

$$\alpha_1 \;=\; \alpha_2. \tag{3.34}$$

Using the reciprocity theorem to analyze a given antenna in transmitting mode or receiving mode. Therefore, we can write the angles α_1 and α_2 from equation (3.31):

$$\alpha_1 \;=\; \arctan\left(\frac{\Delta h_{R_1} + h_{R_1}}{X}\right) \;=\; \arctan\left(\frac{\frac{\delta X^2}{2} + h_t}{X}\right) \tag{3.35}$$

$$\therefore \quad \alpha_1 \;=\; \arctan\left(-\frac{\delta X}{2} + \frac{h_t}{X}\right) \tag{3.36}$$

and,

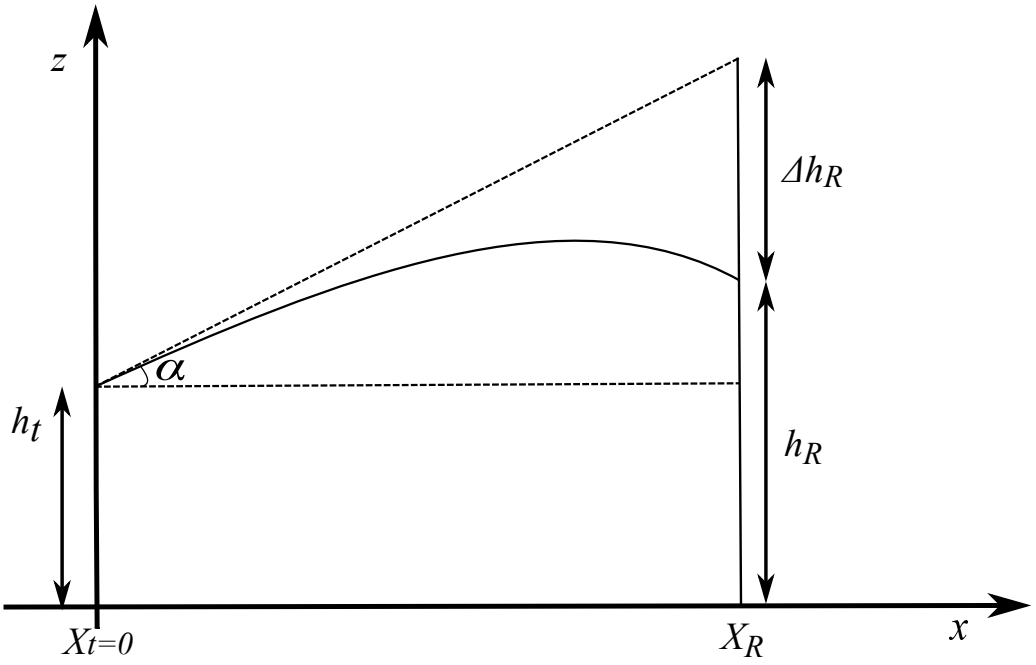

(a)

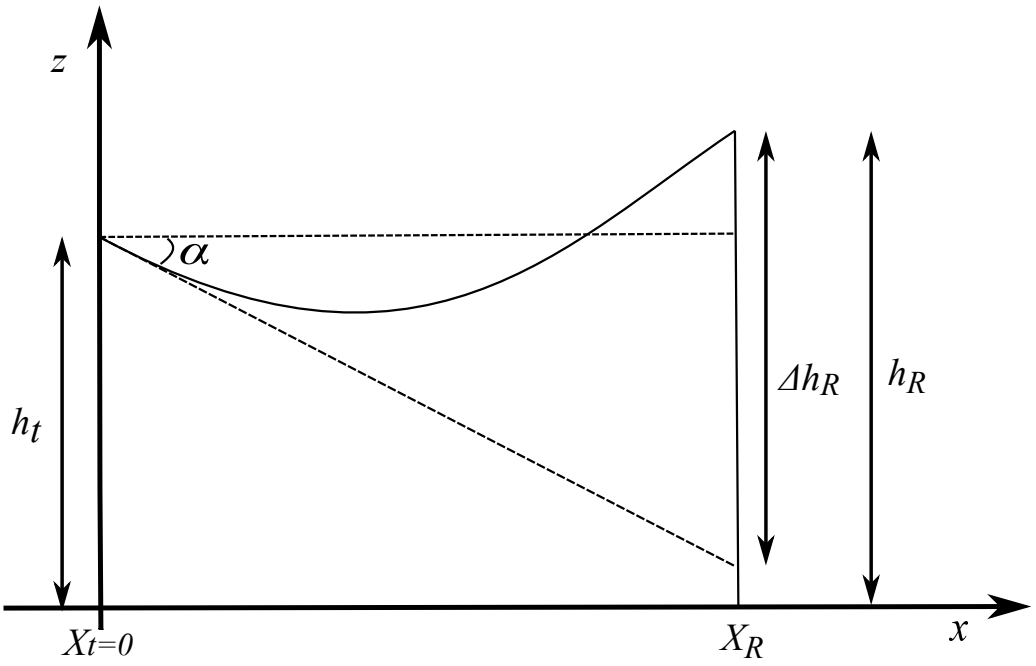

(b)

Figure 15 – Direct ray path under a refractivity gradient (a) $dN/dz > 0$ and (b) $dN/dz < 0$.

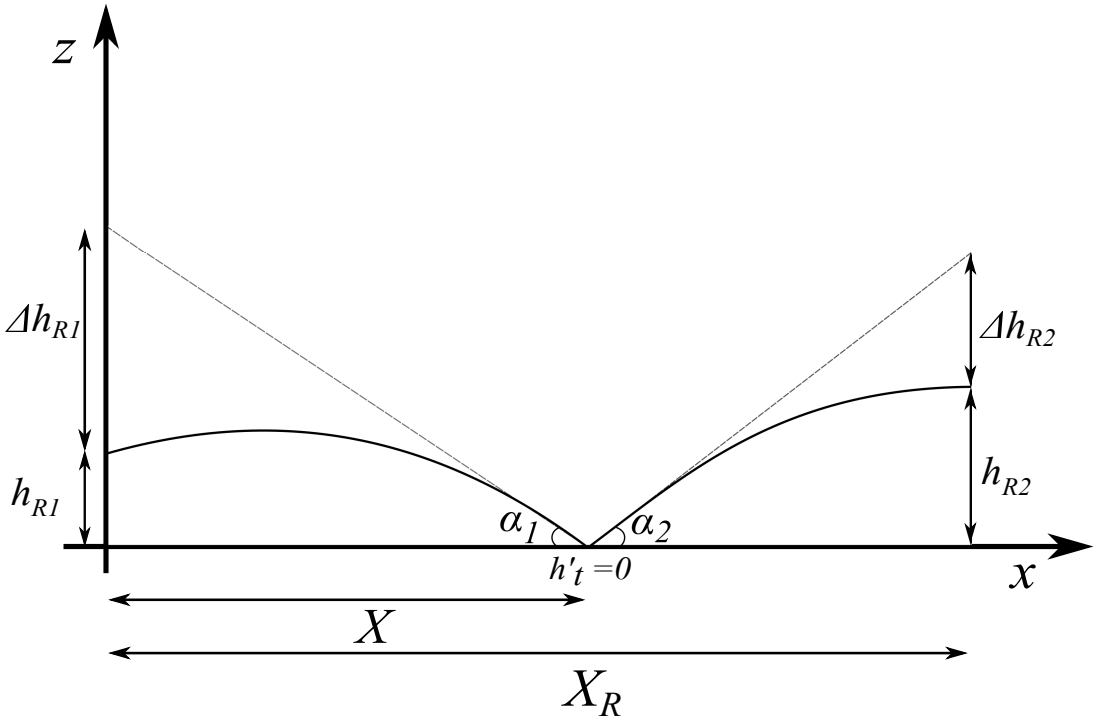

(a)

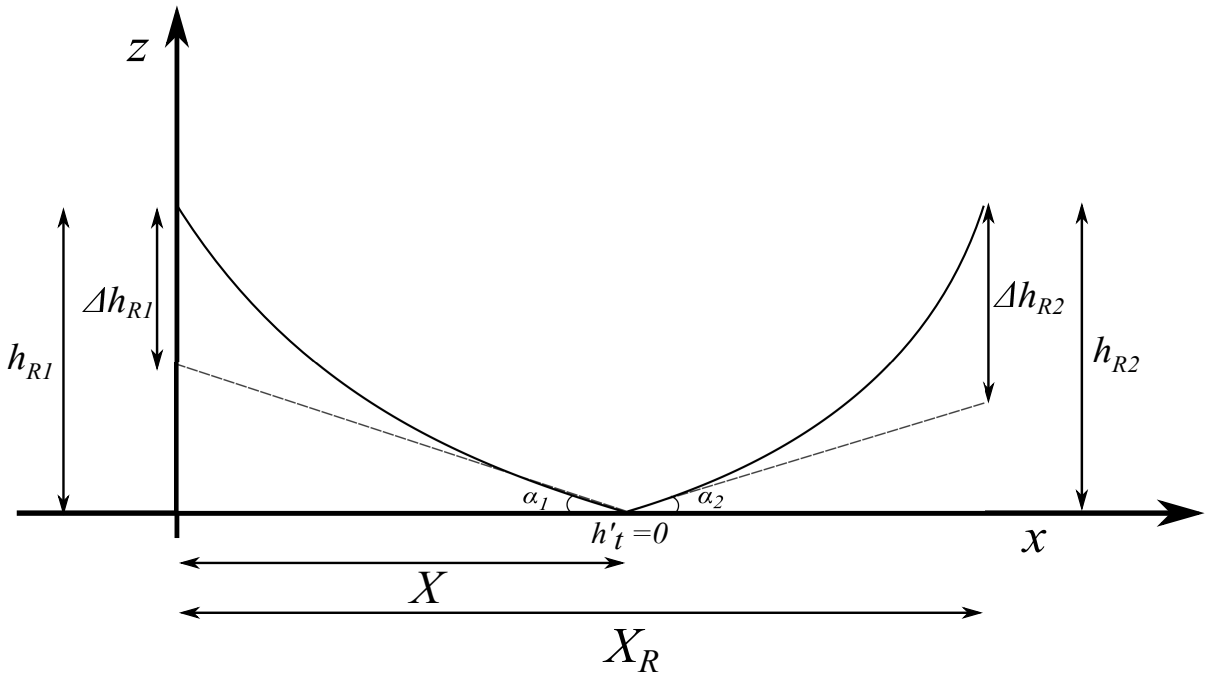

(b)

Figure 16 – Incident and reflected ray paths under a refractivity gradient (a) $dN/dz > 0$ and (b) $dN/dz < 0$.

$$\alpha_2 = \arctan\left(\frac{\Delta h_{R_2} + h_{R_2}}{X_R - X}\right) = \arctan\left(\frac{\frac{\delta(X_R - X)^2}{2} + h_R}{X_R - X}\right) \tag{3.37}$$

$$\therefore \quad \alpha_2 = \arctan\left(\frac{\delta(X_R - X)}{2} + \frac{h_R}{X_R - X}\right). \tag{3.38}$$

Replacing equation (3.36) and equation (3.38) into equation (3.34), reduces it to:

$$\frac{\delta X}{2} + \frac{h_t}{X} = \frac{\delta(X_R - X)}{2} + \frac{h_R}{X_R - X}, \tag{3.39}$$

manipulating mathematically the equation (3.39):

$$\frac{\delta X}{2} - \frac{\delta(X_R - X)}{2} + \frac{h_t}{X} - \frac{h_R}{X_R - X} = 0 \tag{3.40}$$

which is a cubic equation:

$$X^3(\delta) - X^2\left(\frac{3\delta X_R}{2}\right) + X\left(\frac{\delta X_R^2}{2} - h_t - h_R\right) + X_R h_t = 0. \tag{3.41}$$

The unknown X, which is the distance from the transmitter to the point of reflection, whose solution is given by a real root $X = x_1$, minimum and $x_1 > 0$. Figure 17 shows the behavior of rays above a flat terrain. The rays were curved by refractive effects of the standard atmosphere ($dN/dz = -40$ N/km).

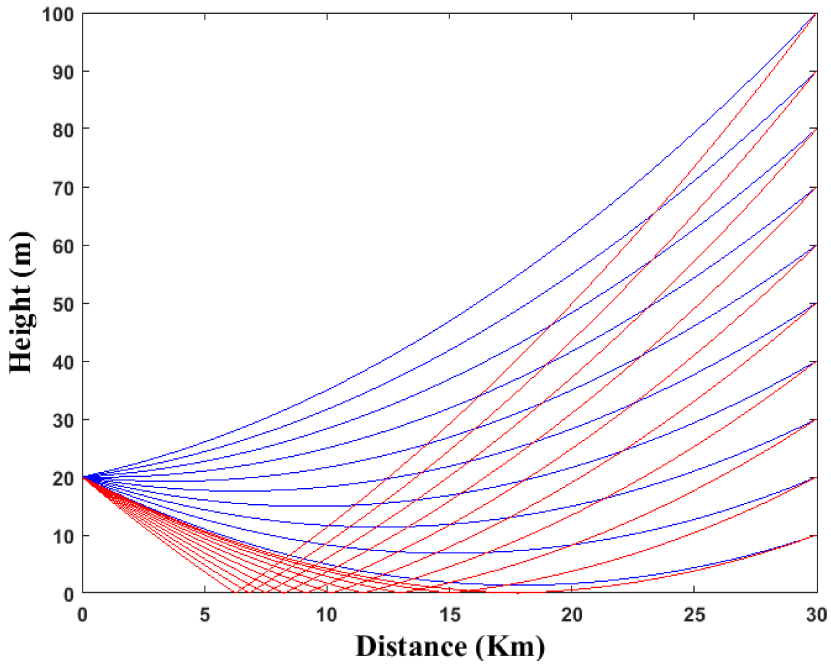

Figure 17 – Ray paths above a flat terrain.

Analysis of reflected ray over sloping terrain

In the same way as in flat terrain case, our purpose is to offer a formulation that calculates a reflection point over sloping terrain. The terrain is modeled as $z = mx$ and Δz_R represents the height of a receiver point over terrain. Figure 18 shows the ray path of a incident and reflected ray over a sloping terrain.

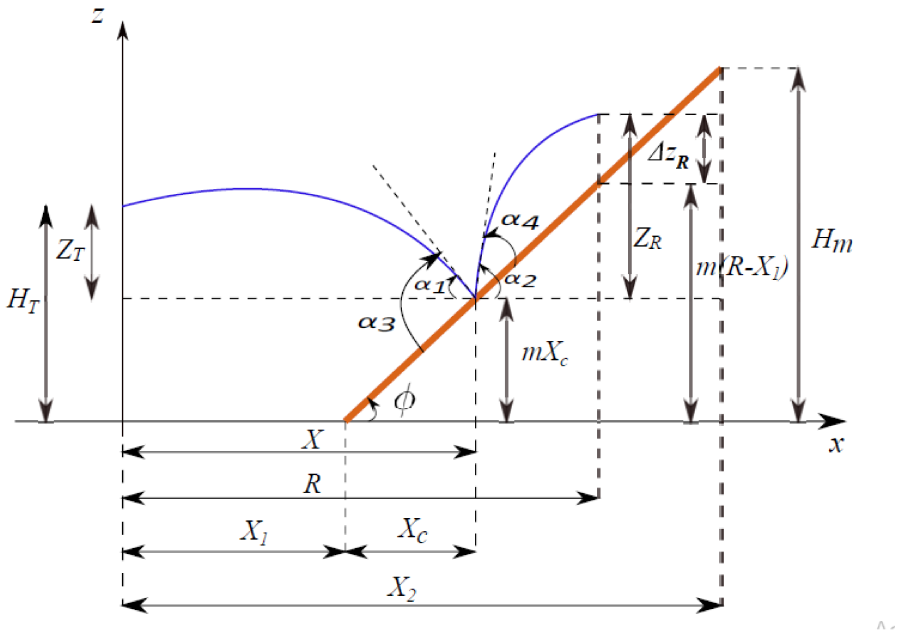

Figure 18 – Incident and reflected ray paths over a sloping terrain.

According to the Figure 18 and based on our works (Parada et al., 2019; Parada et al., 2019):

$$\tan\alpha_1 = -\frac{\delta X}{2} + \frac{Z_T}{X} \tag{3.42}$$

$$\tan\alpha_2 = -\frac{\delta(R-X)}{2} + \frac{Z_R}{R-X} \tag{3.43}$$

$$\tan\phi = \frac{H_m}{X_2 - X_1} = m \tag{3.44}$$

$$X = X_1 + X_c \tag{3.45}$$

$$Z_T = H_T + mX_1 - mX \tag{3.46}$$

$$Z_R = \Delta z_R + mR - mX \tag{3.47}$$

where, as depicted in Figure 18, Δz_R is the height of a receiver point over terrain, ϕ corresponds to the angle associated with the slope of the terrain, H_T refers to the transmitter height for this situation, H_m is the maximum height of the wedge, X_1 represents the distance from the transmitter to the initial location of the sloping terrain, X_C is the distance from the initial location of sloping terrain to the reflection point and X_2 indicates the distance from the transmitter to the final location of the sloping terrain.

From Snell's law:

$$\alpha_3 \;=\; \alpha_4 \quad \rightarrow \quad \alpha_1 + \phi \;=\; \alpha_2 - \phi \tag{3.48}$$

then,

$$\tan(\alpha_1 + \phi) \;=\; \tan(\alpha_2 - \phi). \tag{3.49}$$

by using trigonometric identities in equation (3.49) is obtained:

$$\tan\alpha_1 - \tan\alpha_2 + 2\tan\phi + 2\tan\alpha_1\tan\alpha_2\tan\phi + \tan^2\phi(\tan\alpha_2 - \tan\alpha_1) = 0. \tag{3.50}$$

Substituting (3.42), (3.43) and (3.44) into (3.50), it is possible to reach a fourth degree equation:

$$AX^4 + BX^3 + CX^2 + DX + E = 0, \tag{3.51}$$

where the coefficients are defined in terms of δ and the variables exhibited in Figure 18,as shown from expression (3.52) to (3.56):

$$A \;=\; \delta^2 m, \tag{3.52}$$

$$B \;=\; -2\delta^2 mR \;+\; 2\delta(1+m^2), \tag{3.53}$$

$$C = \delta^2 mR^2 - \delta(3R + 2m\Delta z_R + 2mH_T + 3m^2R + 2m^2X_1), \tag{3.54}$$

$$D = \delta(R^2 - R^2m^2 + 4mRH_T + 4m^2RX_1 - 2m^3R^2) - 2(H_T + mX_1 + \Delta z_R + m^2H_T + m^2\Delta z_R + m^3X_1), \tag{3.55}$$

$$E = -2\delta(mR^2H_T + m^2R^2X_1) + 2(RH_T + RmX_1 + 2mH_T\Delta z_R + m^2RH_T + 2m^2\Delta z_RX_1 + m^3RX_1). \tag{3.56}$$

In (3.51) the solution is given by a real root $X = x_1$, maximum value and $x_1 > 0$. Therefore, the reflection point is at the coordinate $(\ X, m(X - X_1)\ )$.

Figure 19 presents the behavior of rays above a wedge. The rays were curved by refractive effects of the standard atmosphere ($dN/dz = 40$ N/km).

3.2.4 Ray paths under ducting conditions

The standard atmosphere model is not used in cases of anomalous propagation. In anomalous propagation the rays are reflected in the ground and refracted several times, being confined in a thin layer of the atmosphere and being guided over long distances along the Earth's surface (Picquenard, 1974). This layer, in which EM waves are guided, is known as tropospheric duct. Guiding occurs mainly for frequencies above the Ultra High Frequencies (UHF) band and low elevation angle conditions (Hall; Barclay; Hewitt, 1996). Such conditions significantly affect the radio communication links and radar performance (Apaydin; Sevgi, 2017).

Ducts can be formed close to the earth's surface (*surface ducts*) or several meters above it (*elevated ducts*). Surface ducts are generated when a mass of hot air approaches humid ground or over tropical seas (called *evaporation ducts*) (Skolnik; Others, 1980).

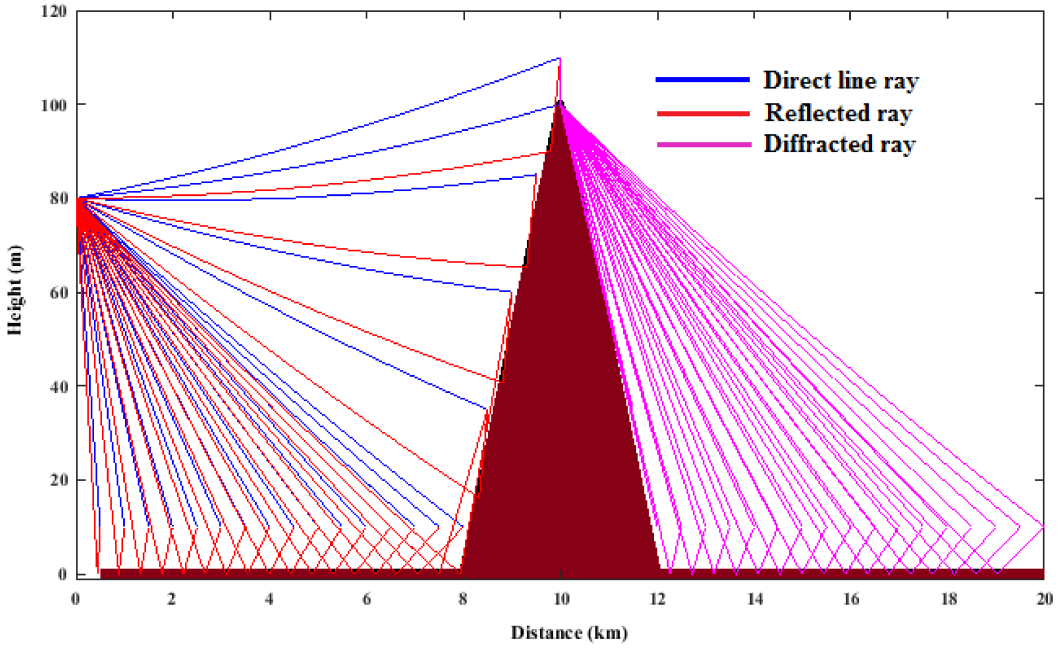

Figure 19 – Ray paths above a wedge.

Elevated ducts appear when a mass of cold air reaches an area of high pressure, a phenomenon that occurs mainly above the clouds and is of interest in UHF communications (Picquenard, 1974).

Previously, ray paths were described under conditions of constant refractivity gradient. The aim of this part is to present a ray path modeling under ducting conditions by using a numerical approximation to solve the equation (3.19) (Valtr, 2017).

Equation (3.19) is rewrite as:

$$\frac{d^2z}{dx^2} = \frac{d}{dz}n(z) \quad \rightarrow \quad z'' = F(z) \tag{3.57}$$

Notice that when using earth flattening transformation the above equation is in fact:

$$\frac{d^2z}{dx^2} = \frac{d}{dz}m(z). \tag{3.58}$$

Figure 20 shows the refractivity dependence with height, two heights (h_1 and h_2) are defined for the formation of ducting conditions. It is also possible to observe the relationship between refractivity (N) and the gradient of refractive index ($g = dn/dz$), which is used to model the ray paths.

Based on Figure 20 the function $F(z)$ is given as:

$$F(z) = \begin{cases} g_1 & for \quad z \leq h_1 \\ g_2 & for \quad h_1 < z \leq h_2 \\ g_1 & for \quad z \geq h_2 \end{cases} \tag{3.59}$$

The following solution is assumed,

$$z(x) = c_0 + c_1(x - x_0) + c_2(x - x_0)^2 + ... = \sum_{n=0}^{\infty} c_n(x - x_0)^n, \tag{3.60}$$

based on Taylor series and initial conditions (equations (3.23) and (3.24)) the equation (3.60) is expressed as:

$$z(x) = z(x_0) + z'(x_0)(x - x_0) + \frac{z''(x_0)}{2!}(x - x_0)^2 + ... = \sum_{n=0}^{\infty} \frac{z^{(n)}(x_0)}{n!}(x - x_0)^n \tag{3.61}$$

Analyzing the derivatives shown in equation (3.61):

$$z'' = F(z), \tag{3.62}$$

$$z'''(x_0) = \frac{dF\{z(x_0)\}}{dz} \cdot \frac{dz(x_0)}{dx}. \tag{3.63}$$

It is possible deduce for higher order derivatives,

$$\frac{d^n F}{dz^n} = 0\ , \quad \forall n > 0 \quad \Rightarrow \quad z^{(n)} = 0\ , \quad \forall\ n > 2 \tag{3.64}$$

Equation (3.61) is rewritten as:

$$z(x) = z(x_0) + z'(x_0)(x - x_0) + \frac{z''(x_0)}{2!}(x - x_0)^2. \tag{3.65}$$

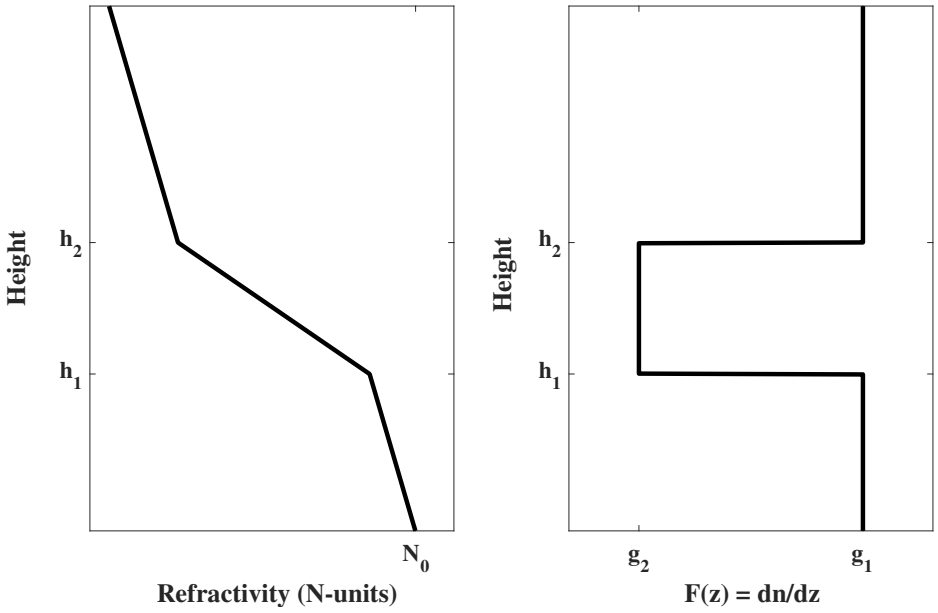

Figure 20 – Refractivity Profile and $F(z)$ Function.

Knowing the z-position of the ray at distance x_0, the z-position at distance $x_0 + \Delta x$ is calculated as:

$$z(x_0 + \Delta x) = z(x_0) + z'(x_0) \cdot \Delta x + \frac{z''(x_0)}{2} \cdot \Delta x^2, \tag{3.66}$$

whose first derivative is:

$$z'(x_0 + \Delta x) = z'(x_0) + z''(x_0) \cdot \Delta x, \tag{3.67}$$

and Δx has to be "small".

Figure 21 presents the results for a radio propagation case that includes the surface-based duct conditions. The ray paths are calculated according to the formulation presented in this Section. The radio wave propagation behavior obtained by the SSPE algorithm is also shown (specifically, it is the distribution of the value of the reduced auxiliar function of the field $u(x, z)$ throughout the analyzed domain). It is possible to observe the agreement between the ray paths (RT approach) and the field distribution achieved with PE numerical solution.

Figure 22 presents the results for a radio propagation case that includes the conditions of a elevated duct. As analyzed in Figure 21, it is possible to infer the agreement between the ray paths and the field distribution achieved with SSPE solution.

3.2.5 Calculation of the ray optical length

In order to calculate the electric field intensity arriving the receiver point, it is necessary to obtain the distance traveled by the ray. The optical length of a ray between points A and B is obtained as (Valtr; Pechac, 2006):

$$l = \int_A^B n(\mathbf{r}) dl, \tag{3.68}$$

where $\mathbf{r}$ is a vector representing the position in space:

$$\mathbf{r}(x, z) = x\hat{\mathbf{x}} + z\hat{\mathbf{z}} \tag{3.69}$$

$$\mathbf{r}(x) = x\hat{\mathbf{x}} + \left(\frac{\delta x^2}{2} + Kx + h_t\right)\hat{\mathbf{z}} \tag{3.70}$$

and l is the optical length. The integral in (3.68) can be solved based on the following:

$$\int_C f ds = \int_a^b f(\mathbf{r}(t)) \left\|\mathbf{r}'(t)\right\| dt, \tag{3.71}$$

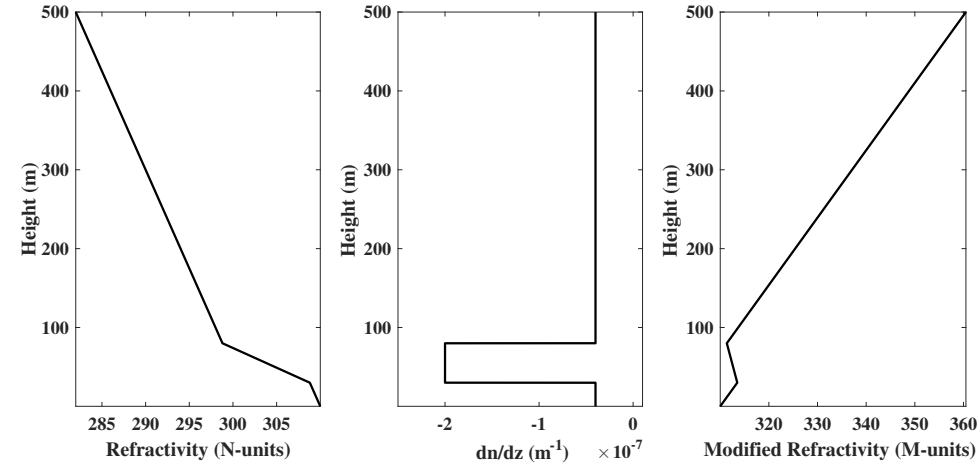

(a)

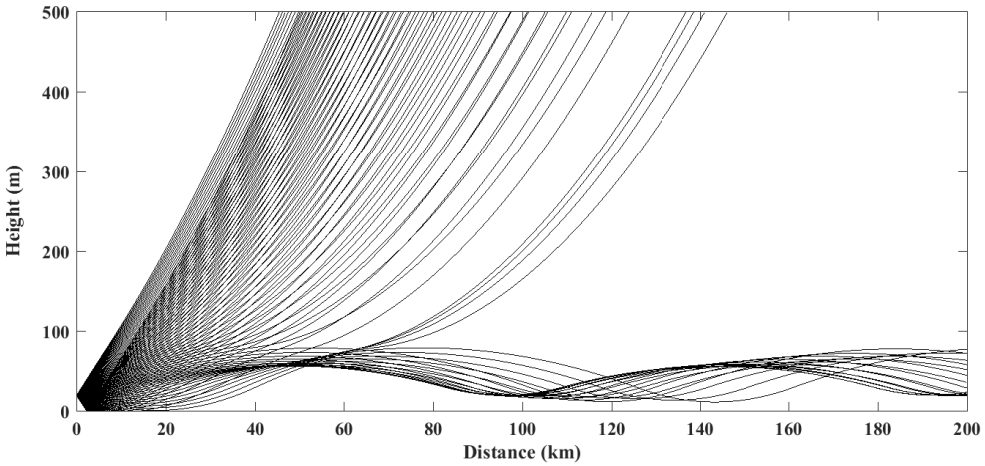

(b)

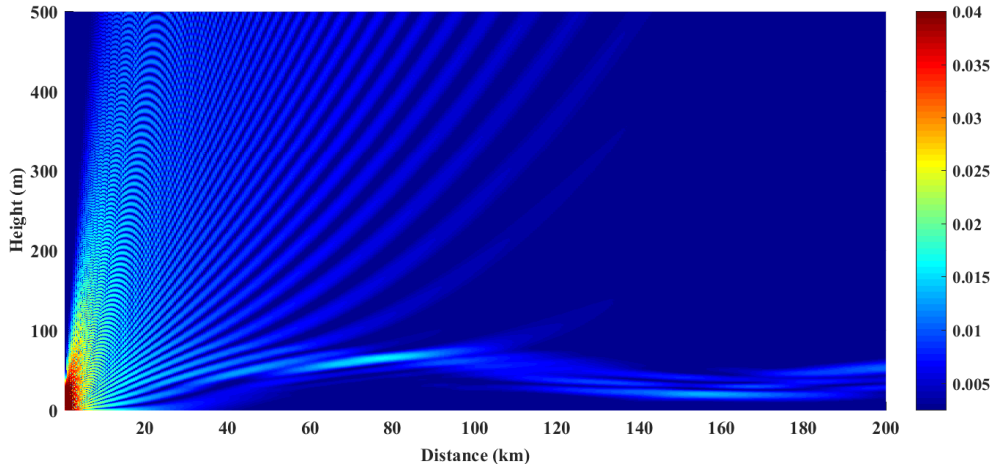

(c)

Figure 21 – Radiopropagation under Surface-based duct conditions (a) Refractivity Profile, (b) Ray paths and (c) Radiopropagation behavior at 15 GHz obtained throught SSPE.

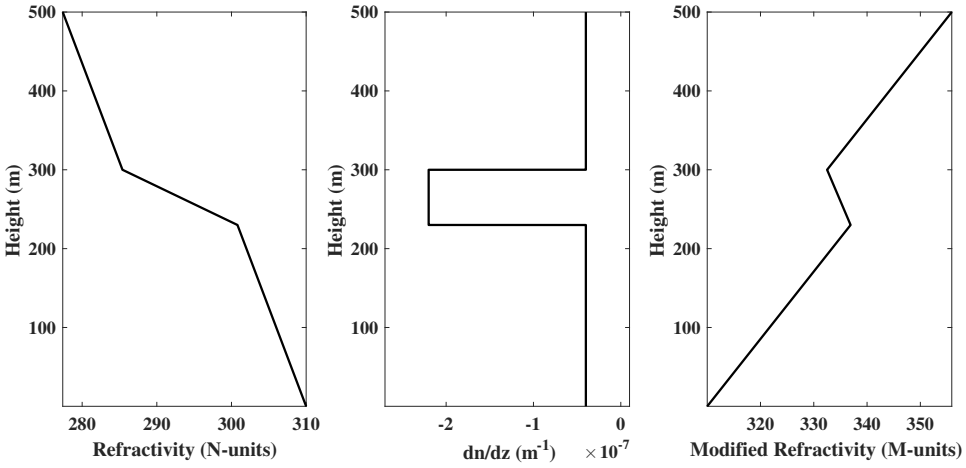

(a)

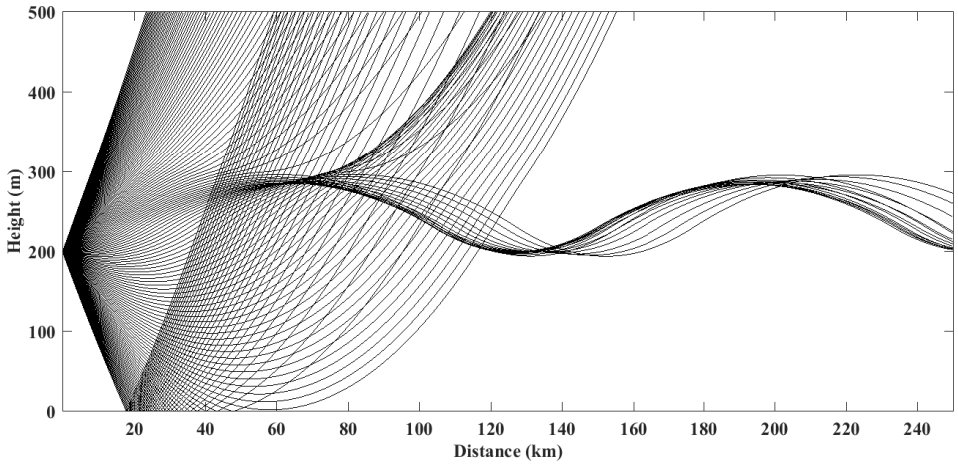

(b)

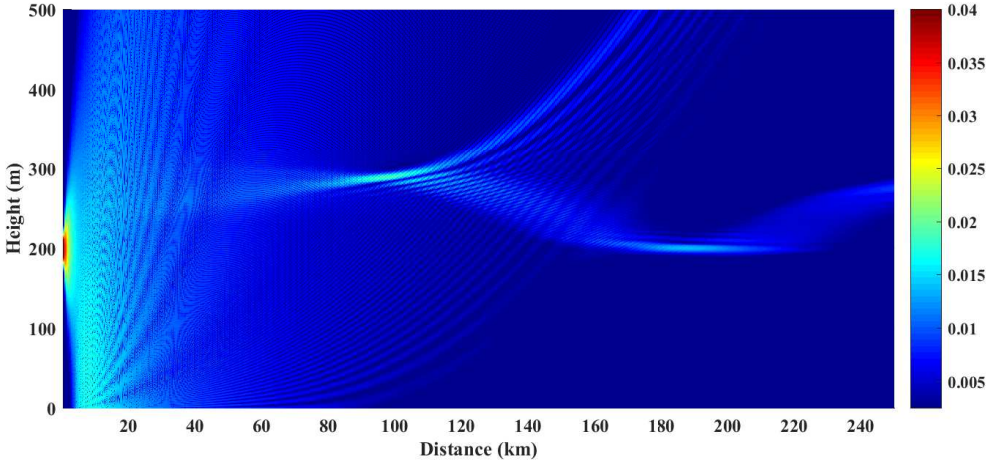

(c)

Figure 22 – Radiopropagation under Elevated duct conditions (a) Refractivity Profile, (b) Ray paths and (c) Radiopropagation behavior at 15 GHz obtained throught SSPE.

where,

$$f(\mathbf{r}(t)) = f(\mathbf{r}(x)) = n_0 + \delta\left(\frac{\delta x^2}{2} + Kx + h_t\right), \tag{3.72}$$

which is a scalar function, and:

$$\|\mathbf{r}'(t)\| = \|\mathbf{r}'(x)\| = \sqrt{1 + (\delta x + K)^2}. \tag{3.73}$$

Therefore, for the length of the direct ray:

$$l_{direct} = \int_0^{X_R} n_0 \left[1 + \delta\left(\frac{\delta x^2}{2} + Kx + h_t\right)\right]\left(\sqrt{1 + (\delta x + K)^2}\right) dx \tag{3.74}$$

and, for the length of the reflected ray:

$$\begin{aligned} l_{reflected} = &\int_0^{X} n_0 \left[1 + \delta\left(\frac{\delta x^2}{2} + Kx + h_t\right)\right]\left(\sqrt{1 + (\delta x + K)^2}\right) dx + \\ &\int_X^{X_R} n_0 \left[1 + \delta\left(\frac{\delta (x-X)^2}{2} + K(x-X) + h_t\right)\right]\left(\sqrt{1 + (\delta (x-X) + K)^2}\right) dx. \end{aligned} \tag{3.75}$$

3.3 Proposed algorithm for a modified radiopropagation multipath model

The algorithm is shown in Figure 23 as a flowchart. The direct ray, reflection and diffraction analysis are implemented by three blocks (see Figure 23) which are executed in parallel. To run those three blocks it is necessary to know the following input parameters: electromagnetic properties, refractivity gradient of the medium, and locations of the transmitter and receiver.

3.3.1 Direct ray analysis

Knowing the input parameters, the launch angle of the direct ray is calculated according to equation (3.31), then the direct ray path is obtained from equation (3.30). In the next step, it is investigated if a direct ray hits the receiver. If the algorithm identifies that the receiver is reached, it proceeds to save the path parameters, and then, continues to post-processing. Otherwise, the algorithm ignores the direct ray path and continues to post-processing.

Two situations can occur so that a ray path does not hit on a receiver point. The first situation is that the algorithm identifies that there is an obstacle that interrupts the ray path. The second one is that due to the curvature of the ray path, it cannot reach the receiver. These above criteria are applied for direct, incident and reflected ray paths.

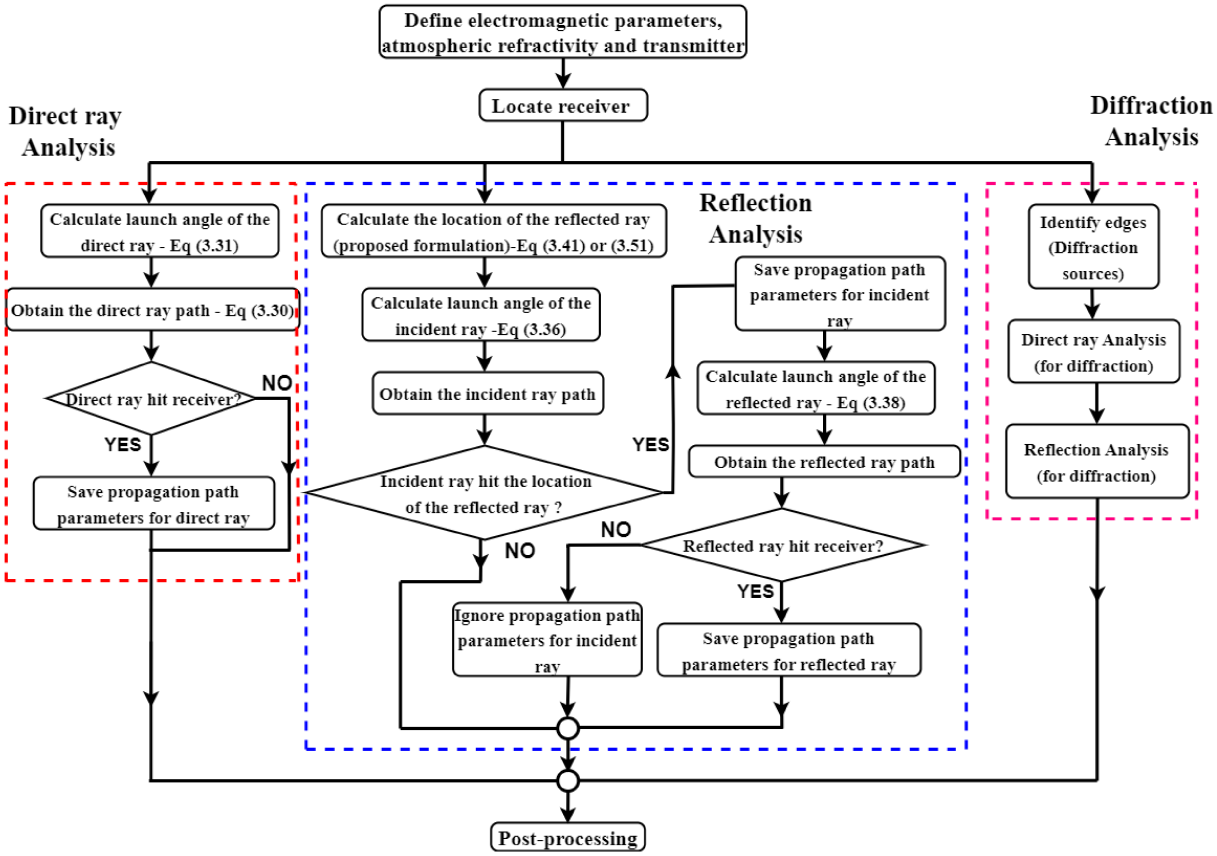

Figure 23 – Flowchart for a modified multipath model based on RT techniques.

3.3.2 Reflection analysis

The location of the reflection point is calculated by using the formulation proposed herein, equation (3.41) or (3.51) is used depending on the situation, either flat or sloping terrain. Once known the location where the ground-reflection occurs, it is possible to calculate the launch angle of the incident ray from equation (3.36), then the incident ray path is obtained. In the next step, it is investigated if the obtained incident ray path hits the location of the point reflection. If the algorithm identifies that the reflection point is reached, it proceeds to save the path parameters. Otherwise, the algorithm ignores the obtained incident ray path and continues to post-processing.

If the incident ray path hits the reflection point, it is possible to calculate the launch angle of the reflected ray from equation (3.38), then, the reflected ray path is obtained as indicated by Figure 23. In the next step, it is learned if the reflected ray path hits the location of the receiver point. If the algorithm identifies that the receiver point is reached, it proceeds to save the path parameters, and then, continues to post processing. Otherwise, the algorithm ignores the obtained reflected ray path and the path parameters for incident ray, consequently, continues to post-processing.

3.3.3 Diffraction analysis

The algorithm has the ability to identify edges that generate diffraction. An analysis of direct, incident and reflected rays associated with the diffraction phenomenon is carried out. The formulation presented in Section 3.1.4 is used by the algorithm for diffraction analysis

3.3.4 Post-processing

Everytime that a ray hits a receiver point, the following path parameters are computed and saved by our algorithm: $\tau_i(t)$: time delay of arrival (TDA) of path, $\overline{T}_i(t)$: polarimetric transmission matrix of path, $\Omega_{T,i}(t)$: direction of departure (DoD) of path and $\Omega_{R,i}(t)$: direction of arrival (DoA) of path. To calculate the total EM field at each receiver point, a coherent sum is computed, taking into account the individual contribution of each multipath component.

In the case studies carried out in this chapter, the following propagation mechanisms are processed by the algorithm: a direct ray path, an incident-reflected ray path, diffraction ray paths and diffraction-reflection combinations arriving at the receiver point, accumulating in maximum two consecutive propagation mechanisms (see Figure 32).

3.4 Case studies

To preliminarily validate our proposal for a modified RT technique, two canonical cases are defined: a flat terrain and wedge. In both cases, it is considered perfect electrical conductor (PEC) surfaces and effects of the standard atmosphere.

3.4.1 PEC flat terrain

This study was done to compare a modified two-ray model and the SSPE method for a specific radiopropagation problem that includes atmospheric effects. The environment is a PEC flat terrain. The simulation use a frequency of 2.0 GHz and the transmitter is located at 100 meters of height. The analysis considers vertical polarization and standard atmosphere. The variation of the index of refraction is modeled as:

$$n(z) = N(z) \times 10^{-6} + 1, \tag{3.76}$$

where,

$$N(z) = 304 - 40z. \tag{3.77}$$

Equations (3.76) and (3.77) model the variations of the index of refraction considering the first kilometers of the standard atmosphere and z corresponds to a certain height position.

Figure 24a shows the comparison between the Ray Tracing and SSPE methods. This graph illustrates the horizontal profiles of attenuation at 120 meters of height. For the first distances, the difference between the two results curves is mainly due to the lack of precision of the SSPE method for distances close to the transmitter, therefore, the result of Ray Tracing in these distances is considered as more reliable. However, it can be observed that both methods have a similar behavior, then is possible to affirm that the atmospheric effects into two-ray model are included favorably.

Figure 24b presents the vertical pathloss profile results calculated with Ray Tracing and SSPE at 25 km. A good agreement is observed between the two pathloss curves. Taking these preliminary results into consideration, it can be validated the proposed formulation for the modified two-ray model when tested in a specific radio propagation problem, considering a PEC flat terrain and standard atmosphere refractivity effects.

3.4.2 PEC wedge

In this case study a radiopropagation problem that includes terrain factors and atmospheric effects is analyzed. The terrain profile is a perfectly conducting wedge centered at 10 km. It is used a frequency of 2.0 GHz, the transmitter is located at 80 m of height and the reception points at 10 m of height along the terrain, from 100 m to 20 km. The analysis considers vertical polarization and the variation of the index of refraction models the first kilometers of the standard atmosphere.

Figure 25 presents the comparison between the proposed Ray Tracing and SSPE method. In this graph, pathloss horizontal profiles are shown for different heights of the

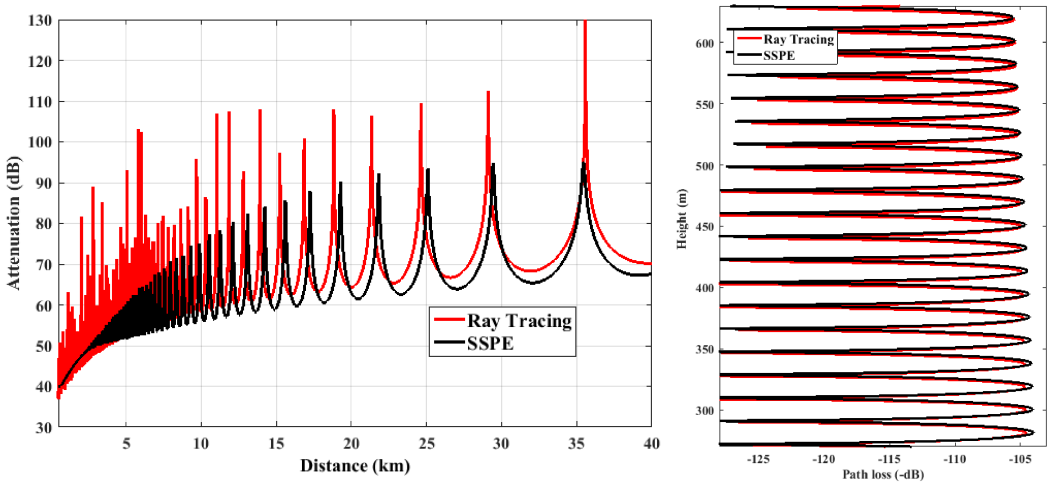

(a) (b)

Figure 24 – Results obtained with Modified RT and SSPE algorithms - PEC flat terrain case: (a) Attenuation at 120 meters of height and (b) Vertical pathloss profile at $x = 25$ km .

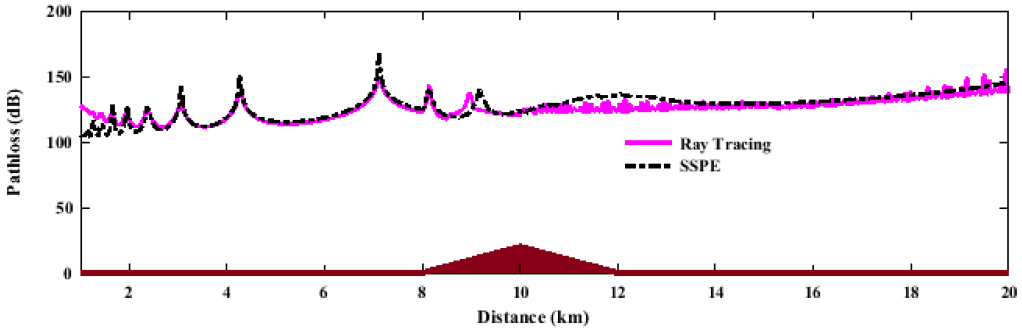

(a)

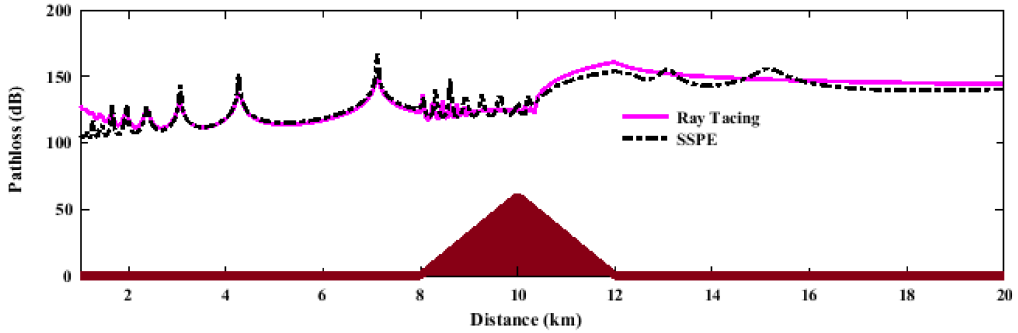

(b)

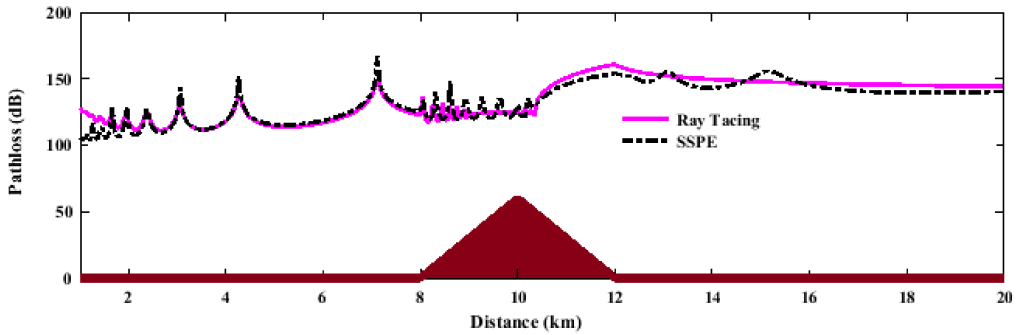

(c)

Figure 25 – Pathloss results of Ray Tracing and SSPE above a perfectly conducting wedge of height: (a) 20 m, (b) 60 m and (c) 100 m.

wedge, 20 m, 60 m and 100 m, respectively. In the three situations, it can be observed that the proposed formulation of a modified ray tracing unified with UTD has a similar behavior regarding to SSPE results.

In Figure 26, pathloss vertical profiles are presented, the curves also shown a good agreement between the two approaches. Then, it is possible to affirm that diffraction and atmospheric effects, into RT technique, are favorably included in this radiopropagation problem.

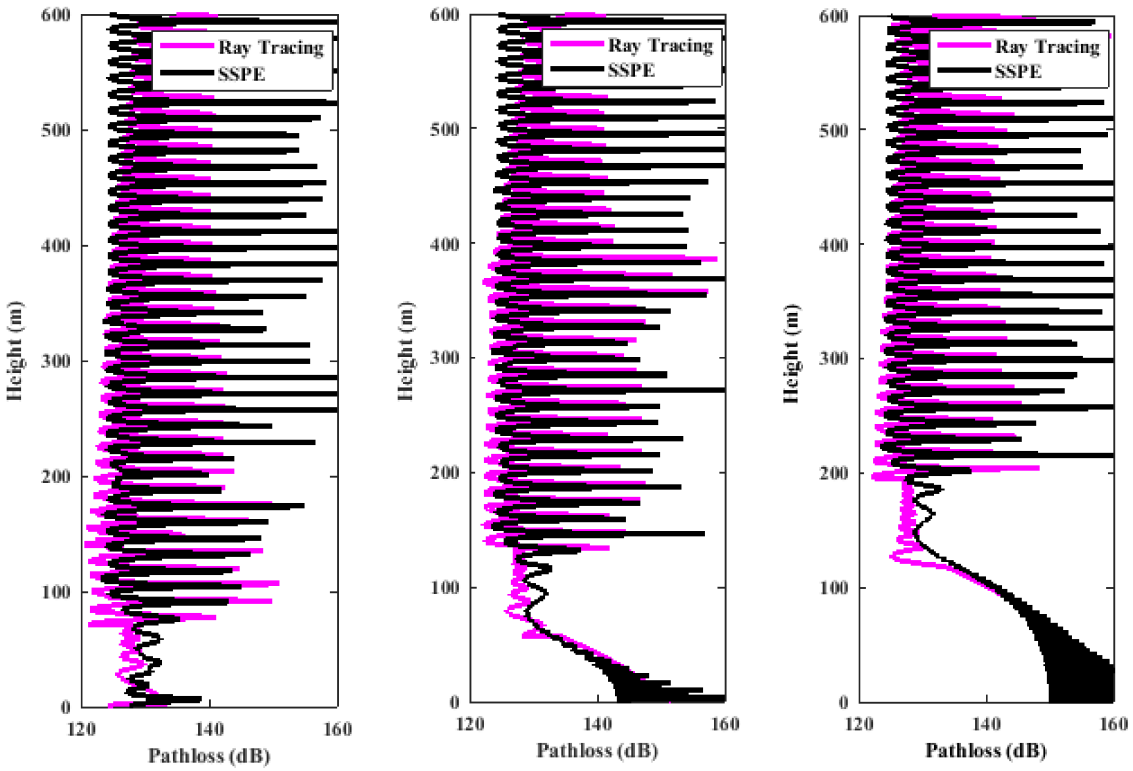

Figure 26 – Pathloss results of a Modified Ray Tracing and SSPE algorithm at 15 km for a case study that includes a perfectly conducting wedge of height: (a) 20 m, (b) 60 m and (c) 100 m.

3.4.3 A comparison between a Modified RT, GO-UTD approach and the DMFT-SSPE methods

This canonical test includes atmospheric effects, terrain factors and lossy surfaces. The terrain profile is a lossy wedge centered at 20 km. It is used a frequency of 2.0 GHz, the transmitter is located at 80 m height and the ground electrical parameters are $\epsilon_r = 15$ and $\sigma = 0.012$ S/m. The case study considers vertical polarization and the variation of the refraction index for the first kilometers of the standard atmosphere.

Figure 27 shows a comparison between the proposed RT technique in this work, the GO-UTD solution and DMFT-SSPE algorithm. In this figure, pathloss horizontal profiles are illustrated for two different heights of the wedge, 60 m and 100 m, respectively. The receiver points are located at 10 m of height along the terrain, from 100 m to 40 km. For both wedge heights, it can be observed that the three curves have a similar behavior. However, at long-range distances the results of the modified RT technique and the DMFT-SSPE numerical solution are closer to each other. The above occurs because at these distances the effects of atmospheric refractivity are more noticeable. Consequently, it is also possible to deduce that the classical GO-UTD approach does not consider the

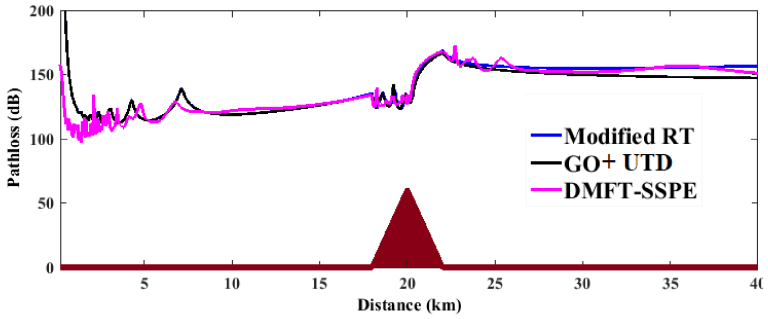

(a)

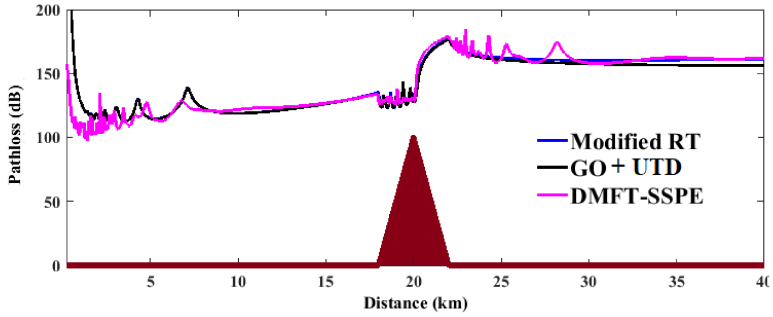

(b)

Figure 27 – Pathloss results of Modified RT, GO-UTD and DMFT-SSPE above a lossy wedge of height: (a) 60 m and (b) 100 m.

curved paths of rays. Therefore, a modified RT technique (proposed in this work) and the DMFT-SSPE algorithm (implemented in this research) are presented as reasonable alternatives to treat this kind of radio propagation problems.

In Figure 28 pathloss vertical profiles calculated at 30 km are presented. It is possible to corroborate the previously discussed, since the modified RT and DMFT-SSPE curves have a good agreement of their results, this being more evident in the first heights.

3.4.4 Mixed scenario

The environment is a mixed scenario, with a total extension of 40 km. The terrain profile is a lossy wedge of 80 m height and centered at 20 km, and whose initial and final positions are located at 12 km and 28 km, respectively. In this case study, the ground region is characterized as a standard ground surface ($\epsilon_r = 15$ and $\sigma = 0.012$ S/m) and a saltwater region ($\epsilon_r = 81$ and $\sigma = 2$ S/m) is placed behind the wedge, from 28 km to 32 km. The refractivity variation is modeled as: $N(z) = 304 - 100z$, a linearly decreasing refractivity altitude profile, which corresponds to a surface duct (Akleman; Sevgi, 2000). In this case, we use a gradient of modified refractive index $dm/dz = dn/dz + 1.57 \times 10^{-7}$ (Valtr; Pechac, 2005a). The transmitter is located at 100 m height, the simulation uses a frequency of 5.4 GHz and vertical polarization.

In order to calculate the pathloss horizontal profile using the Modified RT algorithm,

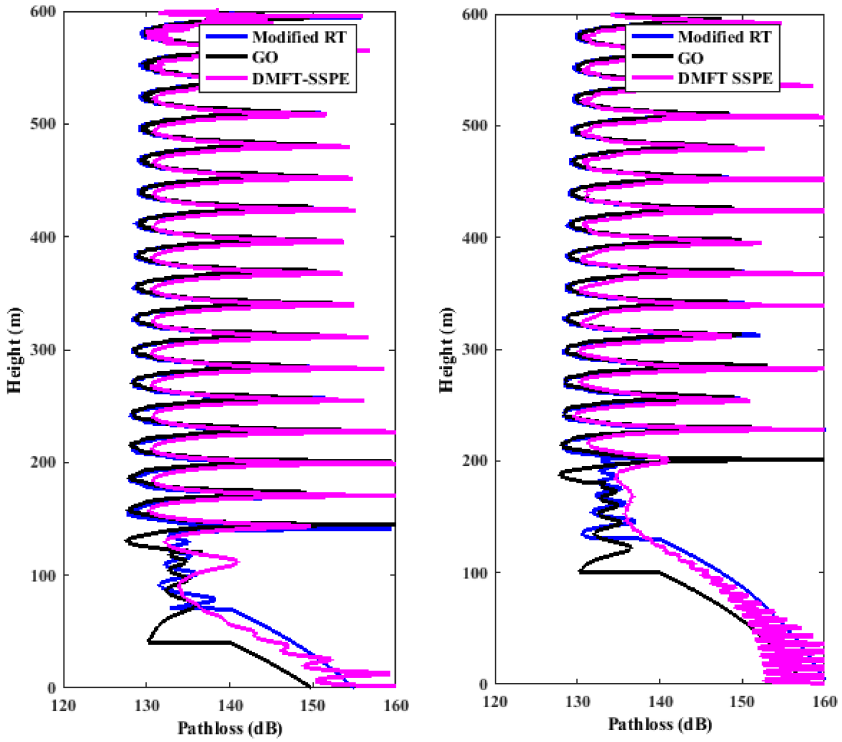

Figure 28 – Pathloss results of Modified RT, GO and DMFT-SSPE at 30 km for a case study that includes a lossy wedge of height: (a) 60 m and (b) 100 m.

it is defined a horizontal step size ($\Delta x = 10$ m) and receiver points located at 10 m height along the terrain. Likewise, the vertical step size ($\Delta z = 0.19$ m) is used to calculate the pathloss vertical profile at $x = 32$ km.

The source is modeled as a Gaussian antenna beam pattern. In most 2-D long-range radiopropagation models, this type of source modeling is chosen because it can adjust beam-width and beam tilt and provide an approximate representation for paraboloid dish antennas (Zhang et al., 2016).

Figure 29 shows the scenario scheme and depicts the conformation of ray paths to calculate the pathloss horizontal using the Modified RT algorithm. Figure 30 depicts the 2-D received power distribution achieved with DMF-SSPE. In this graph, the very low levels of received power that are perceived at the closest distances to the transmitter are not expected, since it does not correspond to a natural behavior of the phenomenon. However, this response is due to the shape of the directional Gaussian antenna pattern used in the simulations. To estimate a pathloss horizontal profile, a correct range of receiver points is chosen, from 1.5 km to 40 km.

In Figure 31 the comparison between the proposed Modified RT and DMFT-SSPE numerical algorithm is shown. The horizontal and vertical profiles for pathloss results are illustrated in Figures 31a and 31b, respectively.

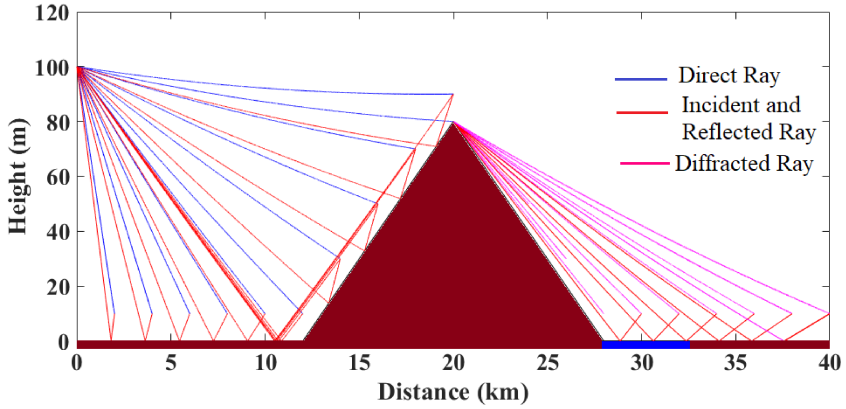

Figure 29 – Scenario scheme and ray paths to calculate a pathloss horizontal profile using $dN/dz = -100$ N/km.

The statistics are summarized in Table 3. It is possible to observe that a good agreement is obtained in statistic comparison between our proposal of a Modified RT and DMFT-SSPE results.

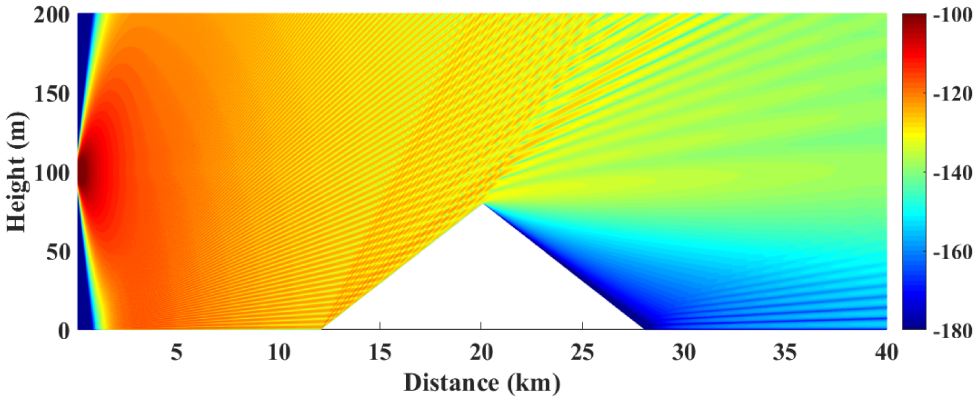

Figure 30 – Received power (dBW) vs. distance-height obtained with DMFT-SSPE for mixed scenario at 5.4 GHz.

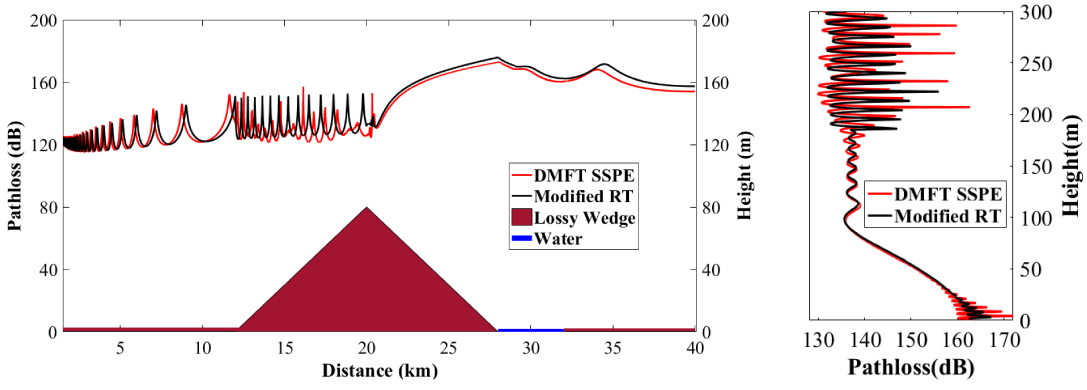

(a) (b)

Figure 31 – Pathloss results: (a) Horizontal Profile at 10 m height and (b) Vertical profile at $x = 32$ km.

Table 3 – Statistic comparison for pathloss results in mixed scenario case

Pathloss Profile	**Mean Absolute Difference (dB)**	**Standard Deviation (dB)**
Horizontal	4.45	6.17
Vertical	2.90	4.92

3.5 Chapter Conclusions

This Chapter proposed a novel formulation to include refractive effects into two-ray model. Subsequently, a modified RT model was implemented. Two case studies was analyzed: PEC flat terrain and PEC wedge, both with standard atmosphere conditions. The obtained results of a RT technique shown a similar behavior compared to the SSPE numerical solution. Canonical tests are useful for analyzing performance of the technique and implementations in controlled environments. The adequate launching angle calculation guarantees the arrival of the reflected ray at a specific receiver point. Consequently, it is possible conclude that the RT based model can includes atmospheric effects into ray paths, maintaining good results. In addition, it can be observed that the proposed formulation of a modified ray tracing unified with UTD has a similar behavior regarding to SSPE results.

4 Modified RT and DMFT-SSPE Algorithms Applied in Colombian Environments

In this Chapter, the Modified RT proposed in this research, and the DMFT-SSPE techniques are applied in Colombian environments, in order to predict radio coverage in environments that demand radiopropagation modeling challenges.

4.1 Radiopropagation challenges in Colombian environments

In addition to mountainous terrain, typical of the Andean countries, there are geographic areas in Colombia, such as the Pacific coast region, which is a rain forest with big mountains and sea, as well as salted water combined with forest. This conditions makes propagation challenging and suitable to experiment with different techniques to predict coverage for wireless systems.

Recently, TV White Spaces (TVWS) technology and 5G applications are projected to provide broadband services in remote rural areas. TVWS is based mainly in the IEEE 802.22 standard, intended to provide wireless broadband service in remote areas, using the spectrum holes in the TV band (Navarro et al., 2022). On the other hand, as explained in Chapter 1, 5G wireless networks are aimed to the meeting of the objectives of high-speed transmission and large increase in channel capacity. Several sub-6 GHz frequencies are being tested, specifically, 2.3 GHz, 3.6 GHz and 5.4 GHz bands are proposed in Latin American countries to be used in 5G communications (Leonor et al., 2022).

In this Chapter, the ability of the DMFT-SSPE and Modified RT algorithms to be used as coverage prediction tools in realistic environments is evaluated. In the previous Chapters, these algorithms were tested in canonical situations.

The most relevant contribution of this Chapter is to demonstrate the applicability of Modified RT and DMFT-SSPE algorithms in realistic situations that consider most of the non-homogeneous conditions of the environments (Parada et al., 2022). The simulation results are obtained for two places: Cúcuta, which is a city surrounded by mountains in Andean region, and Buenaventura, which is a tropical rain forest in Colombian Pacific coast. Additionally, the case studies focus on using projected frequencies to provide connectivity to Colombian rural areas, based on TVWS technology and pioneering 5G applications.

4.2 Simulation and results

The formulations and the corresponding algorithms of a modified RT and DMFT-SSPE are applied to predict coverage in two Colombian environments: Mountainous terrain and Tropical rain forest. In both case studies, the pathloss results obtained with the two techniques are compared with each other.

4.2.1 Cúcuta city case

This realistic scenario is located in Cúcuta city. It consists of a terrain profile with an approximate extension of 15 km, the surface is characterized as a standard ground and the refractivity variation is modeled as: $N(z) = 305.66 - 60z$, according to Recommendation ITU-R P.453-14 for the environmental conditions of the mentioned city. The terrain profile information is collected using the NASA Shuttle Radar Topography Mission (SRTM) Version 3.0 dataset.

The transmitter is located at 100 m height and the simulation uses a frequency of 2.0 GHz and vertical polarization. To calculate the pathloss horizontal profile, both techniques use a horizontal step size ($\Delta x = 50$ m) and the receiver points are located at 10 m height along the terrain.

Figure 32 shows the conformation of ray paths at $x = 1000$ m and 10 m height to calculate Pathloss and the PDP at this receiver point through the Modified RT algorithm. In Figure 33 the PDP is depicted, in this way, the ability of the proposed algorithm to characterize the radio channel is demonstrated.

It is possible to obtain a 2-D received power distribution with DMFT-SSPE, since this numerical approach allows to discretize and calculate the EM field solution of the entire analyzed scenario. Hence, we generate Figure 34 using a DMFT-SSPE algorithm. In Figure 34, it can be seen that at shorter distances there are Non-Line-of-Sight (NLOS)

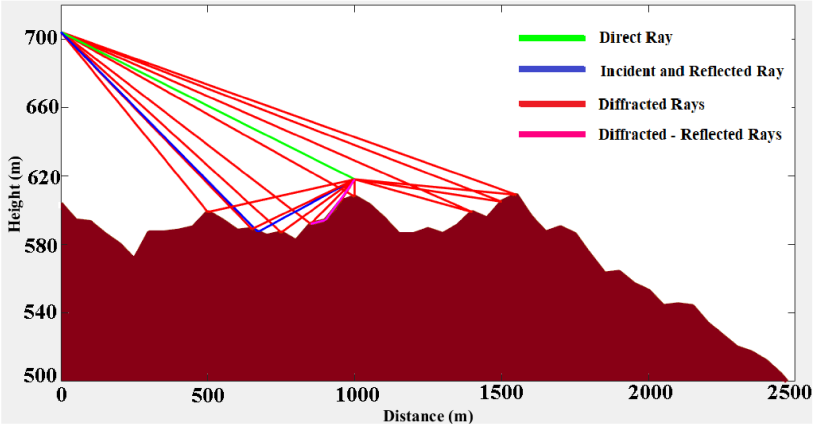

Figure 32 – Ray paths to calculate Pathloss results and PDP by using a Modified RT algorithm.

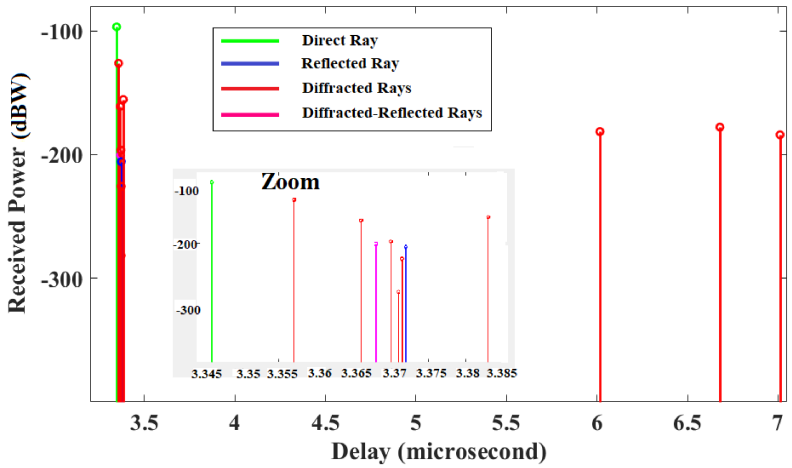

Figure 33 – Power Delay Profile at $x = 1000$ m and 10 m height.

regions, due to the particularities of the terrain profile of the analyzed scenario, and taking into account that the height of the receiver points is 10 m. Furthermore, it is also possible to note that at longer distances there are line-of-sight (LOS) regions, and consequently, this propagation mechanism implies a greater contribution to the final value of received signal intensity at those receiver points. The previously described can be observed in the results of the pathloss curves obtained along the terrain profile (see Figure 35).

In this realistic case, we also obtain results from a RT technique that does not consider atmospheric effects, denominated Non-Modified RT. The purpose is to observe if the inclusion of atmospheric refractivity in the RT technique leads to promising results, when comparing the results obtained with respect to reliable and consolidated techniques, such as the DMFT-SSPE numerical approach. Figure 35a illustrates the comparison of the pathloss horizontal profile results obtained with the Non-Modified RT and DMFT-SSPE tecniques. Similarly, Figure 35b shows the pathloss curves results obtained with the

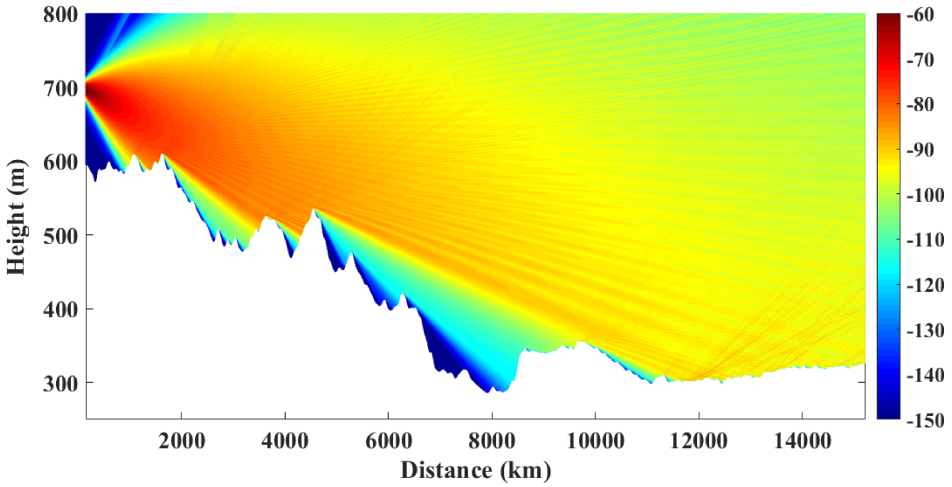

Figure 34 – Received Power (dBW) vs. distance-height obtained with DMFT SSPE for Cúcuta city case at 2.0 GHz.

proposed Modified RT algorithm and DMFT-SSPE solution.

In Figure 35 it can be observed that in some positions no results are obtained, this happens because our RT algorithms use basic combinations of propagation mechanisms and therefore the ray paths do not hit on certain observation points. The proposed alternative is the combination of many more propagation mechanisms, however, this approach generates a high computational cost. The simulations show that the non-hit points of the Non-Modified and the Modified RT are different, which is explained by the slightly different path that the inclusion of atmospheric refractivity effect produces.

Table 4 summarizes the statistics. It can be perceived that a Modified RT algorithm shows a encouraging result in statistical comparison. However, in order to consolidate a conclusion about the results obtained with the proposed algorithm, it is necessary to analyze its performance and behavior in another scenario and at a different frequency band (see Section 4.2.2).

Another of the results obtained in the Cúcuta city scenario are the vertical pathloss profiles calculated at the final position of the radio link, and using the 2.0 GHz and 3.6 GHz frequency bands.

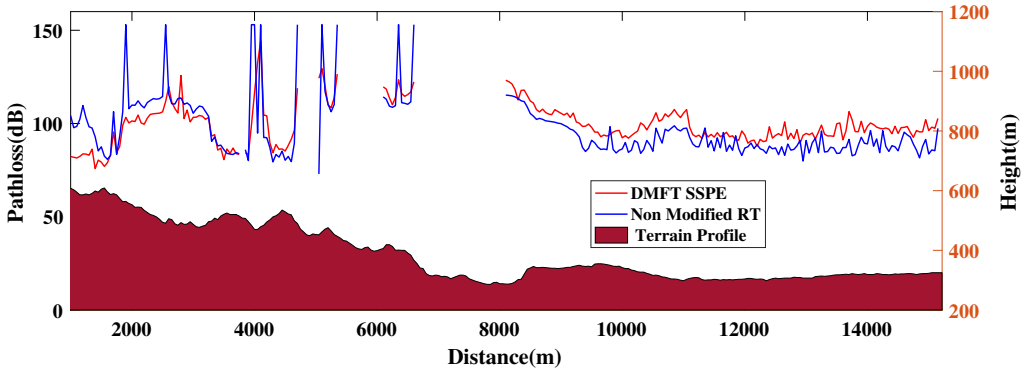

(a)

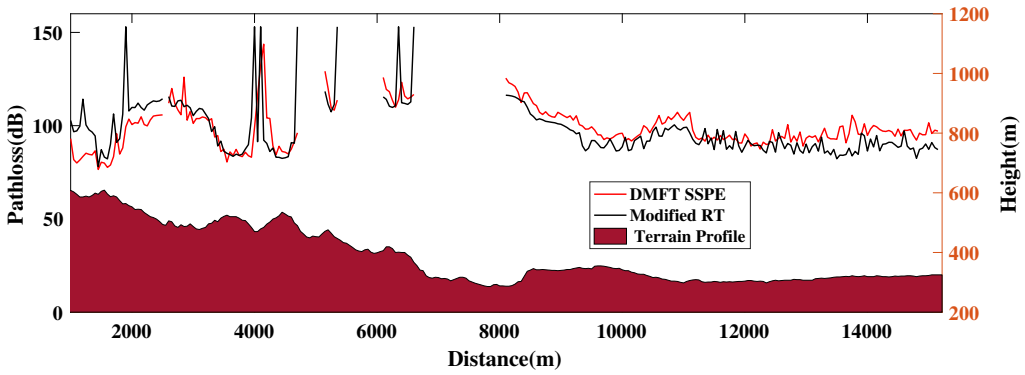

(b)

Figure 35 – Pathloss Horizontal Profile results for Cúcuta city case: (a) Non-Modified RT versus DMFT-SSPE and (b) Modified RT versus DMFT-SSPE.

Table 4 – Statistic comparison for pathloss horizontal results in Cúcuta city case

RT Technique	Mean Absolute Difference (dB)	Standard Deviation (dB)
Non Modified	8.55	11.75
Modified	7.84	11.57

Figure 36 shows the comparison of the vertical pathloss curves obtained with the Modified RT and DMFT-SSPE approach. Figures 36a and 36b depict the results at 2.0 GHz and 3.0 GHz, respectively.

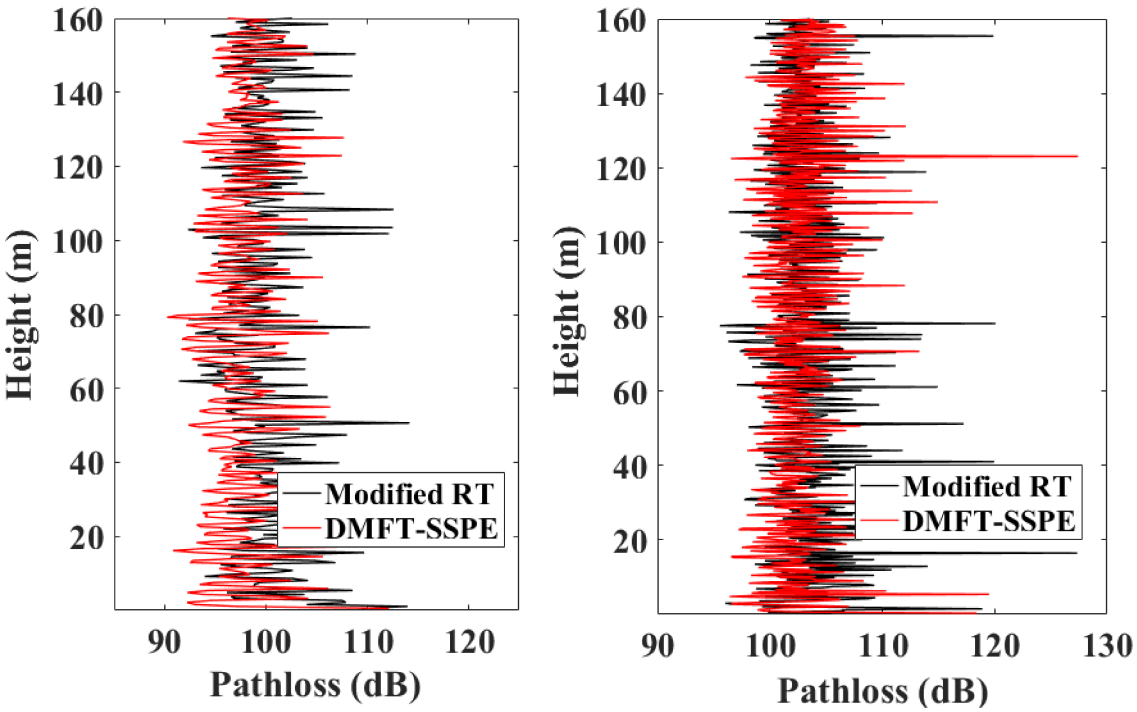

Figure 36 – Pathloss vertical profiles calculated at the final position of the radio link for Cúcuta city case at: (a) 2.0 GHz and (b) 3.6 GHz

Table 5 summarizes the statistical comparison for the two frequency bands analyzed. Based on the results of Figure 36 and Table 5, it is possible to note the good agreement between the vertical pathlos results achieved with both techniques in this realistic scenario and at the 5G frequency bands studied.

Table 5 – Statistic comparison for pathloss vertical results in Cúcuta city case

Frequency band	Mean Absolute Difference (dB)	Standard Deviation (dB)
2.0 GHz	3.75	5.04
3.6 GHz	3.60	4.89

4.2.2 Pacific region case

This realistic scenario is located in the Colombian Pacific Region, which is a tropical rain forest region with dispersed population, adverse geographical conditions and lack of connectivity. It consists of a rural long-distance terrain profile with an approximate extension of 21 km, the surface is characterized as a damp ground ($\epsilon_r = 27$ and $\sigma = 0.02$ S/m) and the refractivity variation is modeled as: $N(z) = 378 - 60z$. The transmitter is located at 25 m of height above terrain, this first simulation uses a frequency of 3.5 GHz and vertical polarization. In order to calculate the pathloss horizontal profile, the radiopropagation techniques use a horizontal step size ($\Delta x = 10$ m) and the receiver points are located at 30 m height along the terrain.

Figure 37 shows the conformation of ray paths at the final position of the radio link. In this situation, the direct ray path and four diffracted ray paths, produced by the terrain influence, are configured. Consequently, the PDP at this receiver point can be generated and is depicted in Figure 38.

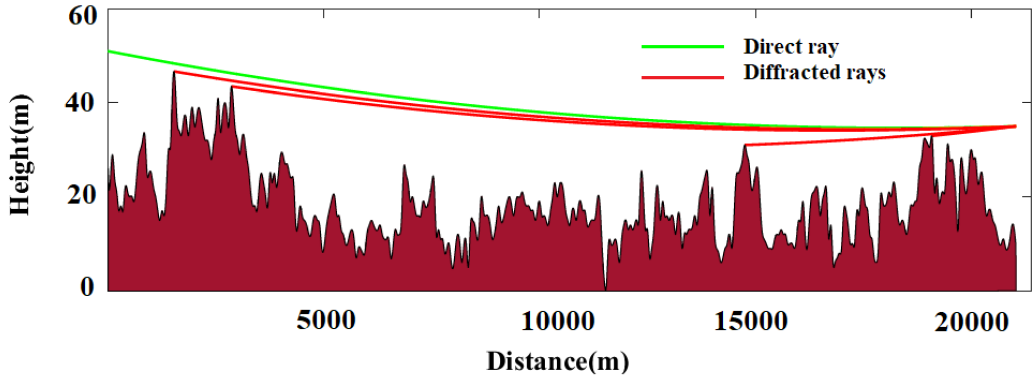

Figure 37 – Ray paths conformation at the final position of the radio link for Colombian Pacific region case.

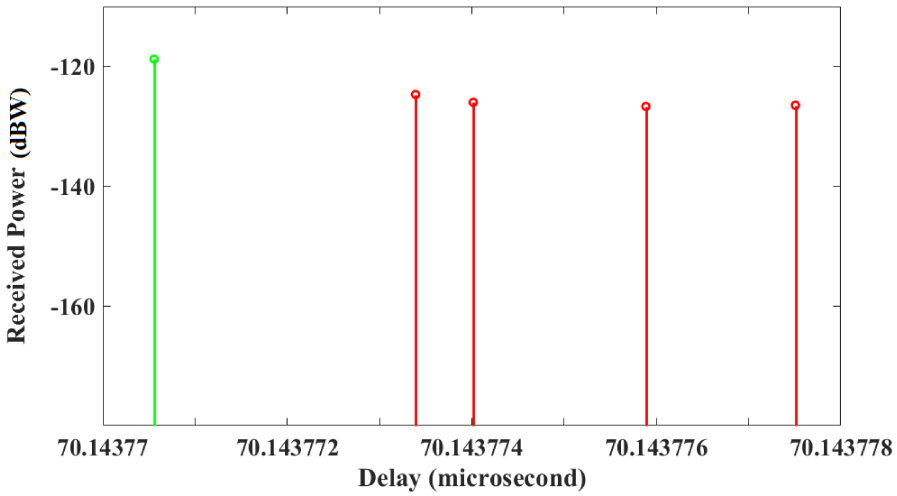

Figure 38 – Power Delay Profile at the final position of the radio link for Colombian Pacific region case.

In the same way as in Cúcuta city case, in this case study we compare the Non-Modified RT and Modified RT results with respect to DMFT-SSPE. In Figure 39, the pathloss curves along the terrain for both situations are illustrated, Figures 39a and 39b, respectively. It can be noted that unlike the first realistic case, in this environment a complete pathloss curve is obtained along the terrain, this is mainly due to the choice of higher receiver points. This means that for all the observation points considered over the Pacific region terrain profile, the proposed multipath approach achieves a combination of ray paths that hit a known receiver point.

Table 6 displays the statistics. Similarly to the Cúcuta city realistic case, it can be observed that a Modified RT algorithm shows a slightly better result in the statistical comparison.

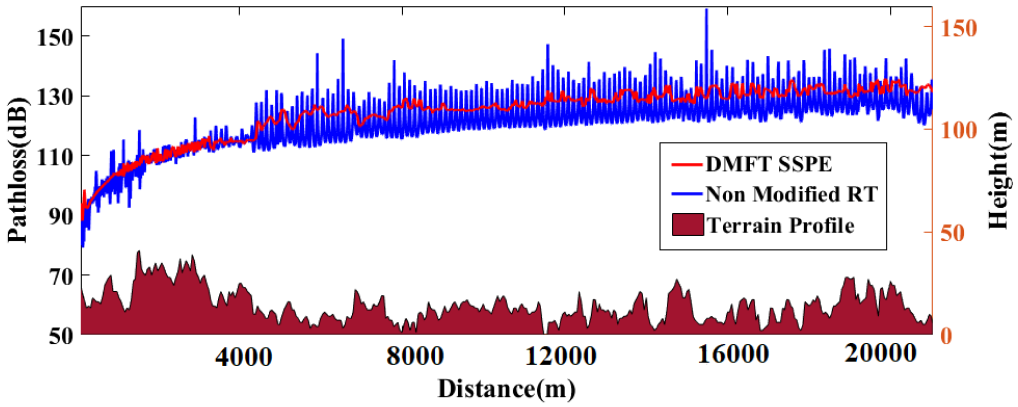

(a)

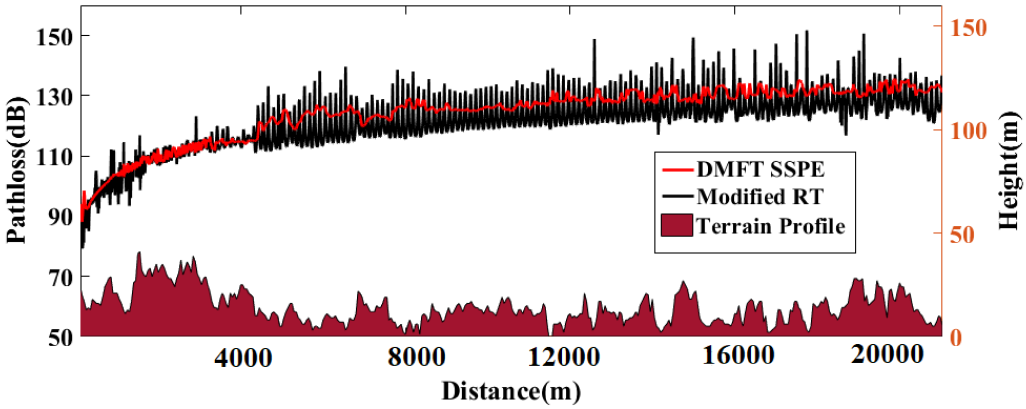

(b)

Figure 39 – Pathloss horizontal Profile results for Pacific region case at 3.5 GHz: (a) Non-Modified RT versus DMFT-SSPE and (b) Modified RT versus DMFT-SSPE.

Table 6 – Statistic comparison for pathloss results in Pacific region case at 3.5 GHz

RT Technique	Mean Absolute Difference (dB)	Standard Deviation (dB)
Non Modified	5.05	6.04
Modified	4.88	5.89

In the second simulation carried out in this scenario, we use the Modified RT and DMFT-SSPE models to estimate coverage for a TVWS system, intended to provide coverage in areas with low population density (less than 1 inhabitant per square km). It is intended to use a technology called Wireless DOCSIS, which is a variation of the cable TV standard DOCSIS 3.0, widely used in some countries like Canada, to provide broadband access in remote areas (Navarro et al., 2022).

It is important to mention that the scenario analyzed in this realistic case simulates the terrain profile between the site located at Universidad del Pacífico campus and "Punta Soldado". In this simulation, we used a frequency of 580 MHz, and the goal was to compare the results obtained with Modified RT and DMFT-SSPE algorithms, as well as try to determine if was possible to get coverage in "Punta Soldado". The location parameters and heights of the transmitter antenna and receiver points are maintained with respect to the first simulation carried out in this scenario.

Figure 40 shows the pathloss results for the Modified RT and DMFT-SSPE along the route. Results in Table 7 shows that prediction difference between DMFT-SSPE and Modified RT are around 7 dB in the entire path. However, we can see in Figure 40 that at the receiver point in "Punta Soldado", the difference is smaller (less than 5 dB).

If we assume the 27 dBm transmitting power and the 10 dBi antenna gain, we can expect a received level of -63 dBm with the Modified RT model and -68 dBm with the DMFT-SSPE model. In both cases, the signal level is acceptable to get a good throughput with the Wireless DOCSIS system. For the type of equipment used, a good received signal should be above -85 dBm, being ideal a level above -75 dBm, which allows the use of the 16 QAM modulation and the higher data rate.

The results obtained in both realistic cases allow to conclude that the proposal of atmospheric refractivity inclusion into a multipath approach, based on RT solutions, is a

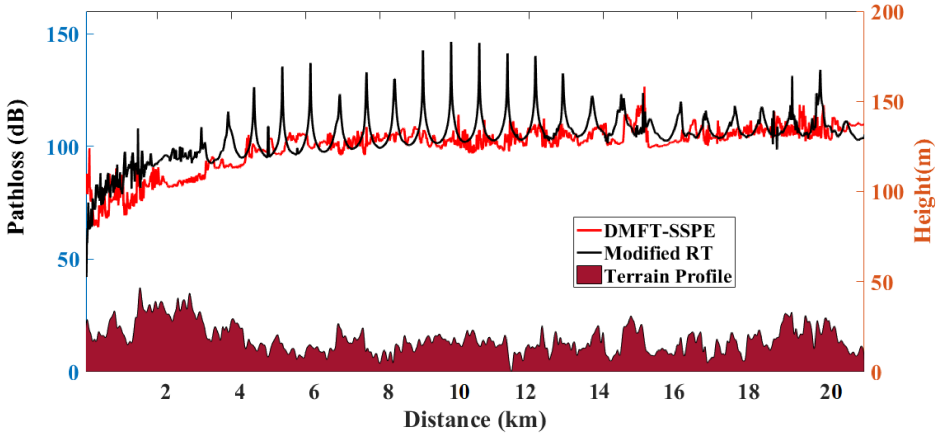

Figure 40 – Pathloss horizontal Profile results obtained with Modified RT and DMFT-SSPE for Pacific region case at 580 MHz.

Table 7 – Statistic comparison for pathloss results in Pacific region case at 580 MHz.

Analyzed Interval	**Mean Absolute Difference (dB)**	**Standard Deviation (dB)**
[70 m - 21040 m]	6.49	8.75

promising propagation model to be applied in this kind of environments. Additionally, the capacity of the proposed algorithms to estimate coverage, and characterize radio channels, at sub-6 GHz (projected for 5G systems operation) and TVWS frequency bands, was also demonstrated.

4.3 Chapter Conclusions

In this Chapter, the simulation results of a modified RT algorithm and DMFT-SSPE technique were obtained. These two propagation models showed promising results when applied in Colombian environments, which presented challenges for radiopropagation modeling. Factors such as atmospheric conditions, terrain profiles, surfaces electromagnetic characterization were adequately processed by both approaches. Additionally, the algorithms present good computational performance to generate results in a short simulation time, and DMFT-SSPE solution did not show numerical instability in the two study cases. The two techniques can be projected as useful tools to predict coverage in the frequency bands that are intended to be used to provide connectivity in remote areas of the Colombian geography.

5 A Proposal of a Modified RT for Horizontally Variable Refractivity

5.1 Chapter motivation

This chapter introduces a novel formulation, proposed by the author of this thesis, for calculation and ground-reflection analysis of ray paths in horizontally variable refractive condition. In (Valtr; Pechac, 2005a), an analytic RT approach for horizontally variable refractive gradient was presented, from which a direct ray path solution was provided. However, ray path solutions associated with other propagation mechanism were not specified. Therefore, in this work an analytical solution is deduced, in order to calculate and analyze the incident and reflected ray paths for the refractivity case mentioned above. In this way, we propose a formulation for ground-reflection analysis, which considers the horizontally stratified variation of the refractivity gradient over flat terrain.

Subsequently, the proposed formulation is implemented within a RT algorithm, called in this work, as Modified RT with atmospheric refractivity effect (Parada et al., 2019) The proposed approach was validated in a canonical scenario, addressing three different situations of horizontally stratified refractivity change. The obtained results were compared with the Split-Step Parabolic Equation (SSPE) numerical solution at 10 GHz. The early results showed a similar behavior for received power calculate, in this canonical test.

5.2 Formulation

5.2.1 Ray path formulation for horizontally variable refractivity

A terrestrial radio link path traveling partly over open terrain or a suburban area and partly through a city center can then be exposed to various refractivity gradients along the path. Figure 41 represents a direct ray path depending on horizontally stratified refractivity gradient variations and knowing the location of a receiver point.

Based on Figure 41 with range dependent gradients, the following equation was proposed in (Valtr; Pechac, 2005a) to calculate the ray path under these refractive conditions:

$$\frac{\mathrm{d}^2 z}{\mathrm{d}x^2} = \delta_1 + \mathbf{1}(x - R_2)[-\delta_1 + \delta_2] + ... + \mathbf{1}(x - R_n)[-\delta_{N-1} + \delta_N]. \tag{5.1}$$

As depicted in Figure 41, Z_t is the transmitter height, Z_R is the receiver point

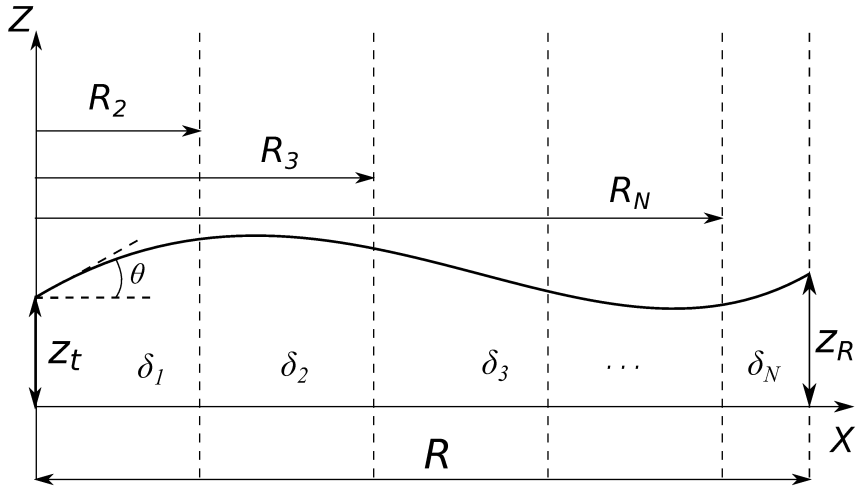

Figure 41 – Direct ray path for refractivity horizontal variation.

height, R is the distance between the receiver point and the transmitter, δ_i represents the range-dependent gradient, R_i are the distances related to those gradients, $R_1 = 0$ and $\mathbf{1}(x)$ is a unit step function defined as:

$$\mathbf{1}(x) = \begin{cases} \mathbf{1}(x) = 0 \quad \text{for} \quad x \leq 0 \\ \\ \mathbf{1}(x) = 1 \quad \text{for} \quad x > 0 \end{cases} \tag{5.2}$$

Equation (5.1) can be solved using Laplace transform and shifting theorem to obtain the solution provided in (Valtr; Pechac, 2005a):

$$z = \frac{\delta_1 x^2}{2} + Kx + Z_t + \sum_{i=2}^{N} \mathbf{1}(x - R_i) \times \left[\frac{\delta_i}{2}(x - R_i)^2 - \frac{\delta_{i-1}}{2}(x - R_i)^2 \right], \tag{5.3}$$

where K is the initial tangent of the launch angle, $K = \tan\theta$.

5.2.2 Reflection analysis for horizontally variable refractivity

In (Valtr; Pechac, 2005a) it was commented that reflections of the ray are not considered in Equation (5.3). Thus, in previous works, the present case of horizontal variation of refractivity was applied in situations where only direct line ray paths were considered. The author of this research propose the following approach to include reflection analysis. Consequently, a new formulation is derived and intended to be used in RT algorithms that include atmospheric refractivity effect.

The formulation is proposed in order to calculate the location of a reflection point. Figure 42 shows the variables involved in the incident and reflected ray paths analysis. In this approach the location of a receptor is known (R, Z_R) and X is the distance from the transmitter to the location of a reflection point.

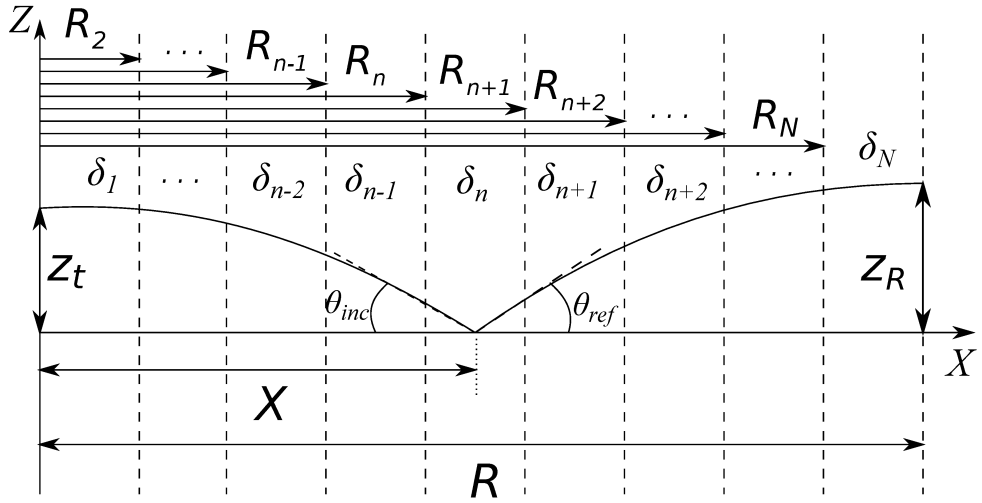

Figure 42 – Incident and reflected paths for horizontal refractive case.

Initially, we isolate K in (5.3):

$$k = \frac{z - Z_t}{x} - \frac{\delta_1 x}{2} - \sum_{i=2}^{N} \mathbf{1}(x - R_i) \times \left[\frac{(x - R_i)^2}{2x} (\delta_i - \delta_{i-1}) \right]. \tag{5.4}$$

Based on Figure 42 and analyzing the incident ray path, the following conditions were considered: $Z_t = 0$, $x = X$, $z = Z_t$ and $\delta_1 = \delta_n$, and substituting them in (5.4), it is possible to reach an expression for k_{inc} as follows:

$$k_{inc} = \frac{Z_t}{X} - \frac{\delta_n X}{2} - \sum_{i=2}^{n} \frac{R_i^2}{2X} (\delta_{i-1} - \delta_i). \tag{5.5}$$

Similarly, analyzing the reflected ray path and according to the Figure 42, the following conditions were considered: $Z_t = 0$, $x = R - X$, $z = Z_R$ and $\delta_1 = \delta_n$, which allows us to obtain an expression for k_{ref} as follows:

$$k_{ref} = \frac{Z_R}{R - X} - \frac{\delta_n (R - X)}{2} - \sum_{i=n+1}^{N} \frac{(R - R_i)^2}{2(R - X)} (\delta_i - \delta_{i-1}). \tag{5.6}$$

In this way, we introduce the following variable changes:

$$A = \sum_{i=n+1}^{N} \frac{(R - R_i)^2}{2} (\delta_i - \delta_{i-1}), \tag{5.7}$$

$$B = \sum_{i=2}^{n} \frac{R_i^2}{2} (\delta_{i-1} - \delta_i), \tag{5.8}$$

$$C = \frac{\delta_n}{2}. \tag{5.9}$$

Consequently, (5.5) and (5.6) can be rewritten as:

$$K_{inc} = \frac{Z_t}{X} - CX - \frac{B}{X}, \tag{5.10}$$

$$K_{ref} = \frac{Z_R}{R - X} - C(R - X) - \frac{A}{(R - X)}. \tag{5.11}$$

From Snell's law: $K_{inc} = K_{ref}$, hence we equate (5.10) and (5.11). Subsequently, it is possible to arrive a cubic equation:

$$(2C)X^3 - (3CR)X^2 + (A + B + CR^2 - Z_t - Z_R)X + (RZ_t - BR) = 0. \tag{5.12}$$

In the solution of (5.12), the following criteria must be met: *i)* $X = x_1$, is a real root and *ii)* $R_n < X < R_{n+1}$. Thus the reflection point is at the coordinate $(X, 0)$, in this radiopropagation case. Once known the location where the ground-reflection occurs, it is possible to calculate the incident and reflected ray paths from (5.3).

5.3 Simulation results

The novel formulation and proposed algorithm of a Modified RT technique for horizontally variable refractivity are applied in three situations, in order to be validated. Therefore, it is compared with the results obtained using the SSPE numerical solution.

The radiopropagation cases are analyzed for a perfectly conducting ground, the simulations use a frequency of 10 GHz and horizontal polarization. The transmitter is located at 30 m height and the receivers points also are located at 30 m height along the scenery. The received power results are plotted versus distance for the three situations.

Figure 43 depicts the results with the refractivity gradient constant δ = -40 N/km throughout the environment. The solution of the classical two-ray model is also presented in this graph, we intend to show the difference of the results when the effects of atmospheric refractivity are considered by radiopropagation techniques. The Free Space Loss represents the results obtained when only the contribution of the direct ray path is considered. Additionally, it is possible to observe that the obtained results of a modified RT and the SSPE method have a similar behavior.

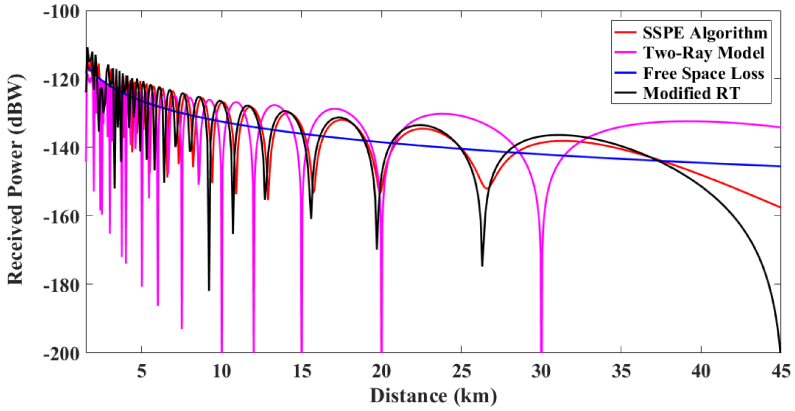

Figure 43 – Validation results for the case of a constant refractivity gradient ($\delta = -40$ N/km).

Figure 44 exhibits the results with a change of gradients $\delta_1 = -40$ N/km and $\delta_2 = -100$ N/km at a distance $d = 15$ km. It is possible to notice that at greater distances from the transmitter the results between Modified RT and SSPE begin to disagree. The maximum and minimum peaks of the curve obtained with RT are formed by the reflections that are still calculated at these distances, on the other hand, the numerical technique shows a smooth fading of signal strength.

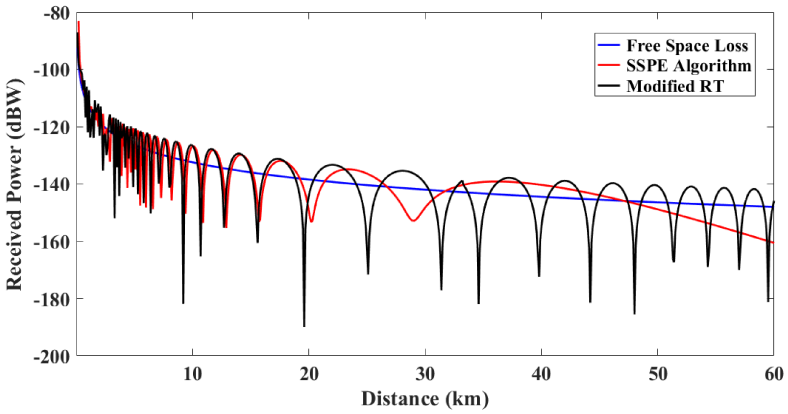

Figure 44 – Validation results for the change of gradients δ_1 = -40 N/km, δ_2 = -100 N/km at d = 15 km.

It is suggested that the application of this case accommodates the smooth variations of the refractivity gradients between two adjacent layers (Valtr; Pechac, 2005a). Therefore the following conditions are proposed: $\delta_1 = -40$ N/km, $\delta_2 = -45$ N/km and $\delta_3 = -50$ N/km, performing the refractivity gradient changes at $d_1 = 15$ km and $d_2 = 30$ km. Figure 45 shows the preliminary results for this simulation conditions.

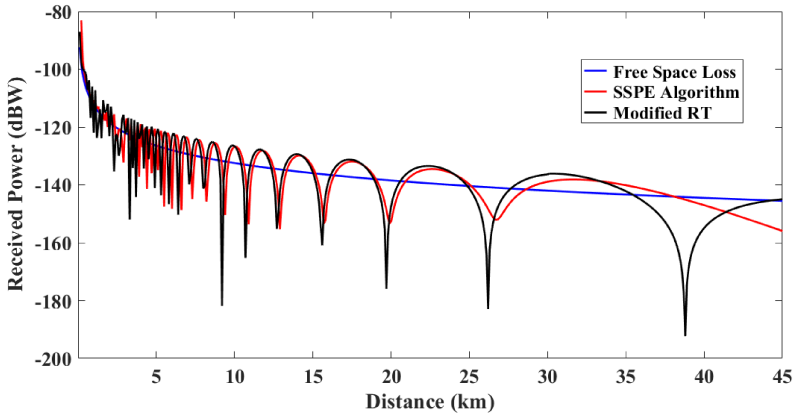

Figure 45 – Validation results for the change of gradients δ_1 = -40 N/km, δ_2 = -45 N/km and δ_3 = -50 N/km.

In the three graphs, the comparison between Modified RT and SSPE results, shows that with minor adjustments, the proposed formulation can be used within a Modified RT algorithm.

5.3.1 Chapter Conclusions

In this chapter, a novel formulation was presented to include ground-reflection analysis within a multipath model based on RT solutions. Specifically, the formulation was derived for the case of horizontally stratified refractivity gradient variation in long-distance scenarios. Preliminary results were obtained in a canonical case and compared with the SSPE numerical technique. The formulation shows promise to be consolidated in the near future.

6 Conclusions and Future Research

6.1 Conclusions

This work presented Parabolic Equation and Ray Tracing formulations for the development of radiowave propagation models in non-homogeneous media. The ability to include realistic factors of the scenarios without involving a high computational cost, is the main motivation for choosing PE and RT approaches.

Previously, a SSPE algorithm had shown a stable formulation to include effects of atmospheric variations and irregular terrain profiles, in propagation problems over perfectly conducting surfaces. Hence, the DMFT method was added in this work in order to incorporate general surfaces with impedance boundary conditions. In this research, the DMFT-SSPE numerical algorithm was used and implemented to solve the PE model, which is the most complete version of the Fourier split-step methods.

This work also proposed a modified RT technique with atmospheric refractivity effect, based on GO, UTD and the mathematical description of ray paths depending on refractivity gradients. The basis of this proposal was to define a two-ray model, which proposes a ground-reflection analysis for curved ray paths under conditions of constant refractivity gradient profiles and horizontally variable refractive. Here, a ground reflected propagation path must exist, and principles, such as Snell's law and the reciprocity theorem for analyzing antennas were used to propose a novel formulation that includes refractive effects into two-ray model. It was possible to affirm that the adequate launching angle calculation guarantees the arrival of the reflected ray at a specific receiver point. Novelty formulations were obtained for the ground-reflection analysis on flat and sloping terrain.

The canonical tests exhibited in Chapter 3 validated the proposed formulation for a modified RT through comparisons made between RT, the SSPE and DMFT-SSPE methods. The obtained results shown a similar behavior for pathloss calculating. For the canonical case of a PEC wedge, it was possible to conclude that the proposed approach of a modified two ray model unified with UTD demonstrated a similar behavior of the results regarding to SSPE algorithm. Thus, diffraction and atmospheric refractivity effect into RT were included favorably. Under lossy ground surface and standard atmosphere effects conditions, the comparative studies maintained the good results. On the whole, it can be observed in Mixed Scenario case that both formulations (PE and RT approaches) presented promising results to coverage prediction in non-homogeneous media.

In Chapter 4, we have shown simulation results of a modified RT algorithm and DMFT-SSPE technique in realistic scenarios. These two propagation models showed

promising results when applied in Colombian environments, which presented challenges for radiopropagation modeling. Factors such as atmospheric conditions, terrain profiles, surfaces electromagnetic characterization were adequately processed by both approaches. Additionally, the algorithms present good computational performance to generate results in a short simulation time, and DMFT-SSPE solution did not show numerical instability in the two study cases. The two techniques can be projected as useful tools to predict coverage in the frequency bands that are intended to be used to provide connectivity in remote areas of the Colombian geography.

Chapter 5 introduced a novel formulation, proposed by the author of this thesis, for calculation and ground-reflection analysis of ray paths in horizontally variable refractive condition. This formulation is implemented within a Modified RT algorithm that includes atmospheric refractivity effect (algorithm proposed in Chapter 3). The proposed approach was validated in a canonical scenario, addressing different situations of horizontally stratified refractivity change. The obtained results were compared with the SSPE numerical solution at 10 GHz. The early results showed promising results for calculating received power, in this canonical tests.

6.2 List of publications

The following journal and conference papers have been performed during the development of this thesis:

- D. Parada, C. G. Rego, D. Guevara, A. Navarro, G. L. Ramos and R. Oliveira, "A Modified Radiopropagation Multipath Model for Constant Refractivity Gradient Profiles" in *Journal of Microwaves, Optoelectronics and Electromagnetic Applications*, 2023. *(Accepted)*.
- D. Parada, C. G. Rego, D. Guevara, A. Navarro and L. E. Royero, "Modified RT and DMFT-SSPE Algorithms Applied in Colombian Environments" in *20º Simpósio Brasileiro de Micro-ondas e Optoeletrônica SBMO*, Natal - RN, 2022.
- A. Navarro, L. Vargas, D. Guevara, D. Parada, C. Amu and C. G. Rego, "Propagation Models Trials for TV White Spaces in Colombian Rain Forest" in *2022 16th European Conference on Antennas and Propagation (EuCAP)*, Madrid, Spain, 2022, pp. 1-5, doi: 10.23919/EuCAP53622.2022.9769611.
- A. Navarro, D. Parada, D. Guevara, C. G. Rego, R. Oliveira, R. Velasquez and L. Gomezjurado, "A Modified Two-Ray Model with UTD and Atmospheric Effects: Analysis of Reflected Ray Over Sloping Terrain" in *2021 15th European Conference on Antennas and Propagation (EuCAP)*, Dusseldorf, Germany, 2021, pp. 1-4, doi: 10.23919/EuCAP51087.2021.9411411.

- A. Navarro, D. Parada, D. Guevara, C. G. Rego and R. A. Badillo, "Modified Two-Ray Model with UTD and Atmospheric Effects" in *2020 14th European Conference on Antennas and Propagation (EuCAP)*, Copenhagen, Denmark, 2020, pp. 1-5, doi: 10.23919/EuCAP48036.2020.9135235.

- D. A. Parada, Dinael Guevara, C. G. Rego, Juliana M. Mendes, Brian Araque and G. L. Ramos. "A Comparison Between a Modified Two-Ray Model with Atmospheric Effects and the SSPE Method for an EM Propagation Case Study" in *13th European Conference on Antennas and Propagation (EuCAP)*, Krakow, 2019.

- J. M. Mendes, C. G. Rego, D. Parada, C. G. Batista and D. Guevara, "SSPE Method Including Backward Term for an EM Propagation Real Case Study" in *2019 IEEE-APS Topical Conference on Antennas and Propagation in Wireless Communications (APWC)*, Granada, Spain, 2019, pp. 289-291, doi: 10.1109/APWC.2019.8870387.

- D. Parada, C. G. Rego, J. Mendes, D. Guevara , R. Daza and G. L, Ramos, "Scattering by a PEC Wedge in a Standard Atmosphere: a Modified Two-Ray Model Versus a SSPE Algorithm" in *SBMO/IEEE MTT-S International Microwave and Optoelectronics Conference (IMOC)*, Aveiro, Portugal, 2019.

- D. A. Parada, C. G. Rego, C. G.Batista and G. L. Ramos "Algoritmos para a Solução de Equações Parabólicas em Problemas de Radiopropagação" in *XXXVI Brazilian Symposium on Telecommunications and Signal Processing (SBrT)*, Campina Grande, PB, 2018.

6.3 Future research

The achieved algorithms in this thesis could be expanded in many research aspects that can be addressed in future works. Suggestions for future work are as follows:

- Extend the formulation (analytical description of trajectories) of ray paths for reflection and diffraction analysis, in other refractivity conditions, for example tropospheric ducts. For this situation of refractivity, this work showed a solution already given by the literature for direct ray paths.

- The preliminary formulation derived in this work for the description of ray paths under the influence of horizontally varying refractivity, must be tested in case studies involving terrain factors. Thus, the diffraction analysis would be added for this refractivity condition.

- Incorporate the backward propagation term in both solutions, analyzing the incidence of such scaterring phenomenon in their results. These models are designed to be used in realistic cases and in higher frequency applications.

- Aiming at the application of the algorithms in Colombian environments, in the near future, it is expected to validate the results obtained through measurement campaigns. This will allow the propagation models to be adjusted.
- Propose case studies to compare precision of results and computational efficiency, with other promising propagation techniques to characterize radio channel.
- Implement 3D algorithms, since Modified RT technique also is promising for wide coverage analysis in three-dimensional scenarios, which are more complex and where many more multipath components are configured.

References

AbouAlmal, A.; Abd-Alhameed, R. A.; Jones, S. M. R.; Al-Ahmad, H. New methodology for predicting vertical atmospheric profile and propagation parameters in subtropical arabian gulf region. *IEEE Transactions on Antennas and Propagation*, IEEE, v. 63, n. 9, p. 4057–4068, 2015.

Akleman, F.; Sevgi, L. A novel finite-difference time-domain wave propagator. *IEEE Transactions on Antennas and Propagation*, IEEE, v. 48, n. 5, p. 839–841, 2000.

Akleman, F.; Sevgi, L. A novel MoM-and SSPE-based groundwave-propagation field-strength prediction simulator. *IEEE Antennas and Propagation Magazine*, IEEE, v. 49, n. 5, p. 69–82, 2007.

Apaydin, G.; Sevgi, L. *Radio wave propagation and parabolic equation modeling.* : John Wiley & Sons, 2017.

Barrios, A. E. Parabolic equation modeling in horizontally inhomogeneous environments. *IEEE Transactions on antennas and propagation*, IEEE, v. 40, n. 7, p. 791–797, 1992.

Barrios, A. E. A terrain parabolic equation model for propagation in the troposphere. *IEEE Transactions on Antennas and Propagation*, IEEE, v. 42, n. 1, p. 90–98, 1994.

Bean, B. R.; Dutton, E. J. *Radio meteorology.* : Superintendentof Documents, US GovernmentPrint. Office, 1966. v. 92.

Bean, B. R.; Thayer, G. D. Models of the atmospheric radio refractive index. *Proceedings of the IRE*, IEEE, v. 47, n. 5, p. 740–755, 1959.

Boan, J. A. *Radio propagation in fire environments.* Tese (Doutorado) — University of Adelaide, Australia, 2009.

Dinc, E.; Akan, O. B. Beyond-line-of-sight communications with ducting layer. *IEEE Communications Magazine*, IEEE, v. 52, n. 10, p. 37–43, 2014.

Dinc, E.; Akan, O. B. Channel model for the surface ducts: large-scale path-loss, delay spread, and AOA. *IEEE Transactions on Antennas and Propagation*, IEEE, v. 63, n. 6, p. 2728–2738, 2015.

Dockery, D.; Kuttler, J. R. An improved impedance-boundary algorithm for Fourier split-step solutions of the parabolic wave equation. *IEEE Transactions on Antennas and Propagation*, IEEE, v. 44, n. 12, p. 1592–1599, 1996.

Donohue, D. J.; Kuttler, J. R. Propagation modeling over terrain using the parabolic wave equation. *IEEE Transactions on Antennas and Propagation*, IEEE, v. 48, n. 2, p. 260–277, 2000.

El Ahdab, Z.; Akleman, F. Radiowave propagation analysis with a bidirectional 3-D vector parabolic equation method. *IEEE Transactions on Antennas and Propagation*, IEEE, v. 65, n. 4, p. 1958–1966, 2017.

Fuschini, F.; Degli-Esposti, V.; Vitucci, E. M. A model for forward-diffuse scattering through a wall. In: IEEE. *Proceedings of the Fourth European Conference on Antennas and Propagation*. 2010. p. 1–4.

Gómez Rojas, J. *Mapas de capacidad de canal para sistemas móviles de quinta gneración*. Tese (Doutorado) — Universidad Pontificia Bolivariana, 2018.

Hall, M. P. M.; Barclay, L. W.; Hewitt, M. T. Propagation of Radiowaves (Institution of Electrical Engineers,). 1996.

Hviid, J. T.; Andersen, J. B.; Toftgard, J.; Bojer, J. Terrain-based propagation model for rural area-an integral equation approach. *IEEE Transactions on Antennas and Propagation*, IEEE, v. 43, n. 1, p. 41–46, 1995.

Iskander, M. F.; Yun, Z. Propagation prediction models for wireless communication systems. *IEEE Transactions on microwave theory and techniques*, IEEE, v. 50, n. 3, p. 662–673, 2002.

Janaswamy, R. A fast finite difference method for propagation predictions over irregular, inhomogeneous terrain. *IEEE transactions on antennas and propagation*, IEEE, v. 42, n. 9, p. 1257–1267, 1994.

Johnson, J. T.; Shin, R. T.; Eidson, J. C.; Tsang, L.; Kong, J. A. A method of moments model for VHF propagation. *IEEE Transactions on antennas and propagation*, IEEE, v. 45, n. 1, p. 115–125, 1997.

Karimian, A.; Yardim, C.; Gerstoft, P.; Hodgkiss, W. S.; Barrios, A. E. Refractivity estimation from sea clutter: An invited review. *Radio Science*, AGU, v. 46, n. 06, p. 1–16, 2011.

Kouyoumjian, R. G.; Pathak, P. H. A uniform geometrical theory of diffraction for an edge in a perfectly conducting surface. *Proceedings of the IEEE*, IEEE, v. 62, n. 11, p. 1448–1461, 1974.

Kuttler, J. R.; Dockery, G. D. Theoretical description of the parabolic approximation/-Fourier split-step method of representing electromagnetic propagation in the troposphere. *Radio science*, Wiley Online Library, v. 26, n. 2, p. 381–393, 1991.

Kuttler, J. R.; Janaswamy, R. Improved Fourier transform methods for solving the parabolic wave equation. *Radio Science*, AGU, v. 37, n. 2, p. 1–11, 2002.

Lentovich, M. A.; Fock, V. A. Solution of Propagation of Electromagnetic Waves Along the Earth's Surface by the Method of Parabolic Equations. *Journal Physics USSR*, v. 10, p. 13–23, 1946.

Leonor, N. R. et al. Site-specific radio propagation model for macrocell coverage at sub-6 GHz frequencies. *IEEE Transactions on Antennas and Propagation*, v. 70, n. 10, p. 9706–9715, 2022.

Levy, M. *Parabolic equation methods for electromagnetic wave propagation*. : IET, 2000.

Luebbers, R. J. A heuristic UTD slope diffraction coefficient for rough lossy wedges. *IEEE Transactions on Antennas and Propagation*, IEEE, v. 37, n. 2, p. 206–211, 1989.

Lytaev, M. S. Nonlocal boundary conditions for split-step padé approximations of the helmholtz equation with modified refractive index. *IEEE antennas and wireless propagation letters*, IEEE, v. 17, n. 8, p. 1561–1565, 2018.

Navarro, A.; Guevara, D.; Gomez, J. Prediction of delay spread using ray tracing and game engine based on measurement. In: IEEE. *2015 IEEE 81st Vehicular Technology Conference (VTC Spring)*. 2015. p. 1–6.

Navarro, A.; Guevara, D.; Gómez, J. A proposal to improve ray launching techniques. *IEEE Antennas and Wireless Propagation Letters*, v. 18, n. 1, p. 143–146, 2019.

Navarro, A.; Parada, D.; Guevara, D.; Rego, C. G.; Badillo, R. A. Modified Two-Ray Model with UTD and Atmospheric Effects. In: *2020 14th European Conference on Antennas and Propagation (EuCAP)*. 2020. p. 1–5.

Navarro, A. et al. Propagation models trials for tv white spaces in colombian rain forest. In: IEEE. *2022 16th European Conference on Antennas and Propagation (EuCAP)*. 2022. p. 1–5.

Ozgun, O.; Apaydin, G.; Kuzuoglu, M.; Sevgi, L. Two-way Fourier split step algorithm over variable terrain with narrow and wide angle propagators. In: IEEE. *2010 IEEE Antennas and Propagation Society International Symposium*. 2010. p. 1–4.

Ozgun, O.; Apaydin, G.; Kuzuoglu, M.; Sevgi, L. PETOOL: MATLAB-based one-way and two-way split-step parabolic equation tool for radiowave propagation over variable terrain. *Computer Physics Communications*, Elsevier, v. 182, n. 12, p. 2638–2654, 2011.

Parada, D. et al. A Comparison Between a Modified Two-Ray Model with Atmospheric Effects and the SSPE Method for an EM Propagation Case Study. In: *2019 13th European Conference on Antennas and Propagation (EuCAP)*. 2019. p. 1–4.

Parada, D.; Rego, C. G.; Guevara, D.; Navarro, A.; Royero, L. E. Modified rt and dmft-sspe algorithms applied in colombian environments. In: SBMO. *20º Simpósio Brasileiro de Micro-ondas e Optoeletrônica SBMO*. 2022. p. 1–5.

Parada, D. et al. Scattering by a PEC Wedge in a Standard Atmosphere: a Modified Two-Ray Model Versus a SSPE Algorithm. *18th edition of the SBMO/IEEE MTT-S International Microwave and Optoelectronics Conference (IMOC)*, Aveiro, p. 1–3, 2019.

Parker, E. A.; Chuprin, A. D.; Langley, R. J. Finite element analysis of electromagnetic wave diffraction from buildings incorporating frequency selective walls. *IEE Proceedings-Microwaves, Antennas and Propagation*, IET, v. 146, n. 5, p. 319–323, 1999.

Picquenard, A. *Radio wave propagation.* : Macmillan International Higher Education, 1974.

Rappaport, T. S. *Wireless communications: principles and practice.* : Prentice hall PTR New Jersey, 1996. v. 2.

Rappaport, T. S. et al. Overview of millimeter wave communications for fifth-generation (5G) wireless networks—With a focus on propagation models. *IEEE Transactions on Antennas and Propagation*, IEEE, v. 65, n. 12, p. 6213–6230, 2017.

Razavi-Ghods, N. *Characterisation of MIMO radio propagation channels*. Tese (Doutorado) — Durham University, 2007.

Sekmen, S. *Modeling of split step parabolic wave equation using the graphics processing unit (MSc thesis)*. : Middle East Technical University, 2014.

Sevgi, L. *Electromagnetic modeling and simulation*. : John Wiley & Sons, 2014.

Sevgi, L.; Uluisik, C.; Akleman, F. A matlab-based two-dimensional parabolic equation radiowave propagation package. IEEE, 2005.

Sirkova, I. Propagation factor and path loss simulation results for two rough surface reflection coefficients applied to the microwave ducting propagation over the sea. *Progress in Electromagnetics Research*, EMW Publishing, v. 17, p. 151–166, 2011.

Skolnik, M. I.; Others. *Introduction to radar systems*. : McGraw-hill New York, 1980. v. 3.

Tami, D. et al. Analysis of heuristic uniform theory of diffraction coefficients for electromagnetic scattering prediction. *International Journal of Antennas and Propagation*, Hindawi, v. 2018, 2018.

Tami Lopez, D. *Métodos assintóticos para caracterização do canal rádio em ambientes externos (MSc thesis)*. : Universidade Federal de Minas Gerais, 2015.

Tappert, F. D. The parabolic approximation method. In: *Wave propagation and underwater acoustics*. : Springer, 1977. p. 224–287.

Ufimtsev, P. Y. *Fundamentals of the physical theory of diffraction*. : John Wiley & Sons, 2014.

Valtr, P. Short Course Computational methods for long-range radio wave propagation prediction. In: *11th European Conference on Antennas and Propagation (EuCAP 2017)*. Paris: , 2017.

Valtr, P.; Pechac, P. The influence of horizontally variable refractive index height profile on radio horizon range. *IEEE Antennas and Wireless Propagation Letters*, IEEE, v. 4, p. 489–491, 2005.

Valtr, P.; Pechac, P. Tropospheric refraction modeling using ray-tracing and parabolic equation. *RADIOENGINEERING-PRAGUE-*, Citeseer, v. 14, n. 4, p. 98, 2005.

Valtr, P.; Pechac, P. Analytic tropospheric ray-tracing model for constant refractivity gradient profiles. In: *2006 First European Conference on Antennas and Propagation*. 2006. p. 1–4.

Wagner, M.; Gerstoft, P.; Rogers, T. Estimating refractivity from propagation loss in turbulent media. *Radio Science*, AGU, v. 51, n. 12, p. 1876–1894, 2016.

Wait, J. R. The scope of impedance boundary conditions in radio propagation. *IEEE Transactions on Geoscience and Remote Sensing*, IEEE, v. 28, n. 4, p. 721–723, 1990.

Wald, I. et al. State of the art in ray tracing animated scenes. In: Wiley Online Library. *Computer graphics forum*. 2009. v. 28, n. 6, p. 1691–1722.

Wang, D.-D.; Xi, X.-L.; Pu, Y.-R.; Liu, J.-F.; Zhou, L.-L. Parabolic equation method for loran-c asf prediction over irregular terrain. *IEEE antennas and wireless propagation letters*, IEEE, v. 15, p. 734–737, 2015.

Wang, S. et al. Estimation of abnormal wave propagation by a novel duct map based on the average normalized path loss. *Microwave and Optical Technology Letters*, Wiley Online Library, v. 62, n. 4, p. 1662–1670, 2020.

Yang, S.; Yang, K.-D.; Yang, Y.-X.; Ma, Y.-L. Experimental verification of effect of horizontal inhomogeneity of evaporation duct on electromagnetic wave propagation. *Chinese physics B*, IOP Publishing, v. 24, n. 4, p. 44102, 2015.

Yun, Z.; Iskander, M. F.; Zhang, Z. Complex-wall effect on propagation characteristics and MIMO capacities for an indoor wireless communication environment. *IEEE Transactions on antennas and propagation*, IEEE, v. 52, n. 4, p. 914–922, 2004.

Zhang, P.; Bai, L.; Wu, Z.; Li, F. Effect of window function on absorbing layers top boundary in parabolic equation. In: IEEE. *Proceedings of 2014 3rd Asia-Pacific Conference on Antennas and Propagation*. 2014. p. 849–852.

Zhang, P.; Bai, L.; Wu, Z.; Guo, L. Applying the parabolic equation to tropospheric groundwave propagation: A review of recent achievements and significant milestones. *IEEE Antennas and Propagation Magazine*, v. 58, n. 3, p. 31–44, 2016.

Zhou, H.; Douvenot, R.; Chabory, A. Modeling the long-range wave propagation by a split-step wavelet method. *Journal of Computational Physics*, Elsevier, v. 402, p. 109042, 2020.